

MULTILAYERS OF BLOCK COPOLYMER MICELLES WITH CORES  
EXHIBITING UPPER CRITICAL SOLUTION TEMPERATURE

A THESIS SUBMITTED TO  
THE GRADUATE SCHOOL OF NATURAL AND APPLIED SCIENCES  
OF  
MIDDLE EAST TECHNICAL UNIVERSITY

BY

CANSU ÜSTOĞLU

IN PARTIAL FULFILLMENT OF THE REQUIREMENTS  
FOR  
THE DEGREE OF MASTER OF SCIENCE  
IN  
CHEMISTRY

DECEMBER 2016



Approval of the thesis:

**MULTILAYERS OF BLOCK COPOLYMER MICELLES WITH CORES  
EXHIBITING UPPER CRITICAL SOLUTION TEMPERATURE**

submitted by **CANSU ÜSTOĞLU** in partial fulfillment of the requirements for the degree of **Master of Science in Chemistry Department, Middle East Technical University** by,

Prof. Dr. Gülbin Dural Ünver  
Dean, Graduate School of **Natural and Applied Science**

\_\_\_\_\_

Prof. Dr. Cihangir Tanyeli  
Head of Department, **Chemistry**

\_\_\_\_\_

Assoc. Prof. Dr. İrem Erel Göktepe  
Supervisor, **Chemistry Dept.** , METU

\_\_\_\_\_

**Examining Committee Members:**

Prof. Dr. Ahmet M.Önal  
Chemistry Dept., METU

\_\_\_\_\_

Assoc. Prof. Dr. İrem Erel Göktepe  
Chemistry Dept., METU

\_\_\_\_\_

Assoc. Prof. Dr. Ali Çırpan  
Chemistry Dept., METU

\_\_\_\_\_

Assoc. Prof. Dr. Gülay Ertuş  
Chemistry Dept., METU

\_\_\_\_\_

Assist. Prof. Dr. Tarık Baytekin  
UNAM, Bilkent University

\_\_\_\_\_

**Date: 28.12.16**

**I hereby declare that all information in this document has been obtained and presented in accordance with academic rules and ethical conduct. I also declare that, as required by these rules and conduct, I have fully cited and referenced all material and results that are not original to this work.**

Name, Last name: Cansu ÜSTOĞLU

Signature:

## ABSTRACT

### MULTILAYERS OF BLOCK COPOLYMER MICELLES WITH CORES EXHIBITING UPPER CRITICAL SOLUTION TEMPERATURE

Üstoğlu, Cansu

M.Sc., Department of Chemistry

Supervisor: Assoc. Prof. Dr. İrem Erel Göktepe

December 2016, 76 pages

Stimuli-responsive films are promising materials to release functional molecules from surfaces. Layer-by-layer (LbL) is a practical and easy technique to construct stimuli responsive thin films. Thickness and composition of the films can be precisely controlled using this technique. Temperature-responsive (thermo-responsive) polymers are one of the most extensively studied polymers in the construction of stimuli responsive LbL films due to relatively easy control of temperature than the other stimulus.

The study presented in this thesis reports on preparation of block copolymer micelles (BCMs) with cores exhibiting upper critical solution temperature (UCST)-type phase behaviour at physiological pH and using such BCMs as building blocks to construct LbL films which can be erased from the surface with increasing temperature. P2VP blocks of P2VP-*b*-PEO was partially quaternized to obtain permanent positive charge on P2VP. Micellization was induced in the presence of multivalent salt ions,  $K_3Fe(CN)_6$ , via electrostatic interactions among the positively charged P2VP block and multivalent salt anions. The concentration of  $K_3Fe(CN)_6$  and the micellization temperature were highly critical on the UCST values of the micellar cores. LbL films of QP2VP+ $[Fe(CN)_6]^{3-}$ -*b*-PEO micelles were prepared using tannic acid (TA) at pH 7.5. The driving force for multilayer assembly was hydrogen bonding interactions

between TA and the PEO-corona of QP2VP+[Fe(CN)<sub>6</sub>]<sup>3-</sup>-*b*-PEO micelles. Multilayers could be erased from the surface with increasing temperature.

This study contributes to the fundamental understanding of the structure-property relationship in hydrogen-bonded multilayers. The results obtained in this study can pave the way to develop multilayer films for controlled release applications from surfaces.

**Keywords:** Stimuli-responsive films, Temperature responsive polymers, Layer-by-Layer technique, Upper critical solution temperature (UCST), Poly (2-vinyl pyridine-*block*-ethylene oxide), Hydrogen-bonded multilayer films.

## ÖZ

### ÇEKİRDEK BÖLGELERİ ÜST KRİTİK ÇÖZELTİ SICAKLIĞI GÖSTEREN BLOK KOPOLİMER MİSELLER İÇEREN ÇOK-KATMANLI FİMLER

Üstođlu, Cansu

Yüksek Lisans, Kimya Bölümü

Tez Yöneticisi: Doç. Dr. İrem Erel Göktepe

Aralık 2016, 76 sayfa

Çevre koşullarına duyarlı polimerler işlevsel moleküllerin yüzeyden salınımı için umut vadeden malzemelerdir. Katman-katman (LbL) kendiliğinden yapılanma tekniđi çevreye duyarlı ince filmler üretmek için pratik ve kolay tekniktir. Bu yöntem ile filmlerin kalınlığı ve içeriđi hassas bir şekilde kontrol edilebilir. Sıcaklığa duyarlı polimerler, sıcaklık kontrolünün diđer uyarılara kıyasla daha kolay kontrol edilebilmesinden dolayı LbL filmlerin üretiminde en fazla çalışılmış polimerlerdendir.

Bu tez çalışması, vücut pH'ında çekirdekleri üst kritik çözelti sıcaklığı (UCST) faz davranış özelliđi gösteren blok kopolimer misellerin (BCMs) hazırlanması ve bu blok kopolimer misellerin sıcaklık artışıyla yüzeyden süpürülebilen LbL filmlerin üretiminde yapıtaşısı olarak kullanılmasını rapor etmektedir. Öncelikle, P2VP-*b*-PEO'nun P2VP bloğunda bulunan piridin birimleri kısmi olarak quaternize edilerek P2VP üzerinde kalıcı pozitif yük elde edildi. Miselizasyon, çok-deđerlikli tuz iyonlarının,  $K_3Fe(CN)_6$ , varlığında, pozitif yüklü P2VP blođu ve çok-deđerlikli tuz anyonları arasındaki elektrostatik etkileşim ile tetiklendi.  $K_3Fe(CN)_6$ 'nın derişimi ve miselizasyonun gerçekleştirildiđi sıcaklık misel çekirdeklerin UCST deđerleri

üzerinde oldukça etkiliydi. QP2VP+[Fe(CN)<sub>6</sub>]<sup>3-</sup>-*b*-PEO misellerini içeren LbL filmler, Tannik Asit (TA) kullanılarak pH 7.5’de hazırlandı. Bu filmlerin üretimindeki birincil itici güç, TA ve QP2VP+[Fe(CN)<sub>6</sub>]<sup>3-</sup>-*b*-PEO misellerine ait PEO-kabuk blokları arasındaki hidrojen bağlarıdır. Çok-katmanlı filmlerin sıcaklık artışıyla yüzeyden süpürülebildiği gösterildi.

Bu çalışma, hidrojen bağlı çok katmanlı filmlerde yapı-özellik ilişkisini anlamaya katkı sağlamaktadır. Bu çalışmada elde edilen sonuçlar, yüzeyden kontrollü salınım uygulamaları için daha gelişmiş çok-katmanlı filmlerin hazırlanması için bir temel oluşturabilir.

**Anahtar kelimeler:** Çevre koşullarına duyarlı polimerler, Sıcaklığa duyarlı polimerler, Poli (2-vinil piridine-*blok*-etilen oksit) (P2VP-*b*-PEO), Katman-katman kendiliğinden yapılanma tekniği, Üst kritik çözelti sıcaklığı (UCST), Hidrojen bağlı çok katmalı filmler.

*To My Precious Family...*

## ACKNOWLEDGMENTS

First and foremost, I would like to thank and express my sincere gratitude to my supervisor Assoc. Prof. Dr. İrem Erel Göktepe for valuable guidance, support, advice throughout the course of this work.

I would like to thank Prof. Dr. Ahmet M. Önal , Assoc. Prof. Dr. Ali Çırpan, Assoc. Prof. Dr. Gülay Ertuş and Assist. Prof. Dr. Tarık Baytekin for taking part as members of my thesis examination committee.

This work was financially supported by The Scientific and Technological Research Council of Turkey, TUBITAK (Grant Number: 113Z586). I also thank TUBITAK for the scholarship from this project between March 1<sup>st</sup>, 2014 and September 28<sup>th</sup>, 2016.

I would also like to thank members of Erel's lab for providing me with a peaceful and enjoyable working environment and supplying help and support.

I am also lucky to have Kübra Narcı, Selda Ata, Merve Karakaş as best friend who always encourage and love me.

Last but not least, I would like to thank my family who have always been there for me; to my mother Özcan, my father Cemil and my brother Oral for their unconditional love, warm affection, endless understanding, and support.

## TABLE OF CONTENTS

ABSTRACT.....	v
ÖZ.....	vii
ACKNOWLEDGMENTS.....	x
TABLE OF CONTENTS.....	xi
LIST OF FIGURES.....	xiv
LIST OF TABLES.....	xvii
LIST OF SCHEMES.....	xviii
LIST OF ABBREVIATIONS.....	xix

### CHAPTERS

1.INTRODUCTION .....	1
1.1. Stimuli responsive polymers .....	1
1.2. Temperature-responsive (thermoreponsive) polymers .....	1
1.3. LCST-type phase behaviour of polymers in aqueous solution.....	3
1.4. UCST-type phase behaviour of polymers in aqueous solution .....	4
1.4.1. Polymers showing UCST-type phase behaviour in aqueous solution via coulomb interactions (C-UCST).....	5
1.4.1.1. Zwitterionic polymers .....	5
1.4.1.2. Polyelectrolytes in presence of multivalent counterions.....	6
1.4.2. Hydrogen-bonded Upper Critical Solution Temperature Polymers .....	7
1.5. Temperature-Responsive Block Copolymer Micelles.....	7
1.5.1. Block Copolymer Micelles Exhibiting LCST-Type Phase Behaviour in Aqueous Solution.....	8
1.5.2. Block Copolymer Micelles Exhibiting UCST-Type Phase Behaviour in Aqueous Solution.....	10

1.6. Layer-by-Layer Self-assembly Technique: Preparation of Ultra-thin Polymer Multilayers.....	12
1.6.1. Temperature Responsive LbL Films of Linear Homo- or Copolymers....	15
1.6.2. Temperature Responsive LbL Films of Block Copolymer Micelles .....	16
1.7. Aim of Thesis .....	19
2.EXPERIMENTAL PART .....	21
2.1. Materials .....	21
2.2. Methods &Instrumentation.....	23
2.3 Quaternization and characterization of P2VP block of PEO- <i>b</i> -P2VP.....	23
2.3.1. <sup>1</sup> H-NMR .....	24
2.3.2. ATR-FTIR.....	24
2.3.3. Dynamic Light Scattering (DLS) and ζ-potential measurements of P2VP- <i>b</i> -PEO and P2QVP- <i>b</i> -PEO in aqueous solution .....	24
2.4. Preparation of (QP2VP+ [Fe(CN) <sub>6</sub> ] <sup>3-</sup> )- <i>b</i> -PEO micelles .....	25
2.5. Deposition of multilayers .....	25
2.6. Stability of multilayers in PBS .....	25
3.RESULTS& DISCUSSION .....	27
3.1. Aqueous Solution Behaviour of P2VP- <i>b</i> -PEO.....	27
3.2. Preparation of P2VP- <i>b</i> -PEO micelles with cores exhibiting UCST-type phase behaviour .....	28
3.2.1. Quaternization of P2VP- <i>b</i> -PEO.....	28
3.3. Multivalent salt-induced Micellization of QP2VP- <i>b</i> -PEO.....	35
3.3.1. Effect of concentration of K <sub>3</sub> Fe(CN) <sub>6</sub> on micellization of QP2VP- <i>b</i> -PEO .....	36
3.3.2. Effect of temperature on multivalent-salt induced micellization of QP2VP- <i>b</i> -PEO.....	38
3.4. Temperature Response of (QP2VP+[Fe(CN) <sub>6</sub> ] <sup>3-</sup> )- <i>b</i> -PEO micelles.....	40
3.4.1. Effect of K <sub>3</sub> Fe(CN) <sub>6</sub> concentration on the temperature-response of (QP2VP+[Fe(CN) <sub>6</sub> ] <sup>3-</sup> )- <i>b</i> -PEO micelles .....	41
3.4.2. Effect of micellization temperature on the temperature-response of (QP2VP+[Fe(CN) <sub>6</sub> ] <sup>3-</sup> )- <i>b</i> -PEO micelles .....	43
3.5. Multilayers of (QP2VP+[Fe(CN) <sub>6</sub> ] <sup>3-</sup> )- <i>b</i> -PEO micelles and Tannic Acid (TA) .....	45

3.5.1. Layer-by-layer deposition of (QP2VP+[Fe(CN) <sub>6</sub> ] <sup>3-</sup> )- <i>b</i> -PEO micelles and TA .....	45
3.5.2. Temperature-response of multilayers .....	50
3.5.2.1. Temperature-response of a monolayer of (QP2VP+[Fe(CN) <sub>6</sub> ] <sup>3-</sup> )- <i>b</i> -PEO micelles.....	50
3.5.2.2. Temperature-response of multilayers of (QP2VP+[Fe(CN) <sub>6</sub> ] <sup>3-</sup> )- <i>b</i> -PEO micelles and TA .....	53
3.5.2.2.1. Temperature-response of multilayers constructed at 25 °C .....	53
3.5.2.2.2. Temperature-response of multilayers constructed at 37.5°C .....	57
3.5.2.2.3 Fluorescence Spectroscopy Studies.....	59
4.CONCLUSIONS AND OUTLOOK.....	61
REFERENCES.....	63
APPENDIX.....	73

## LIST OF FIGURES

### FIGURES

**Figure 1.** Phase diagrams (temperature vs. polymer volume fraction ( $\phi$ )) of polymers exhibiting (a) LCST-type behavior and (b) UCST-type behavior in solution [18]. Modified from Hruby et al. Eur.Polym (2015)..... 2

**Figure 2.** LCST type phase behavior of a polymer in aqueous solution.[17] . Modified from Alarco'n et al. Chem. Soc. Rev. 34 (2005)..... 3

**Figure 3.** Schematic presentation of the effect of pH and temperature on the micellization of poly(acrylic acid)-*block*-poly(N,N-diethylacrylamide) in aqueous solution[49]. Modified from Müller and co-workers, Macromolecular Rapid Communications (2005)..... 9

**Figure 4.** Schematic illustration of the reversible thermoresponsive PEO-*b*-P2VP – K<sub>2</sub>S<sub>2</sub>O<sub>8</sub> micelles in water [52]. Modified from Jia et al./ Chem./ Commun. (2006).. 11

**Figure 5.** Schematic representation of LbL self-assembly process, the chemical structures of PAH and PSS and PAH/PSS multilayers. .... 13

**Figure 6.** Schematic representation of hydrogen bonding interactions among PEG and PMA, PVPON and PMA and PNIPAM and PMA [72]. Modified from Such et al. Chem. Soc. Rev. (2011). .... 14

**Figure 7.** Change in hydrodynamic size of P2VP-*b*-PEO with increasing pH..... 27

**Figure 8.** Schematic representation of the reaction mechanism of the quaternization reaction of P2VP-*b*-PEO using MeI..... 29

**Figure 9.** 1H-NMR spectra of P2VP-*b*-PEO before and after quaternization reaction. .... 30

**Figure 10.** ATR-FTIR spectra before and after quaternization of P2VP-*b*-PEO. .... 32

**Figure 11.** The change in hydrodynamic size of P2VP-*b*-PEO and QP2VP-*b*-PEO in aqueous solution as a function of pH. .... 33

<b>Figure 12.</b> Zeta potential versus pH of P2VP- <i>b</i> -PEO and QP2VP- <i>b</i> -PEO. ....	34
<b>Figure 13.</b> Hydrodynamic size of QP2VP- <i>b</i> -PEO as a function of the concentration of $K_3Fe(CN)_6$ (A), size distribution by number at $3.25 \times 10^{-4} M$ $K_3Fe(CN)_6$ (B) and evolution of hydrodynamic size of QP2VP- <i>b</i> -PEO with time (C) at 25 °C and pH 7.5. ....	37
<b>Figure 14.</b> Hydrodynamic size of QP2VP- <i>b</i> -PEO as a function of concentration of $K_3Fe(CN)_6$ at 37.5 °C and pH 7.5. ....	39
<b>Figure 15.</b> The size distribution by number of QP2VP- <i>b</i> -PEO in the presence of $2.45 \times 10^{-4} M$ $K_3Fe(CN)_6$ at 25 °C (Panel A) and 37.5 °C (Panel B). ....	40
<b>Figure 16.</b> Evolution of hydrodynamic size of $(QP2VP+[Fe(CN)_6]^{3-})-b$ -PEO micelles with increasing temperature (Panel A); the size distribution by number of $(QP2VP+[Fe(CN)_6]^{3-})-b$ -PEO micelles at 25 °C and 45 °C (Panel B). ....	41
<b>Figure 17.</b> Evolution of hydrodynamic size of $(QP2VP+[Fe(CN)_6]^{3-})-b$ -PEO micelles prepared in the presence of $4.05 \times 10^{-4} M$ or $4.83 \times 10^{-4} M$ $K_3Fe(CN)_6$ . ....	42
<b>Figure 18.</b> Size distribution of $(QP2VP+[Fe(CN)_6]^{3-})-b$ -PEO micelles prepared in the presence of $2.45 \times 10^{-4} M$ $K_3Fe(CN)_6$ at 37.5 °C by number at 37.5°C and 42.5 °C (Panel A); size distribution of $(QP2VP+[Fe(CN)_6]^{3-})-b$ -PEO micelles prepared in the presence of $3.25 \times 10^{-4} M$ $K_3Fe(CN)_6$ at 37.5 °C by number at 37.5 °C and 42.5 °C (Panel B). ....	44
<b>Figure 19.</b> Ellipsometric thickness of multi-layer films of $(QP2VP+[Fe(CN)_6]^{3-})-b$ -PEO micelles deposited at pH 7.5 and 25 °C (Panel A) or 37.5 °C (Panel B). ....	49
<b>Figure 20.</b> AFM topography images of a monolayer of $(QP2VP+[Fe(CN)_6]^{3-})-b$ -PEO micelles before and after exposure to 45 °C (Panel A) in PBS solution at pH 7.5 as 2D and 3D; ellipsometric thicknesses (black bars) and rms roughness (red bars) of a monolayer film before after exposure to 45 °C in PBS solution(Panel B). ....	52
<b>Figure 21.</b> Evolution of thickness of 20-layer films of $(QP2VP+[Fe(CN)_6]^{3-})-b$ -PEO micelles and TA at 25°C and 45°C. ....	53
<b>Figure 22.</b> UV-Vis spectra of the $(QP2VP+[Fe(CN)_6]^{3-})-b$ -PEO micelles/TA films at 25°C (Panel A). 37.5°C (Panel B) and 45°C (Panel C). ....	55

<b>Figure 23.</b> Evolution of thickness of 20-layer films of (QP2VP+[Fe(CN) <sub>6</sub> ] <sup>3-</sup> )- <i>b</i> -PEO micelles and TA at 37.5 °C and 42.5 °C. ....	57
<b>Figure 24.</b> UV-Vis spectra of the (QP2VP+[Fe(CN) <sub>6</sub> ] <sup>3-</sup> )- <i>b</i> -PEO micelles/TA films at 37.5°C (Panel A) and 42.5°C (Panel B). ....	58
<b>Figure 25.</b> Fluorescence spectra of the release solutions of the (QP2VP+[Fe(CN) <sub>6</sub> ] <sup>3-</sup> )- <i>b</i> -PEO micelles/TA films which were constructed 25°C and exposed to 45°C (Panel A) and (QP2VP+[Fe(CN) <sub>6</sub> ] <sup>3-</sup> )- <i>b</i> -PEO micelles/TA films which were constructed at 37.5°C and exposed to 42.5°C (Panel B). ....	60
<b>Figure A. 1</b> UV-Vis spectra of QP2VP- <i>b</i> -PEO. ....	73
<b>Figure A. 2.</b> UV-Vis spectra of TA. ....	73
<b>Figure A. 3.</b> UV-Vis spectra of K <sub>3</sub> Fe(CN) <sub>6</sub> . ....	74
<b>Figure A. 4.</b> UV-Visible spectra of multilayers of P2VP- <i>b</i> -PEO micelles/TA at 45°C. ....	74
<b>Figure A. 5.</b> Fluorescence spectra of QP2VP- <i>b</i> -PEO. ....	75
<b>Figure A. 6.</b> Fluorescence spectra of TA , ext λ=260nm. ....	75
<b>Figure A. 7.</b> Fluorescence spectra of K <sub>3</sub> Fe(CN) <sub>6</sub> , ext λ=260nm. ....	76

## LIST OF TABLES

### TABLES

<b>Table 1.</b> Chemical Structures of Polymers and Chemicals .....	22
---	----

## LIST OF SCHEMES

### SCHEMES

**Scheme 1.** Schematic representation of  $K_3Fe(CN)_6$  induced micellization of QP2VP-*b*-PEO at pH 7.5 ..... 35

**Scheme 2.** Schematic representation of the hydrogen bonding interactions among TA and  $(QP2VP+[Fe(CN)_6]^{3-})$ -*b*-PEO micelles (Panel A). Schematic representation of LbL process and multilayers of  $(QP2VP+[Fe(CN)_6]^{3-})$ -*b*-PEO micelles and TA..... 47

## LIST OF ABBREVIATIONS

<b>C-UCST</b>	Coulomb Interaction UCST
<b>DEGMA</b>	Diethylene Glycol Methacrylate
<b>EGMA</b>	Ethylene Glycol Methyl Ether Methacrylate
<b>HB-UCST</b>	Hydrogen Bonding Interaction UCST
<b>LCST</b>	Lower Critical Solution Temperature
<b>P (AAm-<i>co</i>-AN)</b>	Poly (acrylamide- <i>co</i> -acrylonitrile)
<b>PAspAm</b>	Poly (N-acryl asparagin amide)
<b>PBS</b>	Phosphate Buffer Saline
<b>PDEAAM</b>	Poly (N, N)-diethylacrylamide
<b>PDMAEMA</b>	Poly (N, N) - dimethylaminoethyl methacrylate)
<b>PMAm</b>	Poly (methacrylamide)
<b>PNIPAM</b>	Poly (N-isopropylacrylamide)
<b>PVCL</b>	Poly (N-vinylcaprolactam)
<b>UCST</b>	Upper Critical Solution Temperature
<b>PIC</b>	Poly Ion Complex
<b>(PiPrOx-P(Lys))</b>	Poly (2-isopropyl-2-oxazoline)- <i>b</i> -poly (L-lysine)
<b>BCMs</b>	Block Copolymer Micelles
<b>P (AAm-<i>co</i>-AN)</b>	Poly (acrylamide- <i>co</i> -acrylonitrile)

<b>Macro-CTA</b>	Macromolecular Chain Transfer Agent
<b>PS</b>	Polystyrene
<b>PDMA</b>	Poly (dimethylacrylamide)
<b>PEO-<i>b</i>-P2VP</b>	Poly (ethylene oxide)- <i>b</i> -Poly (2-vinylpyridine)
<b>2, 6-NDS</b>	Sodium 2, 6-Naphthalenedisulfonate
<b>LbL</b>	Layer-by-layer
<b>PAA-<i>b</i>-PDEAAm</b>	Poly (acrylic acid)- <i>block</i> -Poly (N, N diethylacrylamide)
<b>PNIPAAm-<i>b</i>-PAA</b>	Poly(N-isopropylacrylamide)- <i>block</i> -Poly(acrylic acid)
<b>(PiPrOx-P (Asp))</b>	Poly (2-isopropyl-2-oxazoline)- <i>b</i> -Poly (aspartic acid)
<b>PNIPAAm-<i>b</i>-PMMA</b>	Poly (N-isopropylacrylamide)- <i>b</i> -methyl methacrylate)
<b>P2VP-<i>co</i>-PNIPAM</b>	Poly (2-vinylpyridine)- <i>co</i> -Poly (N-isopropylacrylamide)
<b>PAH</b>	Poly (sodium-4-styrene sulfonate)
<b>PSS</b>	Poly (sodium-4-styrene sulfonate)
<b>PEG</b>	Poly (ethylene glycol)
<b>PVPON</b>	Poly (N-vinyl pyrrolidone)
<b>PAA</b>	Poly (acrylic acid)
<b>PMAA</b>	Poly (methacrylic acid)
<b>DOX</b>	Doxorubicin
<b>TA</b>	Tannic Acid

<b>PDMA-<i>b</i>-PNIPAM</b>	Poly (2-(dimethylamino) ethyl methacrylate)- <i>b</i> -Poly-(N-isopropylacrylamide)
<b>PDMAEMA-<i>b</i>-PPO-<i>b</i>-PDMAEMA</b>	Poly (N, N-dimethylaminoethyl methacrylate)- <i>b</i> -Poly (propylene oxide)- <i>b</i> -Poly (N, Ndimethylaminoethyl methacrylate)
<b>PMEMA-<i>b</i>-PDPA</b>	Poly [2-(N-morpholino) ethyl methacrylate- <i>b</i> -2-(diisopropylamino) ethyl methacrylate]
<b>BPEI</b>	Branched Poly(ethylenimine)
<b>DMF</b>	N,N- Dimetylformamide
<b>MEI</b>	Methyl Iodide
<b>NMR</b>	Nuclear Magnetic Resonance
<b>DLS</b>	Dynamic Light Scattering
<b>AFM</b>	Atomic Force Microscopy
<b>FTIR-ATR</b>	Fourier Transform Infrared Spectroscopy by Attenuated Total Reflection



# CHAPTER 1

## INTRODUCTION

### 1.1. Stimuli responsive polymers

Polymers which alter their properties, e.g. conformation, hydrophilic/ hydrophobic nature, hydration state, swelling/collapsing and degradation behaviours, upon changing environmental conditions are called “stimuli responsive polymers” [1,2]. Stimuli responsive polymers are also called “smart polymers” or “environmentally sensitive polymers”. These environmental triggers are mainly pH, temperature, ionic strength, electric or magnetic field and biological stimuli [3]. The change in the properties of the polymer is generally reversible, in other words, the polymer returns to its initial state when the trigger is removed [4]. Stimuli responsive polymers find applications in many different areas e.g. switchable hydrophilic-hydrophobic surfaces [5–7], drug delivery [8–10] gene therapy [11,12], thermally switchable optical devices [13], chromatography [14] or bioseparation [15–17]. Among stimuli responsive polymers, temperature-responsive (thermo-responsive) polymers are one of the most extensively studied polymers due to relatively easy control of temperature than the other stimuli. Temperature can be used as both an internal and an external trigger in these systems. For example, the body temperature rises in a disease state making temperature an internal trigger, whereas temperature change can be induced externally in a specific part of the body, e.g. hyperthermia treatment.

### 1.2. Temperature-responsive (thermoreponsive) polymers

Temperature-responsive polymers are a group of polymers which alter their physical properties, e.g. solubility, with changing temperature. This feature makes these polymers advantageous for controlled release applications. The change in the solubility of the polymer with changing temperature simultaneously triggers the release of functional molecules from a polymer matrix. The unique property of

temperature-responsive polymers is that they go into a phase transition at a specific temperature, so called “critical solution temperature” [15]. Temperature-responsive polymers are classified in two groups: i) polymer solutions exhibiting lower critical solution temperature (LCST) and ii) polymer solutions exhibiting upper critical solution temperature (UCST). LCST is the temperature below which the polymer and solvent are miscible. The polymer solution phase separates above LCST [3]. In contrast, polymer solutions exhibiting UCST-type behavior and the solvent are miscible above UCST and the polymer solution phase separates below that critical temperature. Figure 1 shows typical phase diagrams of polymer solutions with LCST-type behavior (Panel A) and UCST-type behavior (Panel B). As shown in the figure, the transition from single-phase to two-phase region occurs upon heating in polymer solutions with LCST-type behavior. In contrast, the transition from single-phase to two-phase region is observed upon cooling in polymer solutions with UCST-type behavior [3].

Solubility of polymers in aqueous environment is driven by the hydrogen bonding interactions between the polymer and the water molecules, whereas the solubility of polymers in organic solvents is ensured by the van der Waals interactions between the polymer and solvent. LCST-type behavior is generally observed in aqueous polymer solutions, while UCST-type behavior is mostly observed in organic solvents. However, there are also polymers which exhibit UCST type behavior in aqueous solution [18].

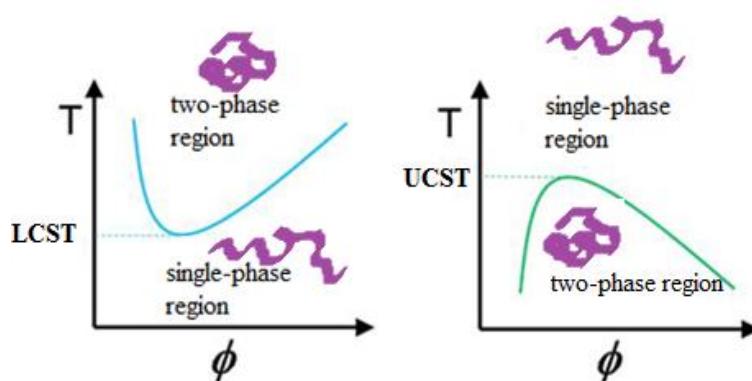


**Figure 1.** Phase diagrams (temperature vs. polymer volume fraction ( $\phi$ )) of polymers exhibiting (a) LCST-type behavior and (b) UCST-type behavior in solution [18]. Modified from Hruby et al. Eur.Polym (2015).

### 1.3. LCST-type phase behaviour of polymers in aqueous solution

Solubility of polymers in aqueous environment is ensured by the hydrogen bonding interactions among the polymer and water molecules below LCST. The polymer adopts extended random coil conformation in the solution below LCST. The solubility of the polymer chains in water decreases as the temperature increases due to disruption of the hydrogen bonds among the polymer chains and water molecules. When the temperature exceeds LCST, the polymer dehydrates resulting in enhanced polymer-polymer interactions. The polymer transforms from extended coil to phase separated globular conformation. The polymer chains then collapse and aggregate in solution [3,16]. Schematic representation of LCST-type phase behavior of a polymer in aqueous solution is shown in Figure 2 [19].

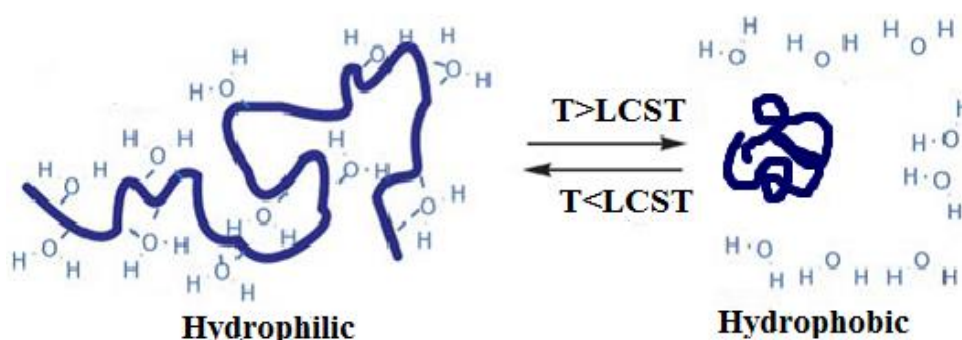


**Figure 2.** LCST type phase behavior of a polymer in aqueous solution.[17] . Modified from Alarco'n et al. Chem. Soc. Rev. 34 (2005).

Poly (N-isopropylacrylamide) (PNIPAM) is one of the most studied polymer which show LCST type behavior in aqueous solution. PNIPAM has a LCST of 32 °C in aqueous solution [20], which is close to body temperature. Therefore, PNIPAM has drawn great attention for use in biomedical applications. PNIPAM displays coil-globule transition when the temperature exceeds 32 °C and significant change in hydrophilicity is observed above the critical temperature [21]. This feature made PNIPAM a promising material for controlled drug delivery applications. Besides PNIPAM, [22–24] there are many other polymers exhibiting LCST-type phase behavior in aqueous solution. These include poly (N,N)-diethylacrylamide

(PDEAAM), poly (vinylmethyl) ether [25,26], poly (2-alkyl-2-oxazoline)s [27,28], poly[oligo(ethylene glycol)methacrylate] [29] and poly(N-vinylcaprolactam) (PVCL) [30].

#### **1.4. UCST-type phase behaviour of polymers in aqueous solution**

Water soluble polymers are preferred for biomedical applications because water is the safe to be used in applications concerning living systems. In addition, it is cheap, thus it is cost-effective to use water during manufacturing [31]. There are many polymers exhibiting LCST-type behavior in aqueous solution and those polymers can be safely used in biomedical applications [1]. In contrast, polymers with UCST-type behavior in solution have not been of interest for biomedical applications as much as the polymers with LCST type have been due to requirement of a water/ organic solvent mixture [32]. Therefore, studies concerning the polymers with UCST-type behavior in water in the absence of organic solvents are limited [33]. The effect of polymer concentration and the ionic strength of the media was another challenge to use polymers with UCST-type behavior in practical applications [34]. Moreover, the synthesis of polymers which show UCST-type behavior in solution is more difficult than the synthesis of polymers with LCST-type behavior. Therefore, the number of polymers with UCST-type behavior in solution is lower than the number of polymers with LCST-type behavior in the literature [35]. For this reason, UCST-type behavior is introduced to polymer solutions by either hydrogen-bonding or Coulomb interactions among polymer chains [36]. Polymers showing UCST in aqueous solution via Coulomb interactions (C-UCST) are also grouped in two different categories: i) zwitterionic polymers and ii) polyelectrolytes in the presence of multivalent counterions. Polymers exhibiting UCST in aqueous solution via hydrogen bonding interactions (HB-UCST) are more preferred for biomedical applications than zwitterionic (charged) polymers. As the electrolyte in the medium significantly affects the UCST of the medium, the use of C-UCST polymers at physiological conditions is limited [37].

## **1.4.1. Polymers showing UCST-type phase behaviour in aqueous solution via coulomb interactions (C-UCST)**

### **1.4.1.1. Zwitterionic polymers**

Polyzwitterions are polymers which have both positively and negatively charged groups on the same repeating unit. If the source of the cation is quaternized ammonium groups, then these polyzwitterions are called polybetains [38]. Polybetains show UCST-type behaviour in pure water or in aqueous solutions with low ionic strength [39,40]. Polybetains are categorized in three groups: i) polycarbobetains; ii) polysulfobetains and iii) polyphosphobetains [38]. Polybetains are insoluble in water below a critical solution temperature due to strong intra- and inter-polymer attractions among the oppositely charged units on the polymer chains, but they are soluble when temperature increases above it [41]. For polysulfobetains, it was found that addition of ions e.g. sodium chloride into an aqueous solution of polysulfobetain increases the solubility of the polysulfobetains due to screening of the zwitterionic units by the salt ions resulting in a decrease in the extent of intra- and inter-molecular interactions among the polymer chains. This enhances the solubility of the polymer and decreases the UCST values [31,34,42]. In addition to electrolyte concentration, UCST of polybetains is highly affected by the molar mass of the polymer. The UCST increases as the molar mass of the polymer increases. For example, Willcock et al. reported that for a cloud point of sulfobetaine block [2-(methacryloyloxy) ethyl] dimethyl-(3-sulfopropyl) ammonium hydroxide (PDMAPS) of diblock or triblock copolymers POEGMA-*b*-PDMAPS between 26 °C and 43°C, the molar mass should vary within a range of 258-448 kg/mol. The cloud point decreased as the molar mass decreased and no cloud point was detected for a polymer with a molar mass of 29 kg/mol [43].

UCST can also be controlled by introducing hydrophobic units to the polymer chain. Woodfield et al. synthesized hydrophobically modified sulfobetaine copolymers and found that UCST varies between 6 °C – 82 °C as the percent of hydrophobic units increase for a polymer with an average molar mass of ~ 30 kg/mol [41]. It is also possible to tune the UCST value by combining two of the factors mentioned above. Same group also demonstrated that benzyl-modified sulfobetaine copolymers showed reversible UCST transition in aqueous solutions containing NaCl. The hydrophobic

units increase the UCST, whereas addition of NaCl in the solution has an opposite effect. As a result, these two effects compensate each other and tunes the UCST value.

#### **1.4.1.2. Polyelectrolytes in presence of multivalent counterions**

UCST-type behaviour can be introduced to aqueous polyelectrolyte solutions in presence of multivalent counterions. The multivalent ions serve as a bridge between the polyelectrolyte chains and enhance the polymer-polymer interactions. These electrostatic interactions are destroyed with increasing temperature and this is how UCST-type phase behaviour is introduced to the polymer solution. For example, Plamper reported that poly (N, N- dimethylaminoethyl methacrylate) (PDMAEMA), which is known with its LCST-type behavior, also shows UCST-type behavior in the presence of hexacyanocobaltate  $[\text{Co}(\text{CN})_6]^{3-}$  counterions. It was shown that LCST-type behavior of PDMAEMA in aqueous environment was not affected by  $[\text{Co}(\text{CN})_6]^{3-}$  counterions. On the other hand, they found that UCST increased as the amount of trivalent counterions increased because of stronger electrostatic interactions between the polymer chains and the counterions. Besides these, they showed that UCST-type behavior of PDMAEMA in aqueous solution was pH-dependent. At high pH (pH > 9), UCST behavior of PDMAEMA disappeared due to unprotonation of the amino groups of PDMAEMA and only LCST-type phase behaviour could be detected. At pH lower than 9, UCST-type phase behavior was observed in the presence of  $[\text{Co}(\text{CN})_6]^{3-}$  counterions [44].

In another study, Hoogenboom et al. also demonstrated the UCST- and LCST- type behaviors of poly( N,N -dimethylaminoethyl methacrylate) PDMAEMA in aqueous environment in the presence of different counterions, i.e.  $[\text{Co}(\text{CN})_6]^{3-}$ ,  $[\text{Fe}(\text{CN})_6]^{3-}$  and  $[\text{Cr}(\text{CN})_6]^{3-}$ . It was found that when the pH was decreased from pH 8 to pH 5, UCST increased due to further protonation of amino groups of PDMAEMA and stronger electrostatic interactions among PDMAEMA and the counterions. In the same study, they also examined the effect of introducing either diethylene glycol methacrylate (DEGMA) or more hydrophobic ethylene glycol methyl ether methacrylate (EGMA) monomers into PDMAEMA via copolymerization on the LCST and UCST transitions. They found that UCST decreased for PDAEMA-*co*-DEGMA due to shielding effect of long diethylene glycol side chains of DEGMA towards the

interactions among PDAEMA and the multivalent counterions. Similar observations were recorded for PDAEMA-*co*-EGMA [45].

#### **1.4.2. Hydrogen-bonded Upper Critical Solution Temperature Polymers**

Some polymers which form intra- and inter-molecular hydrogen bonds among the chains may exhibit UCST-type phase behaviour in solution. For example, poly(methacrylamide) (PMAm) and poly(acrylamide-*co*-acrylonitrile) P(AAm-*co*-AN) belong to this type of polymers [46]. Both polymers cannot dissolve in water below the UCST, however both dissolve in water above UCST due to disruption of the hydrogen bonds between polymer chains with increasing temperature [33]. In the same study, Agarwal reported that UCST of PAAm could be adjusted between in a wide temperature range (6 °C to 60 °C) by adjusting the amount of acrylonitrile units in the P(AAm-*co*-AN) during the copolymerization [46].

It has also been reported that non-vinyl polymers bearing ureido groups could also exhibit UCST-type phase behaviour. Shimada and Maruyama et al. reported that poly(allylurea) copolymer derivatives exhibited UCST-type behavior in water at physiological conditions [47].

In another study, Glatzel et al. investigated UCST-type behavior of poly (N-acryl asparagin amide) (PAspAm) in PBS and showed that UCST of PAspAm depended highly on the degree of polymerization or concentration of the polymer. They reported that UCST increased as the degree of polymerization increased. They also found that UCST was affected by the concentration of the polymer only in dilute solutions [48].

#### **1.5. Temperature-Responsive Block Copolymer Micelles**

Block copolymer micelles (BCMs) are promising drug carriers with their high loading capacities due to their hydrophobic cores which can host drug molecules with low water-solubility. BCMs with stimuli-responsive core and/or coronae are of specific interest for drug delivery applications. In the next two subsections, BCMs with temperature responsive core/corona will be overviewed.

### 1.5.1. Block Copolymer Micelles Exhibiting LCST-Type Phase Behaviour in Aqueous Solution

BCMs with LCST-type phase behavior in aqueous solution are classified in 2 different classes: i) BCMs with cores exhibiting LCST-type phase behavior in aqueous solution; ii) BCMs with coronae exhibiting LCST-type phase behavior in aqueous solution. BCMs which have cores exhibiting LCST-type phase behavior in aqueous solution are formed above LCST of the core blocks and micellar cores are disassembled when the temperature is decreased below LCST. For example, Müller and co-workers demonstrated (Figure 3) formation of crew-cut micelles of poly (acrylic acid)-*block*-poly(N,N diethylacrylamide) (PAA-*b*-PDEAAM) with PDEAAM-cores and PAA-corona above 35 °C at alkaline conditions when the carboxylic acid groups on the PAA coronal blocks were ionized, assuring the water solubility of BCMs. When the temperature was decreased below 35 °C, PAA-*b*-PDEAAM micelles disintegrated. When the pH was decreased to pH 4 at T<35 °C, PAA-*b*-PDEAAM formed inverse micelles with PAA-cores and PDEAAM-coronae [49].

Similar study was performed by Schilli et al. using poly(N-isopropylacrylamide)-*block*-poly(acrylic acid), PNIPAAm-*b*-PAA. They demonstrated the effect of temperature, pH and solvent on the formation of micellar or larger aggregates [50].

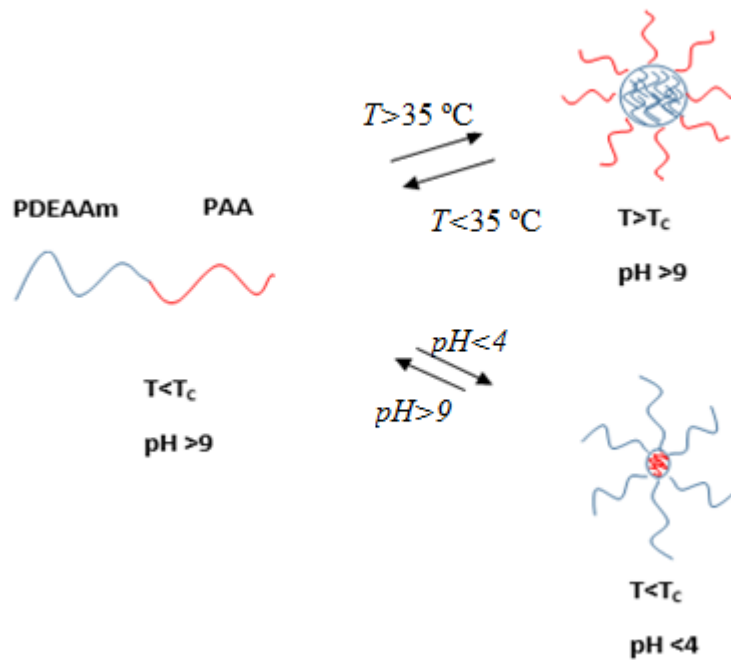


**Figure 3.** Schematic presentation of the effect of pH and temperature on the micellization of poly(acrylic acid)-*block*-poly(N,N-diethylacrylamide) in aqueous solution[49]. Modified from Müller and co-workers, *Macromolecular Rapid Communications* (2005).

BCMs which have coronae exhibiting LCST-type phase behavior in aqueous solution are formed below LCST of the coronal blocks because hydrophilic coronae of BCMs assure the solubility in aqueous environment. For example, Park et al. prepared thermosensitive polyion complex (PIC) micelles using poly(2-isopropyl-2-oxazoline)-*b*-poly(aspartic acid) (PiPrOx-P(Asp)) and poly(2-isopropyl-2-oxazoline)-*b*-poly(L-lysine) (PiPrOx-P(Lys)). The driving force for the formation of PIC micelles was the electrostatic interactions among the anionic P (Asp) and cationic P (Lys) blocks. The temperature-response was provided by the micellar shell composed of PiPrOx which shows LCST-type phase behavior in aqueous solution. The cloud point temperature of these micelles was found as 32 °C at physiological pH, which is important for using such PIC micelles as thermosensitive drug carrier systems [27]. Wei et al. prepared temperature-triggered block copolymer micelles using poly (N-isopropylacrylamide-

*b*-methyl methacrylate) (PNIPAAm-*b*-PMMA) and loaded anti-inflammation drug called as prednisone acetate on hydrophobic inner core. Below LCST of PNIPAAm (26 °C), BCMs was constituted hydrophilic character of PNIPAAm and hydrophobic property of PMMA. However, above LCST of PNIPAAm (40 °C), because of hydrophobicity of PNIPAAm, micelles disintegrated and drugs immersed in core of micelles diffused quickly[51].

### **1.5.2. Block Copolymer Micelles Exhibiting UCST-Type Phase Behaviour in Aqueous Solution**

Similar to BCMs with LCST-type phase behavior, BCMs with UCST-type phase behavior can also be classified in two groups: i) BCMs with cores exhibiting UCST-type phase behavior; ii) BCMs with coronae exhibiting UCST-type phase behavior. BCMs with cores exhibiting UCST-type behaviour in aqueous environment are formed below the UCST and disintegrate above the UCST. Although block copolymer micelles with cores exhibiting UCST-type behaviour in aqueous environment are more promising for biomedical applications than others having cores showing LCST-type behaviour, it is challenging to prepare block copolymer micelles with cores exhibiting UCST-type behaviour because the polymer-polymer interactions in the micellar cores cannot be destroyed and the micellar cores cannot be dissolved even above the boiling point of the solvent [52].

Examples of BCMs with UCST-type behavior were demonstrated by Zhang et al. by using), random copolymer of acrylamide and acrylonitrile P(AAm-*co*-AN) which shows hydrogen-bonded UCST-type phase behavior, as the macromolecular chain transfer agent (macro-CTA) to synthesize three different BCMs: i) P(AAm-*co*-AN)-*b*-PS, ii) P(AAm-*co*-AN)-*b*-PDMA and iii) P(AAm-*co*-AN)-*b*-PDMAEMA. BCMs of P(AAm-*co*-AN)-*b*-PS with PS-core and P(AAm-*b*-AN)-corona were formed when the temperature was higher than UCST of P(AAm-*b*-AN). BCMs of P(AAm-*co*-AN)-*b*-PDMA with P(AAm-*co*-AN)-core and PDMA-corona were prepared below UCST of P(AAm-*co*-AN). BCMs of P(AAm-*co*-AN)-*b*-PDMAEMA with P(AAm-*co*-AN)-core and PDMAEMA-corona were formed below UCST of P(AAm-*co*-AN). On the other hand, BCMs with PDMAEMA-core and P(AAm-*co*-AN)-corona were prepared at  $T > LCST$  of PDMAEMA [37].

Jia et al. introduced UCST-type phase behaviour to the P2VP-cores of poly (ethylene oxide)-*b*-poly (2-vinylpyridine) (PEO-*b*-P2VP) micelles using multivalent counterions (Figure 4). BCMs were produced using potassium persulfate ( $K_2S_2O_8$ ) at strongly acidic conditions when the P2VP block was highly protonated. The driving force for the micellar self-assembly was the electrostatic interactions among P2VP and  $S_2O_8^{2-}$ . UCST-type phase behaviour was observed between 40-70 °C and it was found that the critical temperature could be adjusted by changing the block length of P2VP block. For example, they found that  $PEO_{329}-b-P2VPH^+_{128}-S_2O_8^{2-}$  micelles disintegrated at 40 °C, while  $PEO_{134}-b-P2VPH^+_{251}-S_2O_8^{2-}$  micelles disintegrated at 70 °C [52].

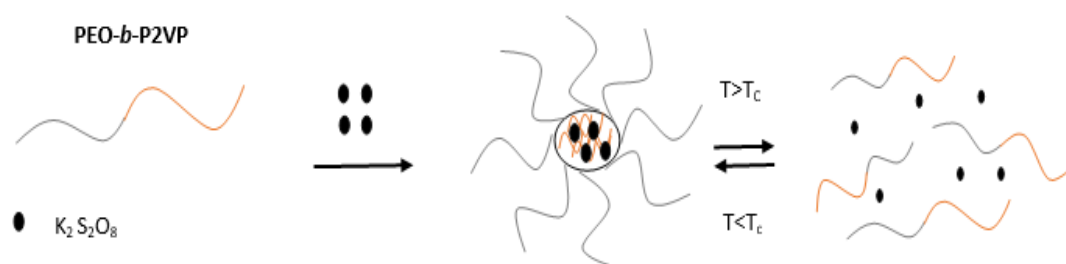


**Figure 4.** Schematic illustration of the reversible thermoresponsive PEO-*b*-P2VP –  $K_2S_2O_8$  micelles in water [52]. Modified from Jia et al./ Chem./ Commun. (2006).

Similarly, Shi and Zhu induced micellization of poly(ethylene oxide)-*b*-poly(4-vinylpyridine) (PEO-*b*-P4VP) using  $SO_4^{2-}$  counterions. BCMs of PEO-*b*-P4VP exhibited thermo-reversible behaviour [53].

In another study, Liu and Yin demonstrated the preparation of core-shell microgels with UCST-type phase behaviour in aqueous solution. They showed that anionic sodium 2,6-naphthalenedisulfonate (2,6-NDS) electrostatically interacts with the P2VP units of (poly(2-vinylpyridine)-*co*-poly(N-isopropylacrylamide) (P2VP-PNIPAM) at acidic conditions inducing formation of (P2VP+2,6 NDS)-*co*-PNIPAM microgels and those microgels exhibited UCST-type phase behaviour in aqueous environment within a temperature range of 20 °C -38 °C [54].

Yusa et al. took advantage of UCST-type phase behaviour of non-vinyl polymers bearing ureido groups to produce BCMs of poly(2-methacryloyloxyethyl phosphorylcholine-*b*-2-ureidoethyl methacrylate (PMPC-*b*-PUEM) with PMPC-corona and PUEM-core exhibiting UCST-type phase behaviour [33].

### **1.6. Layer-by-Layer Self-assembly Technique: Preparation of Ultra-thin Polymer Multilayers**

Layer-by-layer (LbL) self-assembly technique is a practical and an effective thin film preparation method. The LbL technique was first discovered by Iller in 1966. He showed that positively and negatively charged colloidal particles could be deposited alternately onto a substrate [55]. Decher et al. applied this technique to oppositely charged polyelectrolytes in 1997 and showed the first example of polyelectrolyte multilayer films [56]. LbL self-assembly process is based on alternating deposition of oppositely charged polyelectrolytes onto a surface. Each polyelectrolyte deposition step is followed by two rinsing steps to get rid of the loosely bound polymers at the surface. Figure 5 shows schematic representation of the i) LbL self-assembly process; ii) chemical structures of poly(allylamine hydrochloride) (PAH) and poly(sodium-4-styrene sulfonate) (PSS), commonly used polyelectrolytes in LbL assembly; and iii) multilayers of PAH and PSS [56].

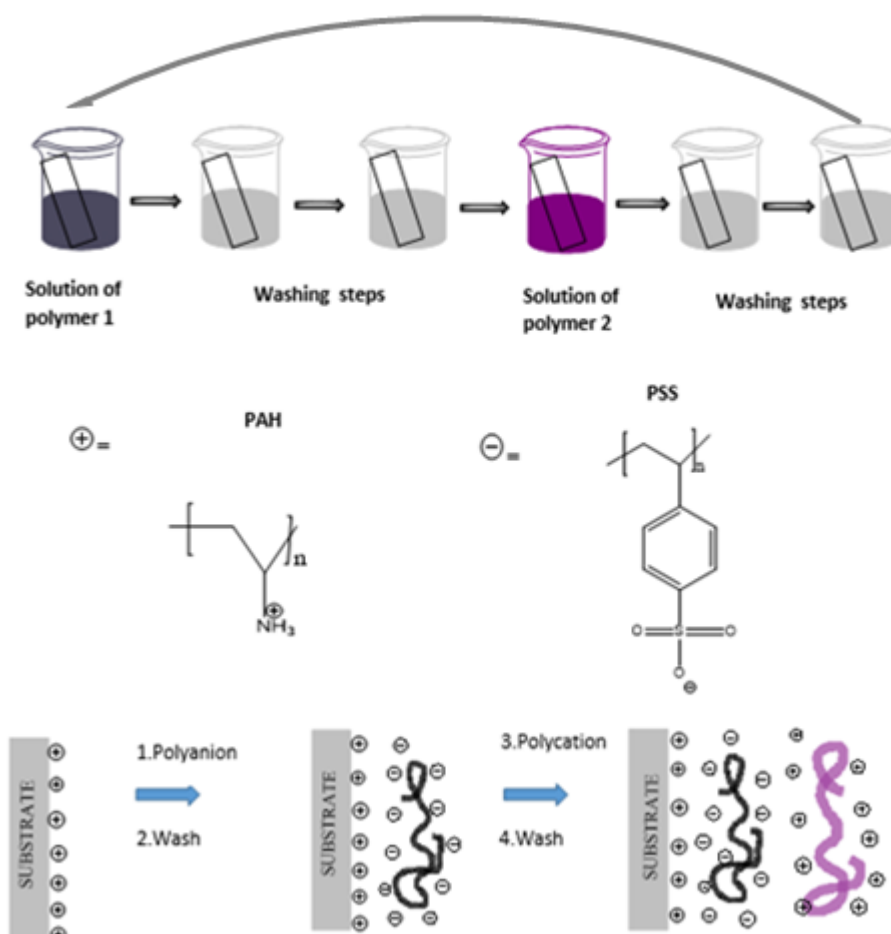


**Figure 5.** Schematic representation of LbL self-assembly process, the chemical structures of PAH and PSS and PAH/PSS multilayers.

As shown in Figure 5, LbL self-assembly process is an easy and economical way of fabricating ultra-thin films. It does not require sophisticated instrumentation. It also allows using aqueous polymer solutions. Therefore, it is suitable for preparation of multilayer films for biomedical applications [57]. There is no limitation in the size and shape of the substrate. Both planar and 3D substrates can be used as templates for LbL self-assembly. The thickness of LbL films can be controlled at the nanoscale by the number of layers deposited at the surface or by tuning the properties of the polymer deposition solutions [58]. For example, film thickness and morphology of multilayer films composed of weak polyelectrolytes can be adjusted by altering the salt concentration and pH of the polyelectrolyte solutions [59].

Besides electrostatically constructed LbL films [60], LbL deposition can also be driven via hydrogen bonding interactions [61], hydrophobic interactions [62], van der Waals forces [63], coordination bonding [64,65], charge-transfer [66], metal-ligand [67–69] and bio-specific [70,71] interactions. Among these, hydrogen-bonded multilayer films are specifically important for biomedical applications. This is because hydrogen-bonded multilayers allow using neutral polymers during self-assembly and neutral polymers are reported to be less toxic than the polycation counterparts [72]. In addition, hydrogen-bonded multilayers show pH-response at mild pH conditions [73]. Similar to the preparation of electrostatic multilayer films, hydrogen-bonded multilayers are constructed by alternating deposition of hydrogen accepting and hydrogen donating polymers at the surface. Poly (ethylene glycol) (PEG) with hydrogen accepting ether oxygens and poly (N-vinyl pyrrolidone) (PVPON) and poly (N-isopropyl acryl amide) (PNIPAM) with hydrogen accepting carbonyl groups are commonly used hydrogen accepting polymers in the construction of hydrogen-bonded multilayers. Polyacids such as poly (acrylic acid) (PAA) or poly (methacrylic acid) (PMAA) are commonly used hydrogen donating polymers in the fabrication of hydrogen-bonded LbL films. Figure 6 shows hydrogen bonding interactions among PEG and PMAA, PVPON and PMAA and PNIPAM and PMAA [72].

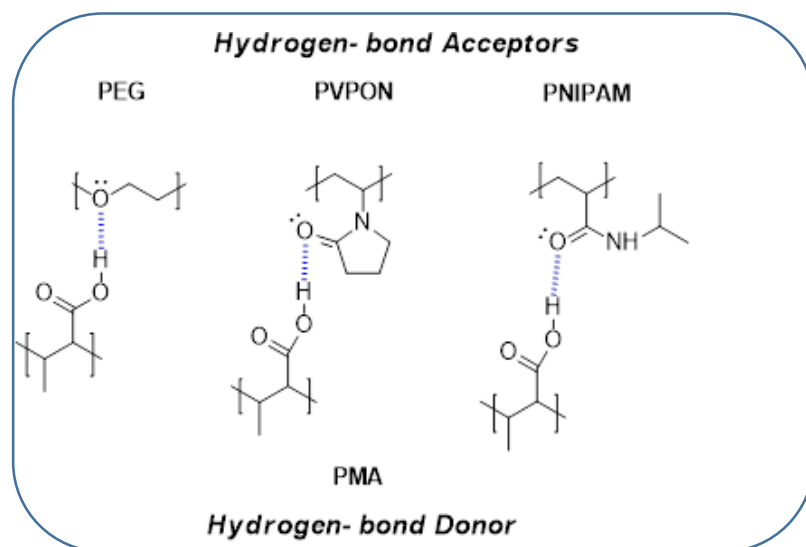


**Figure 6.** Schematic representation of hydrogen bonding interactions among PEG and PMAA, PVPON and PMAA and PNIPAM and PMAA [72]. Modified from Such et al. Chem. Soc. Rev. (2011).

In addition to relatively low toxicity of neutral polymers and pH-response at mild conditions, hydrogen-bonded self-assembly allows incorporation of polymers with low glass transition temperature, e.g. PEO within the multilayers [61]. Moreover, it is also possible to produce single or two-component surface-attached ultrathin hydrogels using hydrogen-bonded multilayer films [74]. Hydrogen-bonded multilayers are generally deposited at strongly acidic conditions when the hydrogen donating polyacid is in the protonated state. It is possible to erase the multilayers from the surface with increasing pH due to ionization of the polyacid and disruption of the hydrogen bonds between the layers [75]. This feature makes hydrogen-bonded multilayers promising ultra-thin materials for embedding functional molecules within the multilayers and then releasing them with a pH-trigger from the surface in a fast manner.

#### **1.6.1. Temperature Responsive LbL Films of Linear Homo- or Copolymers**

There are many studies reported on the temperature-responsive behavior of LbL films. Those films included temperature-responsive either homopolymers [76], copolymers [77], surface attached hydrogels [78] or block copolymer micelles with LCST-type phase behavior in aqueous environment [79]. In general, temperature-triggered release of functional molecules from the surface of LbL films is correlated with the temperature-induced conformational changes in the polymer chains, and the resulting morphological changes within the multilayers which triggers the release of drug molecules from the surface.

Multilayers containing PNIPAM constitutes the majority of temperature-responsive LbL films. This is because of the LCST of PNIPAM ( $\sim 32$  °C) [20] which is close to the body temperature, making PNIPAM containing LbL films promising polymer platforms for biomedical applications. For example, Lyon et al. prepared LbL films of positively charged PAH and negatively charged poly( N-isopropylacrylamide-*co*-acrylic acid) (P(NIPAm-*co*-AAc)) microgels due to the AAc groups existing in their networks. At pH lower than the  $pK_a$  of AAc units, microgels collapsed around the LCST of PNIPAm, 32 °C, due to enhanced polymer-polymer interactions leading to hydrogel deswelling. However, at pH higher than the  $pK_a$  of AAc units, microgels swelling was observed due to electrostatic repulsion of the charged AAc units in the microgel [80]. Same researchers also investigated the temperature-induced release of

insulin [81] and Doxorubicin (DOX) [82] from the multilayers of PAH and P(NIPAM-*co*-AAc) microgels.

Schlenoff and co-workers demonstrated construction of LbL films of oppositely charged PNIPAM copolymers, poly(allylamine hydrochloride)-*co*-poly(*N*-isopropylacrylamide), (PAH-*co*-PNIPAM) and poly(styrene sulfonate)-*co*-poly(*N*-isopropyl acrylamide) (PSS-*co*-PNIPAM) [83].

Johannsmann et al. [84] synthesized thermoresponsive surface-attached gels of PNIPAM. It was found that as the temperature varied around LCST of PNIPAM, the hydrophilic/hydrophobic properties of the gel, the thickness as well as the softness of the surface could be easily tuned [84].

### **1.6.2. Temperature Responsive LbL Films of Block Copolymer Micelles**

Multilayers of block copolymers which exhibit temperature-responsive behavior attracted great attention due to their potential use in drug delivery applications. The studies concerning LbL films containing temperature-responsive polymers can be categorized in two groups: i) LbL films containing block copolymer micelles with temperature-responsive cores and ii) LbL films containing block copolymer micelles with temperature-responsive corona.

An example to LbL films containing block copolymer micelles with temperature-responsive cores was reported by Sukhishvili and co-workers. Using poly (*N*-vinylpyrrolidone)-*b*-poly (*N*-isopropylacrylamide) (PVPON-*b*-PNIPAM), they formed micellar aggregates above 34 °C with PNIPAM-core and PVPON-corona. PVPON-*b*-PNIPAM micelles were then used as building blocks to construct LbL films with poly (methacrylic acid) (PMAA) at strongly acidic conditions. They investigated release of pyrene at temperatures below (20 °C) and above LCST (37 °C) of PNIPAM. They found that PNIPAM-cores could not disintegrate even below the LCST of PNIPAM due to constraint provided by PMAA layers for the conformational changes in the PNIPAM chains. However, despite the stability of block copolymer micelles, release of pyrene at 37 °C is much slower than at 20 °C from multilayers because of strong hydrophobic interaction between pyrene and PNIPAM core at a temperature higher than LCST of PNIPAM [79]. Using the same BCs, PVPON-*b*-PNIPAM

micelles, Sukhishvili and co-workers showed that DOX could be loaded into the PNIPAM-cores at 37 °C (above LCST of PNIPAM-core) and self-assembled at the surface using Tannic Acid (TA). DOX was released from the multilayers at 20 °C when the PNIPAM cores disintegrated [85].

Another study by Sukhishvili and co-workers demonstrated LbL films of block copolymer micelles of poly (2-(dimethylamino) ethyl methacrylate)-*b*-poly-(N-isopropylacrylamide) (PDMA-*b*-PNIPAM) with PNIPAM-core and cationic PDMA-corona with polystyrene sulfonate (PSS) as the polymer counterpart. It was shown that the multilayers were stable against pH variations and incorporating PDMA-*b*-PNIPAM micelles into LbL films prevented temperature-induced disintegration of the PNIPAM-cores. However, release of pyrene from the surface could be regulated by temperature. The rate of pyrene release at temperatures below the PNIPAM's LCST was higher than that at temperatures above LCST. This can be explained with the weaker hydrophobic-hydrophobic interactions among PNIPAM and pyrene below LCST resulting in greater amount of pyrene released from the surface. In contrast, PNIPAM is more hydrophobic above LCST and has stronger hydrophobic-hydrophobic interactions with pyrene, resulting in lower amount of pyrene released from the surface within the same time interval [86].

Electrostatic multilayer films of cationic poly (N,N-dimethylaminoethyl methacrylate)-*b*-poly(propyleneoxide)-*b*-poly(N,Ndimethylaminoethyl methacrylate) (PDMAEMA-PPO- PDMAEMA) with pH-responsive PDMAEMA and temperature-responsive PPO blocks were constructed using either anionic PAA or PSS by Tan et al. PDMAEMA-PPO-PDMAEMA was incorporated within the multilayers either in the form of unimers or micelles. They found that multilayers exhibited dual response, i.e. temperature- and pH-response. They also reported that the polyanion type and assembly conditions were critical on the temperature-response of the multilayers [87].

There are also studies concerning LbL films containing BCMS with temperature responsive corona. Erel et al.[88] prepared dually responsive hydrogen-bonded LbL films of dicationic poly [2-(N-morpholino) ethyl methacrylate-*b*-2-(diisopropylamino) ethyl methacrylate] (PMEMA-*b*-PDPA) and TA at pH 7.4. Release of pyrene from PDPA-cores, increased as the acidity of the solution was increased due to protonation of the amino groups of PDPA and disintegration of the micellar cores. In addition to

pH-response, PMEMA coronal chains of PMEMA-*b*-PDPA micelles exhibited LCST-type phase behaviour in aqueous solution with a critical temperature of 40 °C. The conformational changes in the PMEMA chains resulted in formation of void-like structures within the multilayers leading to greater amount of pyrene released from the multilayers. In another study of Erel, similar phenomenon was observed in the multilayers of BCMs with zwitterionic coronal chains exhibiting UCST-type phase behaviour in aqueous solution at temperatures below UCST [89].

## 1.7. Aim of Thesis

The aim of this thesis was to develop a fundamental study to prepare i) BCMs at physiological pH with cores exhibiting UCST-type behaviour in aqueous solution within a physiologically related temperature range and ii) LbL films which could be erased from the surface with increasing temperature.

Several research groups have worked on introducing UCST-type phase behaviour to polymer solutions [90,91]. These studies accomplished obtaining UCST-type phase behaviour in aqueous solution either at strongly acidic conditions or at temperatures far from the physiologically related temperature values. This study differs from those by introducing UCST-type behaviour to QP2VP-*b*-PEO at physiological pH. Moreover, critical temperatures varied near above the body temperature (42.5-45°C).

The work presented in this thesis is also the first example of hydrogen-bonded LbL films which could be erased from the surface with increasing temperature. There are many studies concerning pH-induced erosion of hydrogen-bonded multilayers from the surface. However, erasable multilayers via temperature increase have not been reported before.

This study constitutes fundamental knowledge on the structure-property relationship in hydrogen-bonded multilayer films and can serve as a model to develop advanced nanostructures for controlled release applications from surfaces.



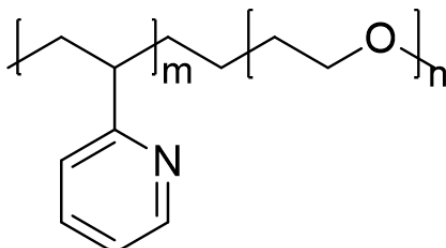
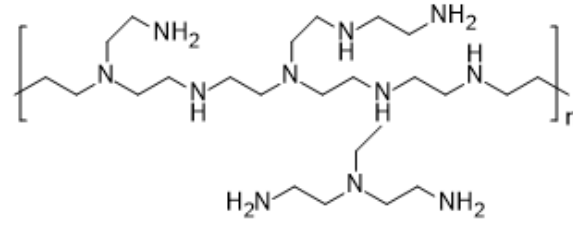
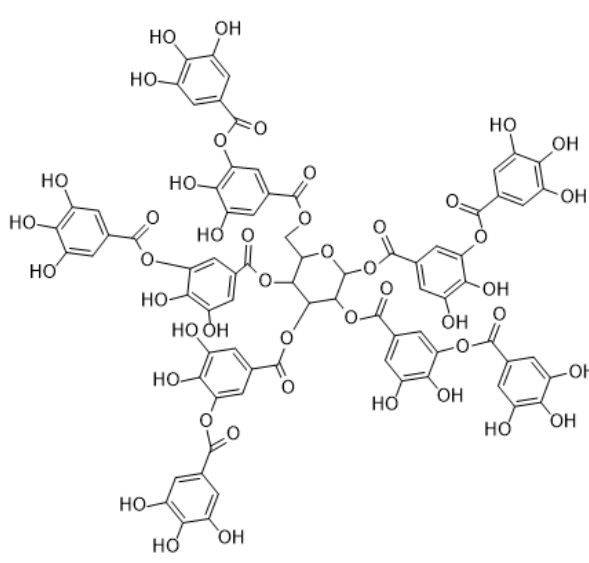
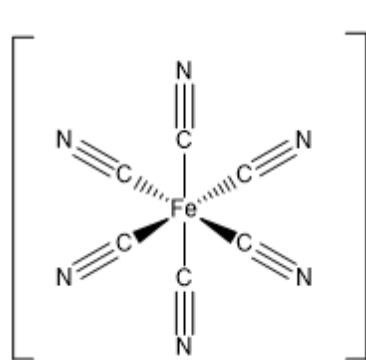
## CHAPTER 2

### EXPERIMENTAL PART

#### 2.1. Materials

Poly(2-vinylpyridine-*b*-ethylene oxide) (P2VP-*b*-PEO)  $M_n$ :P2VP (13500)-PEO(21000) was purchased from Polymer Source, Inc. Branched poly(ethylenimine) (BPEI;  $M_w$  25,000); phosphate buffer saline (PBS); sodium hydroxide, hydrochloric acid, N,N- Dimethylformamide (DMF) (>99%) were purchased from Sigma-Aldrich Chemical Co. Monobasic sodium phosphate, methyl iodide (MEI) (>99%) , Sulfuric acid (98%) and Tannic acid (TA;  $M_w$  1701.20); were purchased from Merck Chemicals.  $K_3Fe(CN)_6$  was purchased from Horasan Kimya. The deionized (DI)  $H_2O$  was purified by passage through a Milli-Q system (Millipore) at 18.2  $M\Omega$ . SpectroPor7 regenerated cellulose dialysis membrane, molecular weight cutoff: 3.5 kDa was used for dialysis.

**Table 1. Chemical Structures of Polymers and Chemicals**

<p><b>Poly (2-vinylpyridine-b-ethylene oxide)</b></p>  <p>The structure shows a copolymer chain with two repeating units. The first unit, labeled with subscript 'm', is a 2-vinylpyridine unit where the vinyl group is attached to the 2-position of a pyridine ring. The second unit, labeled with subscript 'n', is an ethylene oxide unit consisting of a two-carbon chain with an oxygen atom bridging them.</p>	<p><b>Branched Poly(ethyleneimine)</b></p>  <p>The structure shows a branched poly(ethyleneimine) chain. The main chain is enclosed in brackets with a subscript 'n'. It consists of repeating units of -[CH2-CH2-NH]-. A branched unit is attached to the main chain, consisting of a -CH2-CH2-NH- group connected to a nitrogen atom that is also bonded to two ethylamine groups (-CH2-CH2-NH2).</p>
<p><b>Tannic Acid</b></p>  <p>The structure of Tannic Acid is a complex polyphenolic compound. It features a central gallic acid unit (a benzene ring with three hydroxyl groups) that is esterified to a glucose molecule. This glucose molecule is further esterified to multiple gallic acid units, forming a large, branched, and highly hydroxylated structure.</p>	<p><b>Potassium Ferricyanide</b></p>  <p>The structure shows the ferricyanide complex ion, [Fe(CN)6]3-. The central iron atom (Fe) is coordinated to six cyanide ligands (C≡N) in an octahedral geometry. The complex is enclosed in large square brackets with a 3- charge indicated at the top right.</p>

## 2.2. Methods & Instrumentation

**Nuclear Magnetic Resonance (NMR):**  $^1\text{H}$ -NMR measurements were implemented at room temperature using Bruker Spectrospin Avance DPX-400 Ultra shield instrument operating at 400 MHz.

**Dynamic Light Scattering (DLS) and Zeta-potential Measurements:** Hydrodynamic size and zeta-potential measurements were carried out by using Zetasizer Nano-ZS equipment (Malvern Instruments Ltd., U.K.).

**Ellipsometry:** Dry film thickness measurements were performed using a spectroscopic ellipsometer of Optosense, USA (OPT-S6000).

**Atomic Force Microscopy (AFM):** AFM imaging of the films was performed using an NT-MDT Solver P47 AFM in tapping mode using Si cantilevers. Roughness values were taken from images with 5 x 5  $\mu\text{m}$  scan size.

**pH Meter:** Starter 3000 bench pH meter was utilized for adjusting pH of solutions. Calibration of pH meter was performed using three standard buffer solutions at pH 4, pH 7 and pH 10.

### **Fourier Transform Infrared Spectroscopy by Attenuated Total Reflection (FTIR-ATR):**

Nicolet iS10 FTIR-ATR was utilized to perform qualitative and quantitative analysis for P2VP-*b*-PEO and QP2VP-*b*-PEO.

**UV-VIS Spectrometer :** Varian Cary 100 UV-Visible Spectrometer was used.

## 2.3 Quaternization and characterization of P2VP block of PEO-*b*-P2VP

34 mg P2VP-*b*-PEO was dissolved in 9.6 mL DMF. After complete dissolution, 9.0  $\mu\text{L}$  MeI was added into the solution. The solution was stirred for 3 days at room temperature. It was protected from sunlight during stirring. The color of the solution turned from colorless to slightly yellow after 3 days. DMF and unreacted methyl iodide was removed using a rotary evaporator. In this way, the reaction solution was concentrated under reduced pressure. The product was then dissolved in water and dialyzed against deionized water for 3 days. At the end of this step, the product was

successfully transferred to aqueous phase. Finally, the solution was lyophilized and QP2VP-*b*-PEO was obtained.

### 2.3.1. <sup>1</sup>H-NMR

3.0 mg P2VP-*b*-PEO or QP2VP-*b*-PEO was dissolved in 600 μL deuterated chloroform, CDCl<sub>3</sub> for <sup>1</sup>H-NMR analysis.

### 2.3.2. ATR-FTIR

0.1 mg P2VP-*b*-PEO or QP2VP-*b*-PEO was used for ATR-FTIR analysis. ATR-FTIR technique was used to confirm the quaternization of the P2VP blocks as well as to determine the percent quaternization. The % quaternization was calculated as follows [90] the difference between the areas under the peaks centered at 1590 cm<sup>-1</sup> wavenumber of P2VP-*b*-PEO and QP2VP-*b*-PEO was summed up with the area under the peak centered at 1630 cm<sup>-1</sup> wavenumber of QP2VP-*b*-PEO (the sum is denoted as X). X was divided by the area under the peak centered at 1590 cm<sup>-1</sup> of P2VP-*b*-PEO (the ratio is denoted as Y) and this was multiplied by 100. The percent quaternization was calculated as ~ 60 %.

**X:** (Difference between area under the peak centered at 1590 cm<sup>-1</sup> of P2VP-*b*-PEO and 1590 cm<sup>-1</sup> of QP2VP-*b*-PEO) + (Area under the peak centered at 1630 cm<sup>-1</sup> of QP2VP-*b*-PEO)

**Y:** (Area under the peak centered at 1590 cm<sup>-1</sup> of P2VP-*b*-PEO)

**% Quaternization=(X/Y)x 100**

### 2.3.3. Dynamic Light Scattering (DLS) and ζ-potential measurements of P2VP-*b*-PEO and P2QVP-*b*-PEO in aqueous solution

Zetasizer Nano-ZS equipment (Malvern Instruments Ltd., U.K.) was used to measure the hydrodynamic size and ζ-potential of P2VP-*b*-PEO and QP2VP-*b*-PEO. 0.1mg/mL P2VP-*b*-PEO or QP2VP-*b*-PEO was prepared by dissolving 1 mg/mL P2VP-*b*-PEO or QP2VP-*b*-PEO in 0.01 M NaH<sub>2</sub>PO<sub>4</sub> buffer (H<sub>3</sub>PO<sub>4</sub>/ H<sub>2</sub>PO<sub>4</sub><sup>-</sup>) at pH 7.5 and diluting the solutions to a final concentration of 0.1 mg/mL. For hydrodynamic size and zeta-potential measurements performed as a function of pH, P2VP-*b*-PEO solution was

prepared at pH 3 and the pH of the solution was gradually increased to higher values. However, in case of QP2VP-*b*-PEO, 0.01 M NaH<sub>2</sub>PO<sub>4</sub> buffer solutions were prepared at varying pH which were then used to dissolve QP2VP-*b*-PEO solutions.

#### **2.4. Preparation of (QP2VP+ [Fe(CN)<sub>6</sub>]<sup>3-</sup>)-*b*-PEO micelles**

1 mg/mL poly (N-methyl-2-vinylpyridiniumiodide-*block*-ethyleneoxide) (QP2VP-*b*-PEO) was prepared in 0.01M NaH<sub>2</sub>PO<sub>4</sub> buffer at pH 7.5, and then diluted to final concentration of 0.1 mg/mL. Micellization was induced by adding various volumes of 0.0166 M K<sub>3</sub>Fe(CN)<sub>6</sub> into 0.1 mg/mL QP2VP-*b*-PEO at pH 7.5 at either 25°C or 37.5°C. (QP2VP+[Fe(CN)<sub>6</sub>]<sup>3-</sup>)-*b*-PEO micelles were obtained after gentle stirring for 60 minutes.

#### **2.5. Deposition of multilayers**

The silicon wafers/quartz slides were treated with concentrated sulfuric acid for 85 minutes and then thoroughly rinsed with DI water. The silicon wafers/quartz slides were then immersed into 0.25 M NaOH solution for 10 minutes, followed by thorough rinsing with DI water. To increase the adhesion of multilayer films onto the substrate, BPEI was deposited as a precursor layer onto the silicon wafers/quartz slides. The concentration of BPEI was 0.5 mg/mL (prepared in 0.01 M phosphate buffer) and the deposition was performed at pH 5.5.

The precursor layer was deposited in all the experiments except the monolayer film presented in Section 3.5.2.1. Multilayers were constructed by alternating deposition of (QP2VP+ [Fe(CN)<sub>6</sub>]<sup>3-</sup>)-*b*-PEO micelles and TA (0.1 mg/mL at pH 7.5) for 15 min each with two intermediate rinsing steps using 0.01 phosphate buffer at pH 7.5.

#### **2.6. Stability of multilayers in PBS**

Temperature-stability of multilayers were followed by ellipsometry or UV-Visible Spectroscopy. For ellipsometry, 20-layer films were prepared onto silicon wafers. For UV-Visible spectroscopy, 20-bilayer films were deposited on both sides of the quartz slides. Multilayers were exposed to PBS solutions (prepared dissolving 1 tablet into 200 mL deionized water yields 0.01 M phosphate buffer, 0.0027 M potassium chloride

and 0.137 M sodium chloride, pH 7.4 at 25 °C) at different temperatures for a determined period of time.

### **2.7. Deposition of the monolayer film for AFM imaging**

Monolayer film was prepared at pH 7.5 and 25 °C by exposing the silicon wafer into (QP2VP+ [Fe(CN)<sub>6</sub>]<sup>3-</sup>)-*b*-PEO micelle solution for 1 hour which was followed 2 rinsing steps using a phosphate buffer solution at pH 7.5. AFM imaging was performed on the dried monolayer film. The same film was then exposed to PBS solution at 45 °C for 1 hour. The film was dried prior to AFM imaging.

## CHAPTER 3

### RESULTS & DISCUSSION

#### 3.1. Aqueous Solution Behaviour of P2VP-*b*-PEO

P2VP-*b*-PEO is soluble in aqueous solution at acidic conditions. P2VP-*b*-PEO self-assembles into micellar aggregates above the  $pK_a$  of P2VP block ( $\sim 4.5$ [54]). This is because of the unprotonation of the pyridine units as the acidity decreased, resulting in enhanced hydrophobic interactions among the P2VP blocks, inducing the self-assembly of P2VP-*b*-PEO and the formation of BCMs [91]. Figure 7 shows the change in hydrodynamic size of P2VP-*b*-PEO with increasing pH. The sharp increase in hydrodynamic size above pH 4.5 was attributed to the formation of micellar aggregates.

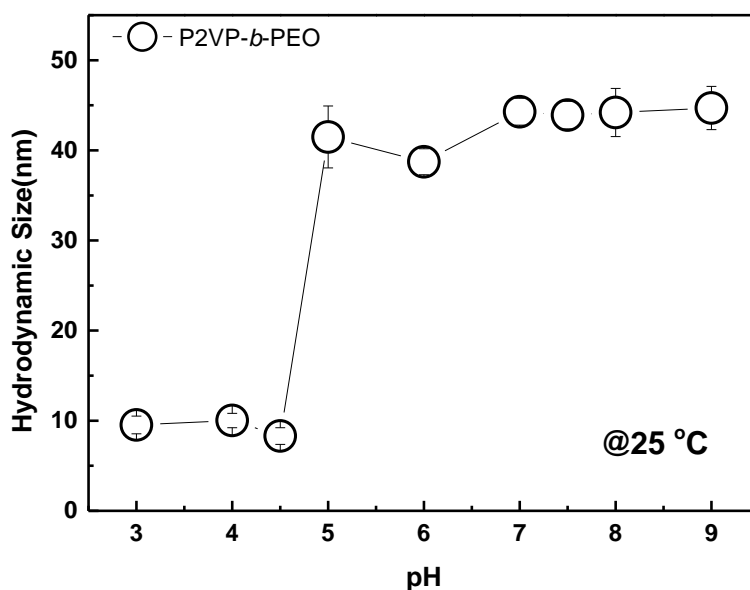


**Figure 7.** Change in hydrodynamic size of P2VP-*b*-PEO with increasing pH.

As seen in Figure 7, P2VP-*b*-PEO was in the micellar form at physiological pH (pH 7.5) with hydrophilic PEO-corona and pH-responsive P2VP-core structure. As

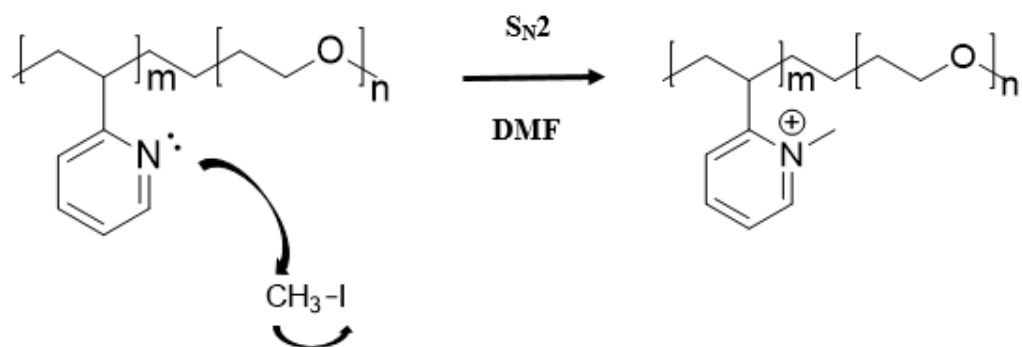
mentioned in Section 1.7, one of the aims of this study was to obtain BCMs with cores exhibiting UCST-type behaviour in aqueous solution within a physiologically related temperature range. Next section will explain a different route for the preparation of P2VP-*b*-PEO micelles so that P2VP micellar cores would show UCST-type phase behaviour.

### **3.2. Preparation of P2VP-*b*-PEO micelles with cores exhibiting UCST-type phase behaviour**

To obtain P2VP-*b*-PEO micelles with cores exhibiting UCST-type phase behavior, micellization was induced in the presence of multivalent salt ions via electrostatic interactions among the positively charged P2VP block and multivalent salt anions. In this way, electrostatic interactions would disrupt as the temperature was increased leading to an UCST-type behaviour in the micellar cores. However, such BCMs could only be obtained at acidic conditions when P2VP was positively charged. Increasing pH to physiological conditions would result in loss of electrostatic interactions among P2VP and multivalent salt anions resulting in disintegration of the BCMs. To obtain BCMs which were stable at physiological pH but disintegrate with increasing temperature, P2VP block of P2VP-*b*-PEO should bear positive charge at pH 7.5. To achieve this goal, P2VP block of P2VP-*b*-PEO was quaternized using methyl iodide. Next section presents the details of quaternization reaction of P2VP-*b*-PEO.

#### **3.2.1. Quaternization of P2VP-*b*-PEO**

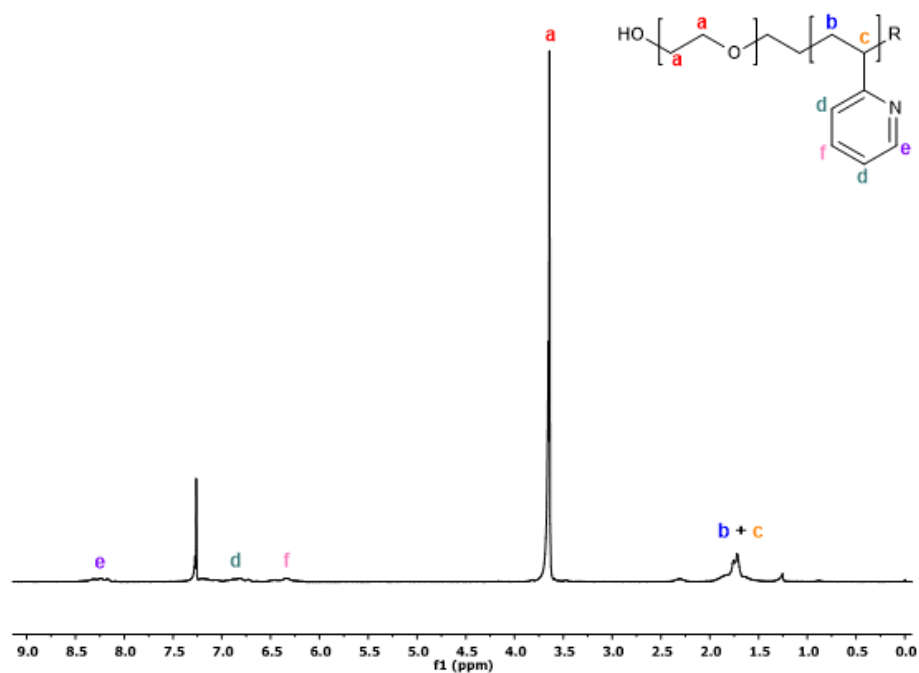
Quaternization (N-alkylation) of P2VP-*b*-PEO with methyl iodide follows an S<sub>N</sub>2-type reaction mechanism. As seen in Figure 8, nitrogen atom of the pyridine unit of P2VP with a lone-pair electron acts as a nucleophile. MeI, being a good electrophile, is open to nucleophilic attacks and the nucleophilic addition reaction occurs resulting in iodide cleavage.



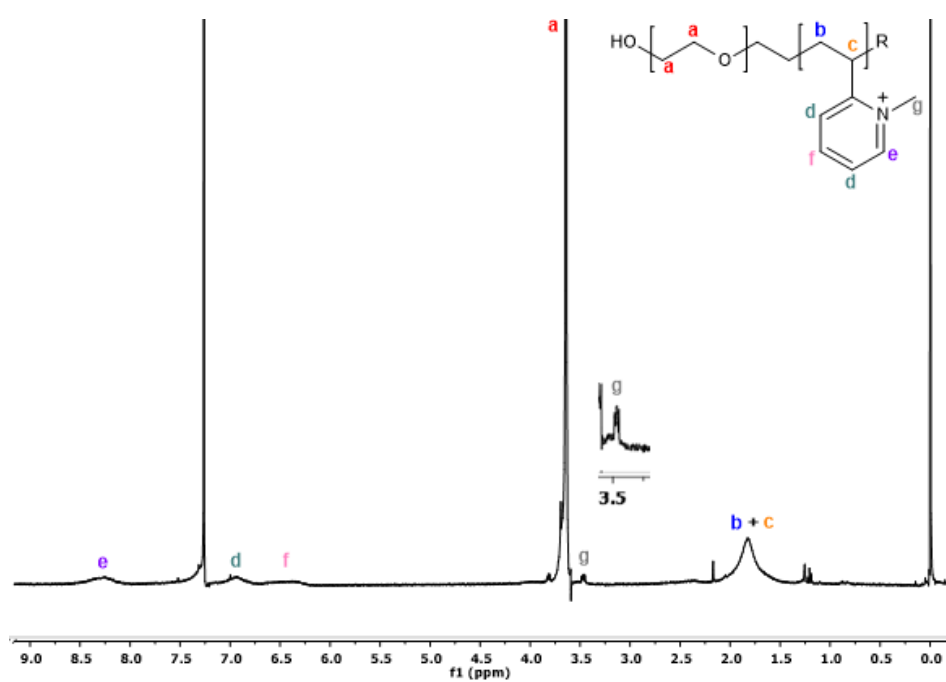
**Figure 8.** Schematic representation of the reaction mechanism of the quaternization reaction of P2VP-*b*-PEO using MeI.

Figure 9 shows the  $^1\text{H-NMR}$  spectra of P2VP-*b*-PEO before and after the quaternization reaction. Quaternization of P2VP-*b*-PEO was confirmed by the methyl protons of the pyridinium units at 3.5 ppm. Ethylene protons of PEO block were detected at 3.6 ppm with a strong singlet. Aromatic protons of P2VP located adjacent to nitrogen are represented by the broad peak at 8.3 ppm, whereas other aromatic protons were detected between 6.3-7.3 ppm. Aliphatic protons of P2VP block overlapped in the range of 1.8-2.2 ppm [90].

### P2VP-*b*-PEO-( Before Quaternization)



### QP2VP-*b*-PEO-(After Quaternization)

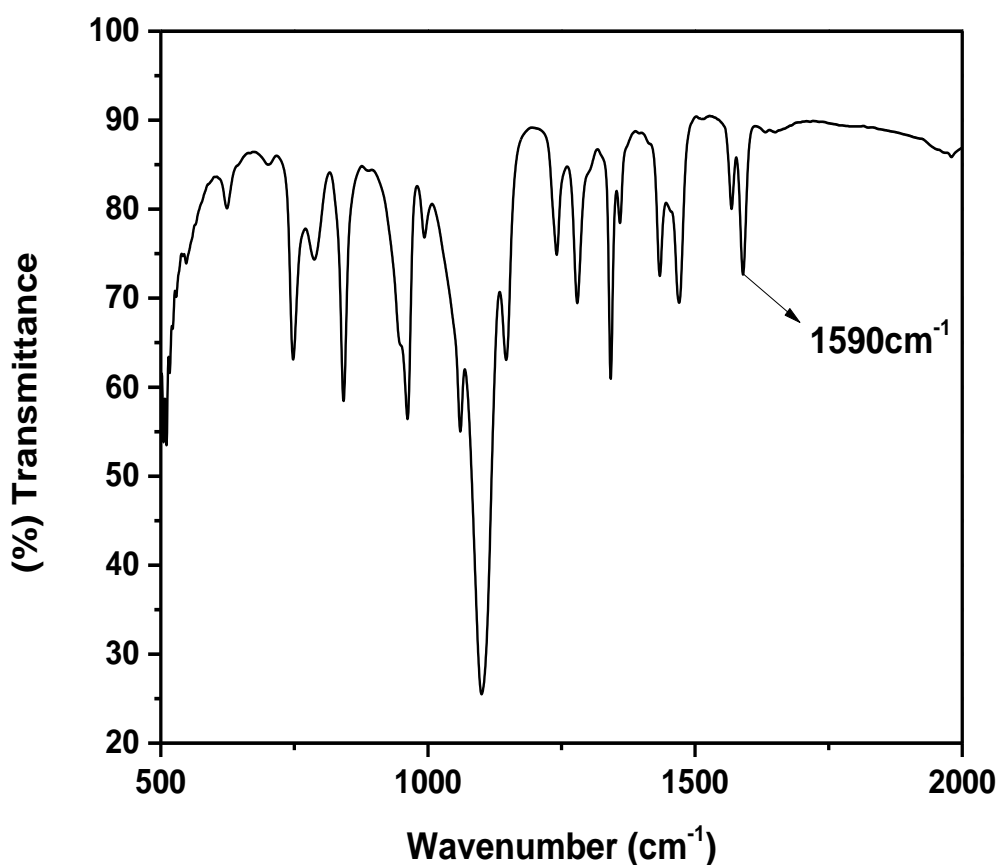


**Figure 9.1**  $^1\text{H-NMR}$  spectra of P2VP-*b*-PEO before and after quaternization reaction.

Quaternization of P2VP-*b*-PEO was further characterized by ATR-FTIR. The spectra of P2VP-*b*-PEO and QP2VP-*b*-PEO are presented in Figure 10.

The peak at 1590 cm<sup>-1</sup> correlates with the absorption band of P2VP (C=C stretching vibration of pyridine ring). The intensity of this peak decreases or the peak even disappears as the percent degree of quaternization increases. The peak at 1630 cm<sup>-1</sup> is correlated with the N-methylation of the pyridine ring and this peak is not observed in the spectrum of a non-quaternized polymer. Thus, the presence of the peak at 1630 cm<sup>-1</sup> confirms the successful quaternization of the pyridine units of P2VP[92]. The degree of quaternization was estimated as ~ 60%.

### P2VP-*b*-PEO-Before Quaternization



### QP2VP-*b*-PEO-After Quaternization

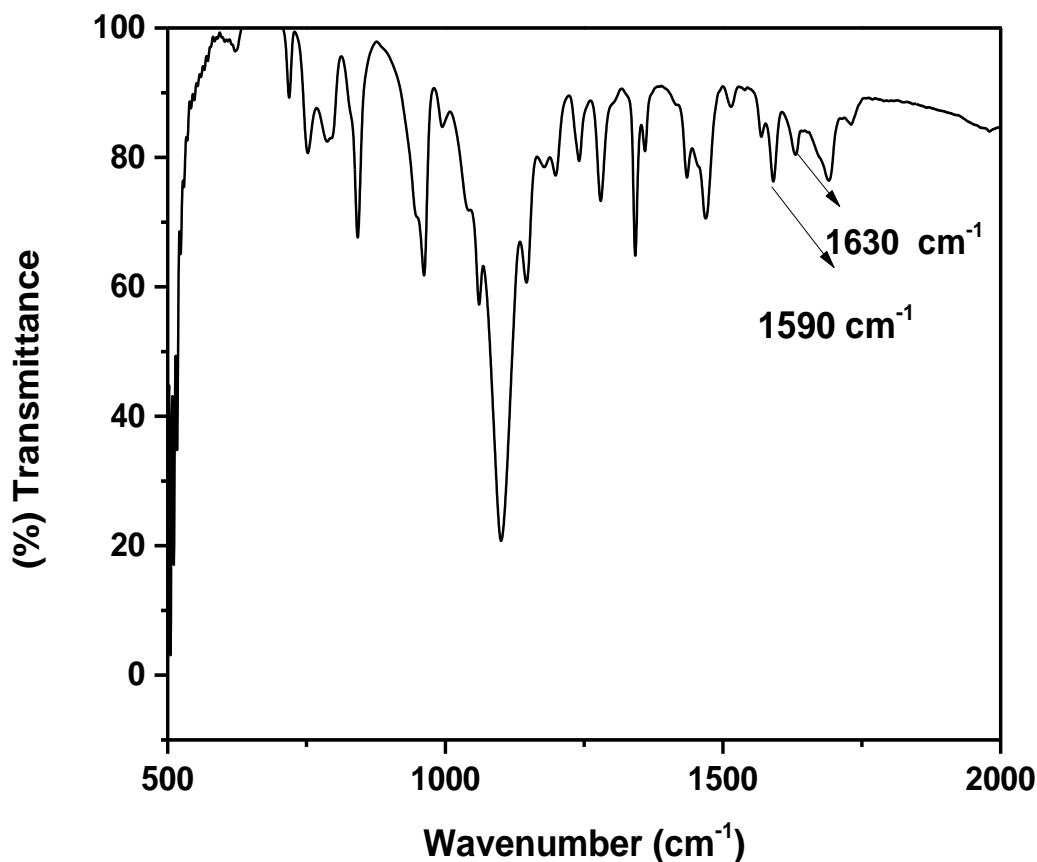


**Figure 10.** ATR-FTIR spectra before and after quaternization of P2VP-*b*-PEO.

Aqueous solution properties of QP2VP-*b*-PEO was studied using dynamic light scattering technique. The hydrodynamic size of QP2VP-*b*-PEO was followed as a function of pH (Figure 11). The data for the non-quaternized polymer, which was previously presented in Figure 7, is plotted for comparison. In contrast to P2VP-*b*-PEO, which showed a sharp increase in hydrodynamic size above the  $pK_a$  of P2VP units, no significant increase in hydrodynamic size of QP2VP-*b*-PEO was detected above the  $pK_a$  of the P2VP. QP2VP-*b*-PEO existed as unimers with a size of approximately ~10 nm within a wide pH range. The difference in the aqueous solution behaviour of P2VP-*b*-PEO and QP2VP-*b*-PEO can be explained by the quaternized pyridine units which rendered QP2VP water soluble within a wide pH range and

prevented the pH-induced micellization at physiological pH. Of note, the electrostatic repulsion among the QP2VP blocks is another reason why micellization did not occur in case of QP2VP-*b*-PEO.

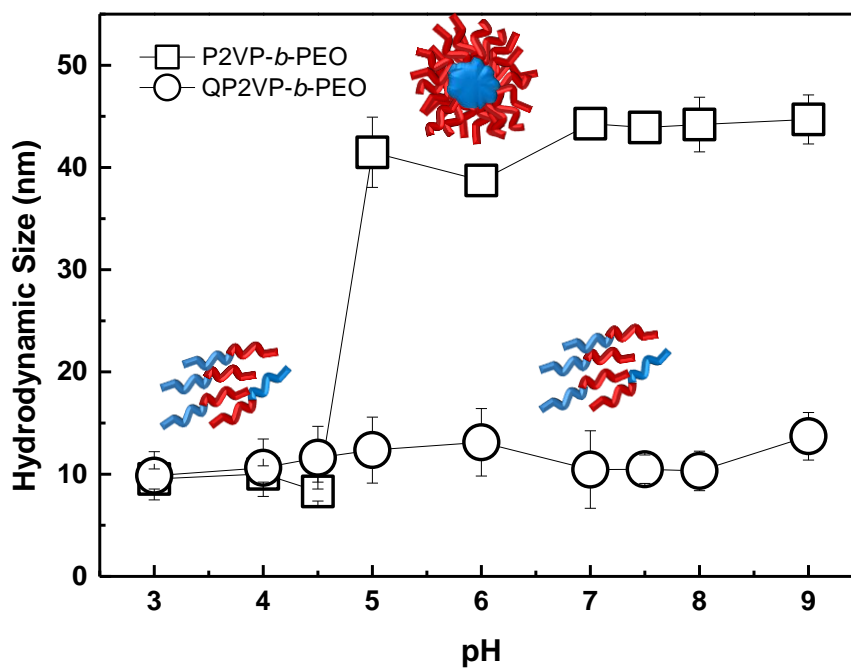


**Figure 11.** The change in hydrodynamic size of P2VP-*b*-PEO and QP2VP-*b*-PEO in aqueous solution as a function of pH.

Zeta-potential of QP2VP-*b*-PEO was also followed as a function of pH and zeta potential values of P2VP-*b*-PEO are plotted in the same graph for comparison (Figure 12). At strongly acidic conditions, when the polymers existed as unimers, both polymers has positive zeta potential, associated with the protonated pyridine units of P2VP. The zeta potential of QP2VP-*b*-PEO was slightly higher at pH 3 probably due to greater number of positively charged units as a result of the quaternization reaction. Zeta potential values decreased for both of the polymers as the acidity of the solution decreased. QP2VP-*b*-PEO carried slightly positive zeta potential between pH 5-9. Of note, QP2VP constitutes ~ 21 mol percent of the block copolymer and ~ 60% of the units were found to be quaternized. Thus, it is reasonable to have slightly positive zeta potential for QP2VP-*b*-PEO. P2VP-*b*-PEO showed a similar trend in evolution of zeta

potential values with increasing pH. However, P2VP-*b*-PEO carried slightly negative zeta-potential above pH 5. The self-assembly of P2VP-*b*-PEO starts above pH 4.5 and P2VP-*b*-PEO micelles were expected to be neutral above the critical pH. The negative zeta potential could arise from the salt ions which might have adsorbed on the coronal PEO chains, making P2VP-*b*-PEO micelles slightly negatively charged. Importantly, as discussed above, different from P2VP-*b*-PEO micelles, QP2VP-*b*-PEO was slightly positively charged within the same pH region. The positive zeta potential arising from the pyridinium units could compensate the negative zeta potential arising from the adsorbed salt ions on the coronal chains, resulting in positive zeta potential values.

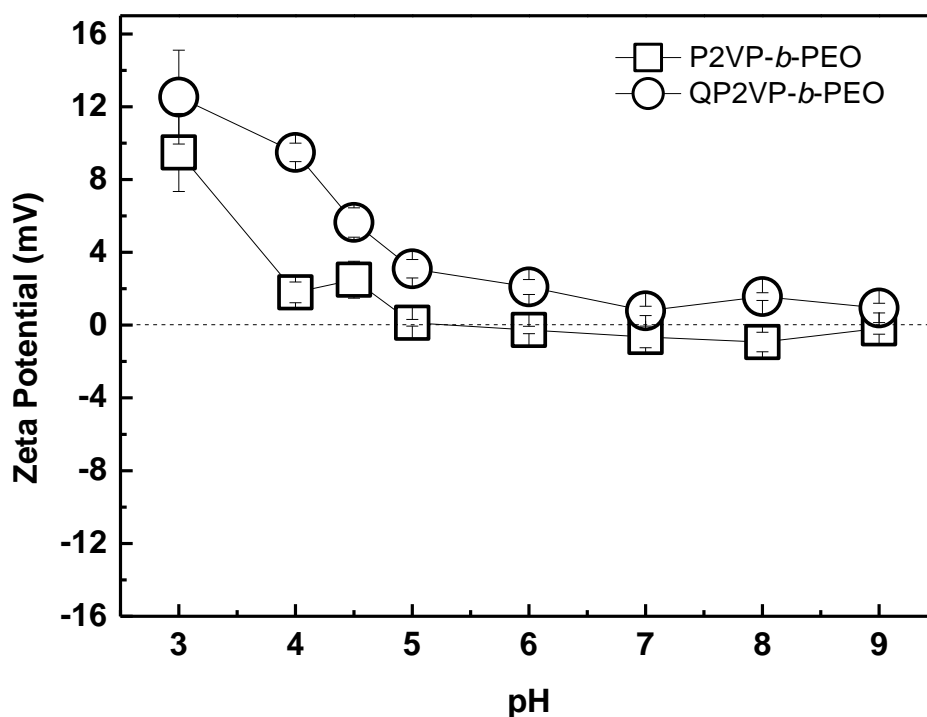
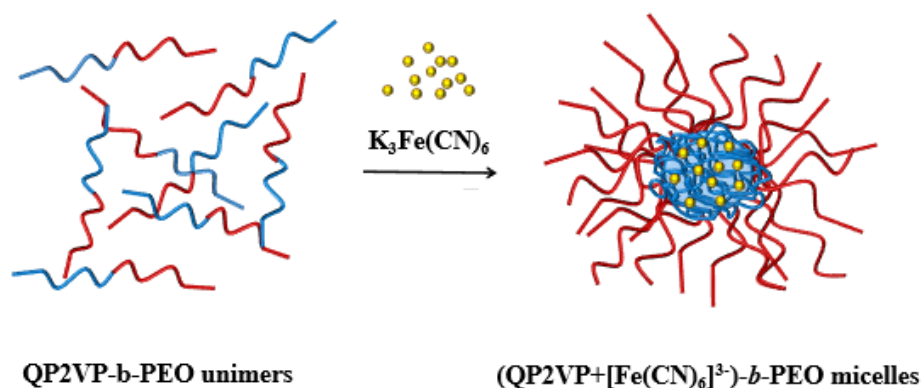


**Figure 12.** Zeta potential versus pH of P2VP-*b*-PEO and QP2VP-*b*-PEO.

### 3.3. Multivalent salt-induced Micellization of QP2VP-*b*-PEO

As discussed in Section 3.1, QP2VP-*b*-PEO existed as unimers at pH 7.5. Micellization was induced by addition of a multivalent salt,  $\text{K}_3\text{Fe}(\text{CN})_6$  into aqueous solution of QP2VP-*b*-PEO at pH 7.5. The driving force for the self-assembly of QP2VP-*b*-PEO was the electrostatic interactions among the positively charged pyridinium units of QP2VP and  $[\text{Fe}(\text{CN})_6]^{3-}$  anions resulting in formation of micellar aggregates with (QP2VP+ $[\text{Fe}(\text{CN})_6]^{3-}$ )-core and PEO-corona structures. The solubility of (QP2VP+ $[\text{Fe}(\text{CN})_6]^{3-}$ )-*b*-PEO micelles in aqueous solution was assured by the hydrophilic PEO corona. Scheme 1 represents the  $\text{K}_3\text{Fe}(\text{CN})_6$ -induced micellization of QP2VP-*b*-PEO at pH 7.5. It is important to note that using a multivalent salt was crucial to induce the micellization. Each  $[\text{Fe}(\text{CN})_6]^{3-}$  anion could associate with more than one QP2VP-*b*-PEO chain and could trigger the self-assembly process among the QP2VP-*b*-PEO chains.  $[\text{Fe}(\text{CN})_6]^{3-}$  was preferred as a trivalent counterion because of its low toxicity when compared to other trivalent counterions such as  $[\text{Co}(\text{CN})_6]^{3-}$  [45].

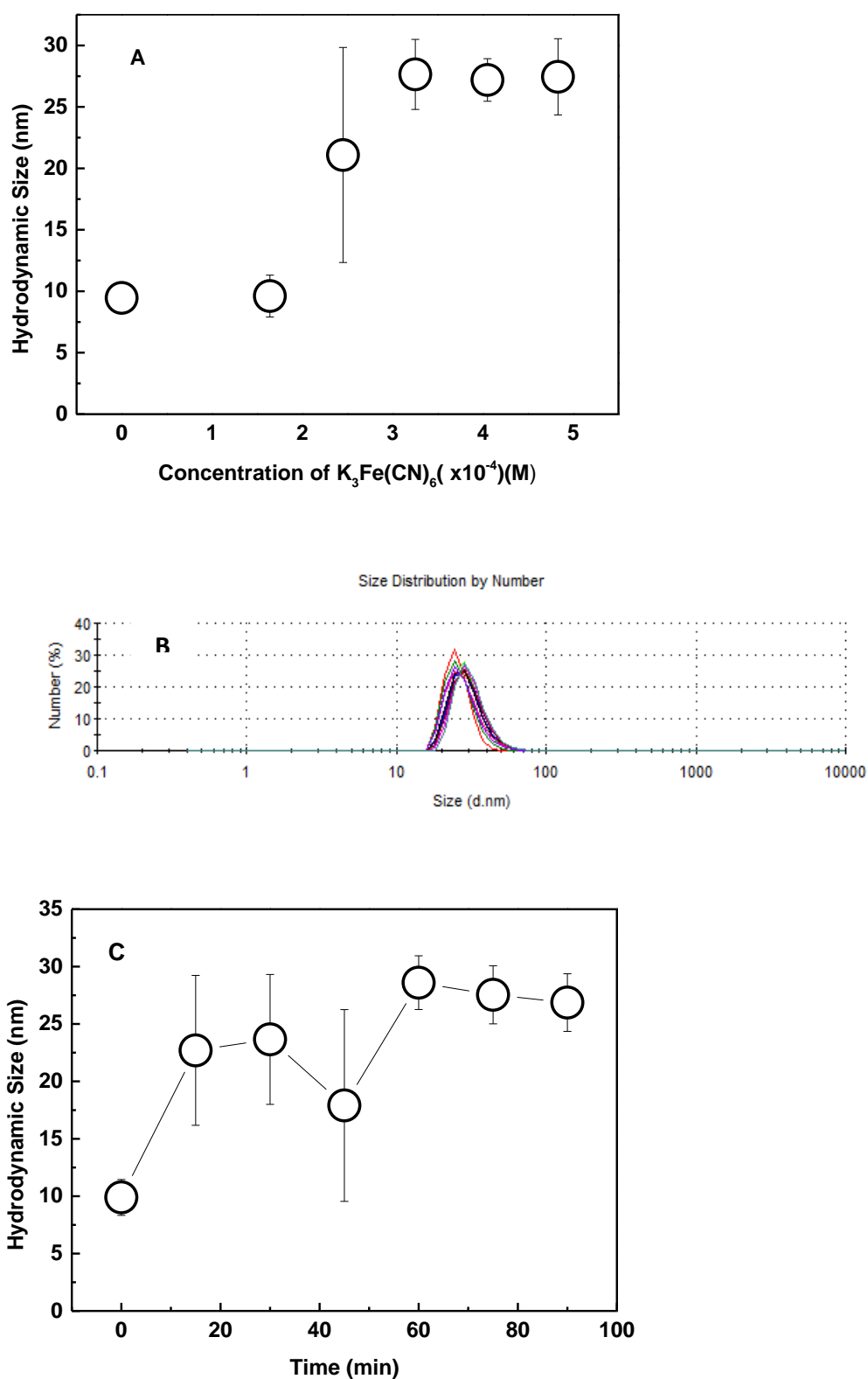


**Scheme 1.** Schematic representation of  $\text{K}_3\text{Fe}(\text{CN})_6$  induced micellization of QP2VP-*b*-PEO at pH 7.5

### 3.3.1. Effect of concentration of $K_3Fe(CN)_6$ on micellization of QP2VP-*b*-PEO

To monitor the micellization, the hydrodynamic size of QP2VP-*b*-PEO was measured after addition of  $K_3Fe(CN)_6$  into QP2VP-*b*-PEO solution. Figure 13A shows the hydrodynamic size of QP2VP-*b*-PEO as a function of the concentration of  $K_3Fe(CN)_6$  in the solution. At  $1.64 \times 10^{-4}$  M of  $K_3Fe(CN)_6$ , no micellization was observed. The hydrodynamic size of QP2VP-*b*-PEO remained almost same with the size in the absence of  $K_3Fe(CN)_6$ . Increasing  $K_3Fe(CN)_6$  concentration to  $2.45 \times 10^{-4}$  M led to an increase in the hydrodynamic size of QP2VP-*b*-PEO, i.e. an increment from  $\sim 10$  nm to  $\sim 20$  nm  $\pm 8.75$ . The large standard deviation is correlated with the existence of both unimers and micelles with varying size in the aqueous solution. Although, micellization could be induced at  $2.45 \times 10^{-4}$  M of  $K_3Fe(CN)_6$ , the amount of  $[Fe(CN)_6]^{3-}$  ions was not enough to form solely micelles with uniform size. Therefore, unimers and micelles with varying size existed together in the solution. At  $3.25 \times 10^{-4}$  M of  $K_3Fe(CN)_6$ , (QP2VP+ $[Fe(CN)_6]^{3-}$ )-*b*-PEO micelles with a hydrodynamic size of  $\sim 30$  nm  $\pm 2.84$  formed. The small standard deviation showed that the amount of  $[Fe(CN)_6]^{3-}$  ions was enough to form (QP2VP+ $[Fe(CN)_6]^{3-}$ )-*b*-PEO micelles with uniform size. Further increasing the  $K_3Fe(CN)_6$  concentration did not result in a significant change in the micellar size. The hydrodynamic size of (QP2VP+ $[Fe(CN)_6]^{3-}$ )-*b*-PEO micelles at  $4.05 \times 10^{-4}$  M and  $4.83 \times 10^{-4}$  M  $K_3Fe(CN)_6$  were almost at the same magnitude with the micelles formed upon addition of  $3.25 \times 10^{-4}$  M  $K_3Fe(CN)_6$ . Figure 13B represents the size distribution by number at  $3.25 \times 10^{-4}$  M  $K_3Fe(CN)_6$ .

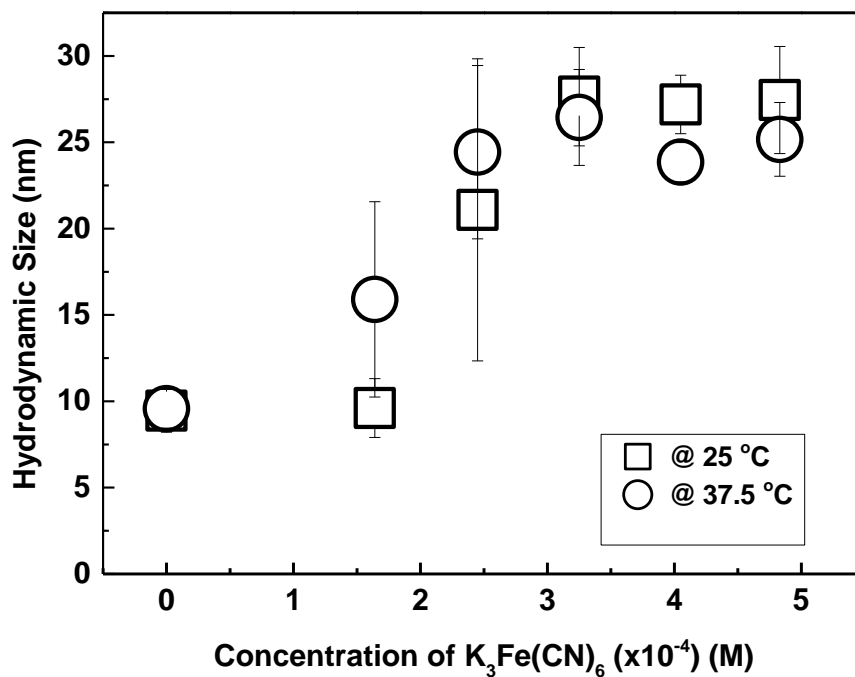
It is important to mention that the size data were collected after 60 min the  $K_3Fe(CN)_6$  was added into QP2VP-*b*-PEO solution in Figure 13A. The duration for self-assembly was determined by monitoring the size at a certain  $K_3Fe(CN)_6$  concentration as a function of time (Figure 13C). It was found that although (QP2VP+ $[Fe(CN)_6]^{3-}$ )-*b*-PEO micelles formed in the first 15 minutes after the addition of  $K_3Fe(CN)_6$ , micelles reached a more uniform size after 60 minutes. Therefore, the micellization time was kept as 60 minutes.



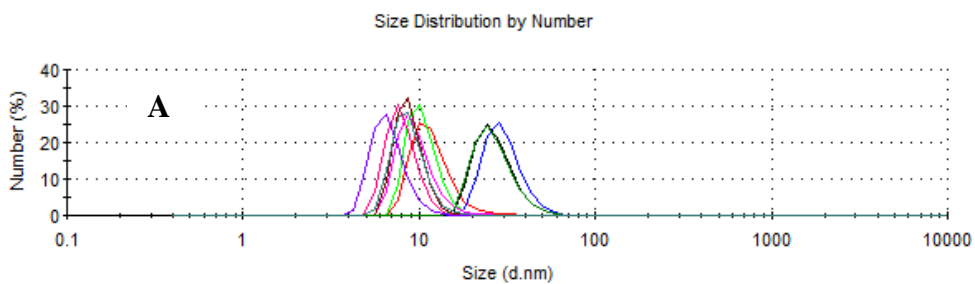
**Figure 13.** Hydrodynamic size of QP2VP-*b*-PEO as a function of the concentration of  $K_3Fe(CN)_6$  (A), size distribution by number at  $3.25 \times 10^4$  M  $K_3Fe(CN)_6$  (B) and evolution of hydrodynamic size of QP2VP-*b*-PEO with time (C) at 25 °C and pH 7.5.

### 3.3.2. Effect of temperature on multivalent-salt induced micellization of QP2VP-*b*-PEO

In this part of the study, micellization was induced at 37.5 °C. For comparison with the data at 25 °C, similar  $K_3Fe(CN)_6$  concentrations were examined to induce micellization. Figure 14 shows the change in hydrodynamic size of QP2VP-*b*-PEO as a function of concentration of  $K_3Fe(CN)_6$  at pH 7.5 and 37.5 °C. The data obtained at 25 °C was plotted for comparison. Interestingly, (QP2VP+[Fe(CN)<sub>6</sub>]<sup>3-</sup>)-*b*-PEO micelles could be formed at lower concentrations of  $K_3Fe(CN)_6$  at 37.5 °C. For example, at  $1.64 \times 10^{-4}$  M  $K_3Fe(CN)_6$ , no change in hydrodynamic size of QP2VP-*b*-PEO was recorded at 25 °C, while ~ 15 nm micellar aggregates coexisted with the unimers at 37.5 °C. Similarly, at  $2.45 \times 10^{-4}$  M  $K_3Fe(CN)_6$ , micelles with hydrodynamic size of ~23 nm was formed at 37.5 °C, while micelles with varying size and even unimers coexisted in solution at 25 °C. Figure 15 contrasts the size distribution by number of QP2VP-*b*-PEO in the presence of  $2.45 \times 10^{-4}$  M  $K_3Fe(CN)_6$  at 25 °C and 37.5 °C. The difference in the micellization between 25 °C and 37.5 °C is correlated with the LCST-type phase behaviour of PEO in aqueous solution. Although, PEO has a LCST of ~ 100°C [93], its solubility, in other words, degree of hydration decreases as the temperature rises even well below the LCST value. This results in enhanced hydrophobic-hydrophobic interactions among the PEO chains which might have contributed to the formation of micellar aggregates at lower salt concentrations. In another study, it was reported that increasing the temperature of solution of micellar aggregates with PEO-coronae led to transformation from cylinders to vesicles. Researchers explained this phenomenon by the decrease in the volume of the swollen PEO layer in water. They suggested that the interfacial area ( $a_0$ ) at the hydrophilic-hydrophilic interface decreased as the temperature rised resulting in an increase in the packing parameter and a transformation from cylinders to vesicles [94].



**Figure 14.** Hydrodynamic size of QP2VP-*b*-PEO as a function of concentration of  $K_3Fe(CN)_6$  at 37.5 °C and pH 7.5.



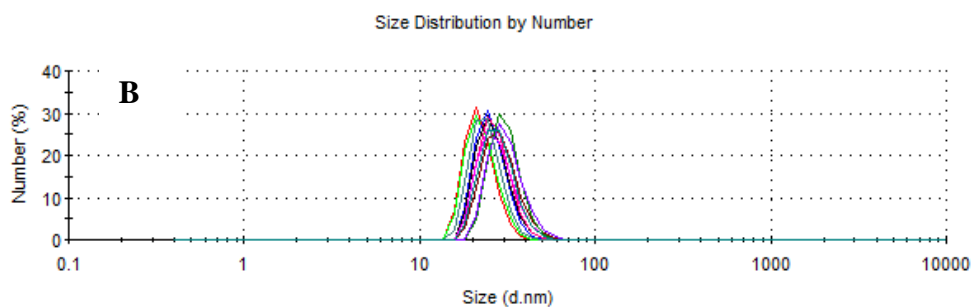


**Figure 15.** The size distribution by number of QP2VP-*b*-PEO in the presence of  $2.45 \times 10^{-4}$  M  $\text{K}_3\text{Fe}(\text{CN})_6$  at 25 °C (Panel A) and 37.5 °C (Panel B).

### 3.4. Temperature Response of (QP2VP+[Fe(CN)<sub>6</sub>]<sup>3-</sup>)-*b*-PEO micelles

We have examined the temperature-response of (QP2VP+[Fe(CN)<sub>6</sub>]<sup>3-</sup>)-*b*-PEO micelles by monitoring the hydrodynamic size of micelles with increasing temperature using dynamic light scattering.

First, hydrodynamic size of (QP2VP+[Fe(CN)<sub>6</sub>]<sup>3-</sup>)-*b*-PEO micelles which were prepared in the presence of  $3.25 \times 10^{-4}$  M  $\text{K}_3\text{Fe}(\text{CN})_6$  at 25 °C was followed as a function of temperature by 5°C steps from 25°C to 45°C. As seen in Figure 16A, no significant change in hydrodynamic size of BCMs was recorded until 45°C. Further increasing temperature to 45°C resulted in a decrease in the hydrodynamic size of BCMs by 50 %. At 45°C, the hydrodynamic size decreased to ~14 nm. Figure 16B contrasts the size distribution by number of (QP2VP+[Fe(CN)<sub>6</sub>]<sup>3-</sup>)-*b*-PEO micelles at 25°C and 45°C to emphasize the shift in the size distribution to lower values with increasing temperature. The decrease in hydrodynamic size can be explained by the partial disintegration of the (QP2VP+[Fe(CN)<sub>6</sub>]<sup>3-</sup>)-*b*-PEO micelles due to loss in electrostatic interactions among QP2VP and  $\text{Fe}(\text{CN})_6^{3-}$  as the temperature was increased.

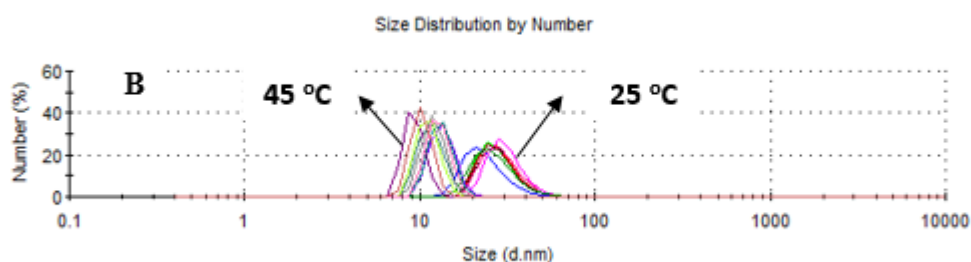
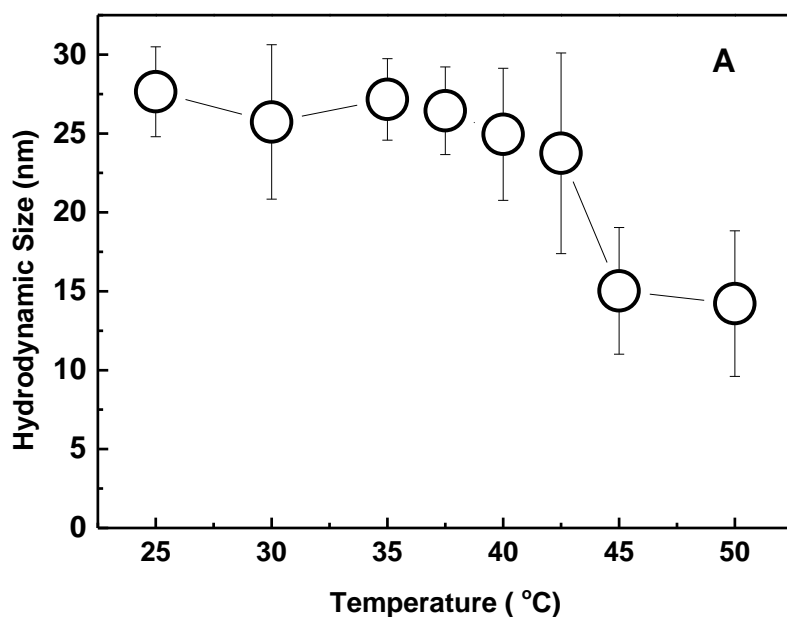


**Figure 16.** Evolution of hydrodynamic size of (QP2VP+[Fe(CN)<sub>6</sub>]<sup>3-</sup>)-*b*-PEO micelles with increasing temperature (Panel A); the size distribution by number of (QP2VP+[Fe(CN)<sub>6</sub>]<sup>3-</sup>)-*b*-PEO micelles at 25 °C and 45 °C (Panel B).

### 3.4.1. Effect of K<sub>3</sub>Fe(CN)<sub>6</sub> concentration on the temperature-response of (QP2VP+[Fe(CN)<sub>6</sub>]<sup>3-</sup>)-*b*-PEO micelles

It was found that temperature-response of (QP2VP+[Fe(CN)<sub>6</sub>]<sup>3-</sup>)-*b*-PEO micelles strongly depended on the concentration of K<sub>3</sub>Fe(CN)<sub>6</sub> used in the preparation of the micelles. (QP2VP+[Fe(CN)<sub>6</sub>]<sup>3-</sup>)-*b*-PEO micelles became less responsive to temperature changes as the amount of K<sub>3</sub>Fe(CN)<sub>6</sub> in the BCMs increased. This can be explained by the stronger interactions among the QP2VP and [Fe(CN)<sub>6</sub>]<sup>3-</sup> ions in the

micellar cores as the amount of  $\text{K}_3\text{Fe}(\text{CN})_6$  increased in the  $(\text{QP2VP}+[\text{Fe}(\text{CN})_6]^{3-})$ -*b*-PEO micelles and requirement for higher temperature to disrupt the interactions within the micellar cores. Figure 17 shows the evolution of hydrodynamic size of  $(\text{QP2VP}+[\text{Fe}(\text{CN})_6]^{3-})$ -*b*-PEO micelles prepared in the presence of  $4.05 \times 10^{-4}$  M or  $4.83 \times 10^{-4}$  M  $\text{K}_3\text{Fe}(\text{CN})_6$ . In contrast to BCMs prepared in the presence of  $3.25 \times 10^{-4}$  M  $\text{K}_3\text{Fe}(\text{CN})_6$ , no change in hydrodynamic size was recorded in a temperature range between 25-50 °C.

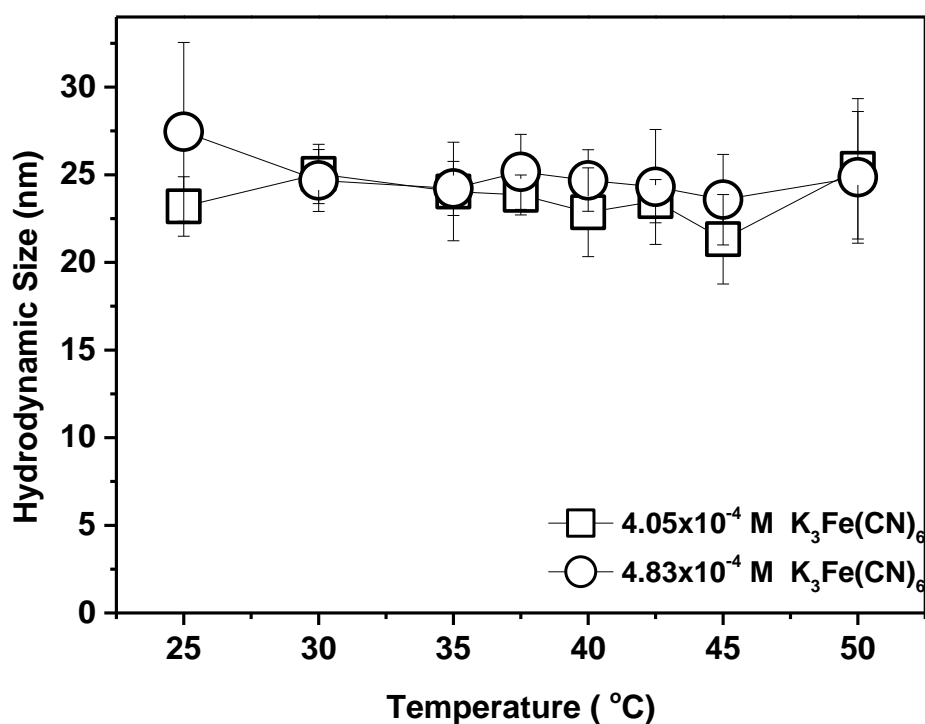


**Figure 17.** Evolution of hydrodynamic size of  $(\text{QP2VP}+[\text{Fe}(\text{CN})_6]^{3-})$ -*b*-PEO micelles prepared in the presence of  $4.05 \times 10^{-4}$  M or  $4.83 \times 10^{-4}$  M  $\text{K}_3\text{Fe}(\text{CN})_6$ .

### 3.4.2. Effect of micellization temperature on the temperature-response of (QP2VP+[Fe(CN)<sub>6</sub>]<sup>3-</sup>)-*b*-PEO micelles

It was found that (QP2VP+[Fe(CN)<sub>6</sub>]<sup>3-</sup>)-*b*-PEO micelles which were prepared in the presence of  $2.45 \times 10^{-4}$  M K<sub>3</sub>Fe(CN)<sub>6</sub> at 37.5 °C were responsive to increasing temperature in a more narrow temperature range. BCMs partially disintegrated in a temperature range between 37.5-42.5 °C.

Figure 18A contrasts the size distribution of (QP2VP+ [Fe(CN)<sub>6</sub>]<sup>3-</sup>)-*b*-PEO micelles by number at 37.5°C and 42.5 °C. It is important to remind that (QP2VP+[Fe(CN)<sub>6</sub>]<sup>3-</sup>)-*b*-PEO micelles which were prepared in the presence of  $3.25 \times 10^{-4}$  M K<sub>3</sub>Fe(CN)<sub>6</sub> at 25 °C only slightly disintegrated at 42.5 °C. To further understand the effect of micellization temperature on the temperature-response of micelles, the hydrodynamic size of (QP2VP+[Fe(CN)<sub>6</sub>]<sup>3-</sup>)-*b*-PEO micelles, prepared in the presence of  $3.25 \times 10^{-4}$  M K<sub>3</sub>Fe(CN)<sub>6</sub> at 37.5 °C was monitored as a function of temperature (Figure 18B). In contrast to BCMs prepared at 25 °C at the same K<sub>3</sub>Fe(CN)<sub>6</sub> concentration, disintegration of (QP2VP+[Fe(CN)<sub>6</sub>]<sup>3-</sup>)-*b*-PEO micelles, prepared in the presence of  $3.25 \times 10^{-4}$  M, was observed below 45°C. Figure 18B represents the size distribution of (QP2VP+[Fe(CN)<sub>6</sub>]<sup>3-</sup>)-*b*-PEO micelles by number at 37.5 °C and 42.5 °C .

These results show that the BCMs which were prepared at 37.5 °C were more responsive to temperature increase. This can be explained by the weaker interactions formed at 37.5 °C among the QP2VP blocks and Fe(CN)<sub>6</sub> ions at 37.5 °C which was relatively easier to destruct as the temperature increased compared to BCMs prepared at 25°C.

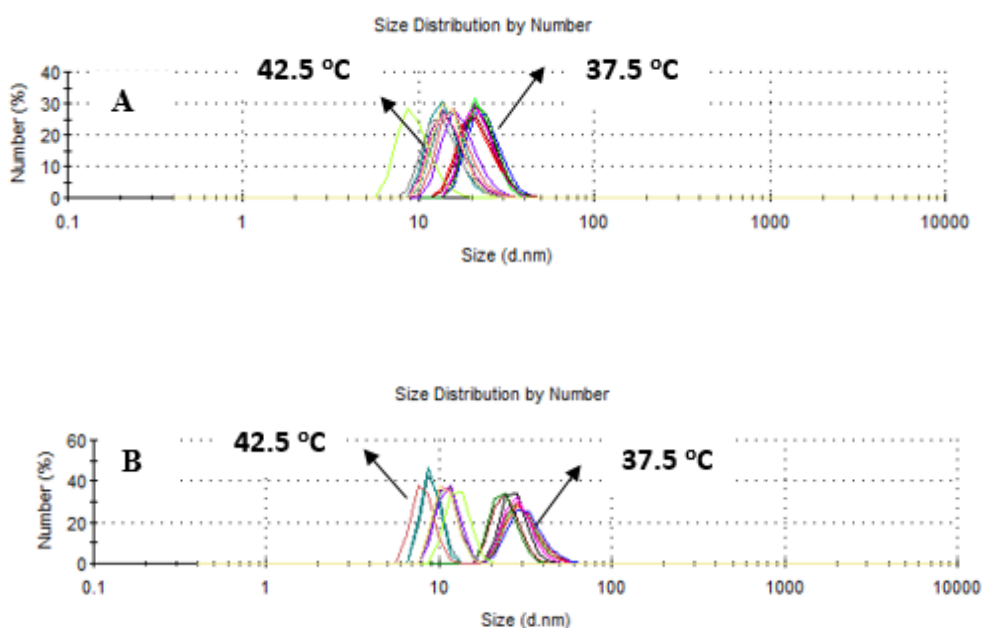


**Figure 18.** Size distribution of (QP2VP+[Fe(CN)<sub>6</sub>]<sup>3-</sup>)-*b*-PEO micelles prepared in the presence of  $2.45 \times 10^{-4}$  M K<sub>3</sub>Fe(CN)<sub>6</sub> at 37.5 °C by number at 37.5 °C and 42.5 °C (Panel A); size distribution of (QP2VP+[Fe(CN)<sub>6</sub>]<sup>3-</sup>)-*b*-PEO micelles prepared in the presence of  $3.25 \times 10^{-4}$  M K<sub>3</sub>Fe(CN)<sub>6</sub> at 37.5 °C by number at 37.5 °C and 42.5 °C (Panel B).

Several research groups have worked on introducing UCST-type phase behaviour to polymer solutions. For example, Plamper et al. reported that poly(*N,N*-dimethylaminoethyl methacrylate) (PDMAEMA) exhibited UCST-type phase behaviour in the presence of [Co(CN)<sub>6</sub>]<sup>3-</sup> trivalent counterions below pH 9 and UCST was highly dependent on the pH [44]. In another study, Jia et al. used a divalent counterion, potassium persulfate (K<sub>2</sub>S<sub>2</sub>O<sub>8</sub>) to introduce UCST-type phase behaviour to P2VP-*b*-PEO. However, micellar aggregates via electrostatic interactions among P2VP and K<sub>2</sub>S<sub>2</sub>O<sub>8</sub> could only be formed at acidic conditions when P2VP was in the protonated form at strongly acidic conditions. Therefore, UCST-type phase behaviour which was observed between 40-70 °C depending on the P2VP chain length, was only present at strongly acidic conditions [52]. In the study of Liu and co-workers, UCST-type phase behaviour was introduced to poly (2-vinylpyridine)-*b*-poly (N-isopropylacrylamide) (P2VP-*b*-PNIPAM) using 2,6-naphthalenedisulfonate (2,6-NDS). Similar to the study of Jia et al., formation of BCMs via electrostatic

interactions among P2VP and 2,6 NDS could only be induced at strongly acidic conditions when P2VP was in the protonated state, thus UCST-type phase behaviour was only present at strongly acidic conditions between 20-38 °C [54].

This study differs from those by introducing UCST-type behaviour to P2VP-*b*-PEO at physiological pH by quaternizing some of the pyridine units and imparting permanent charge on P2VP. In this way, uncontrollable disintegration of BCMs can be prevented when exposed to physiological pH. In addition, this study achieved producing BCMs which were stable at physiological temperature but showed response near above the body temperature which is important for biological applications.

### **3.5. Multilayers of (QP2VP+[Fe(CN)<sub>6</sub>]<sup>3-</sup>)-*b*-PEO micelles and Tannic Acid (TA)**

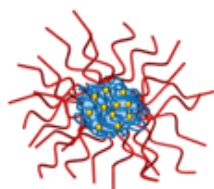
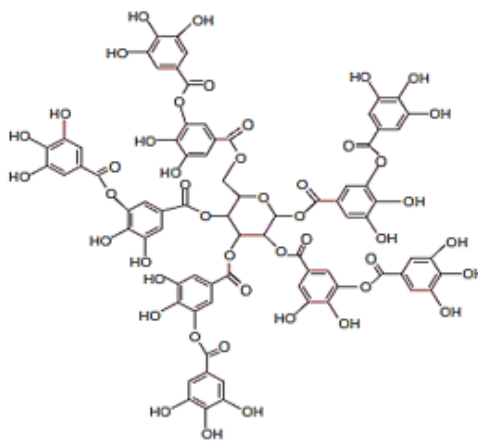
#### **3.5.1. Layer-by-layer deposition of (QP2VP+[Fe(CN)<sub>6</sub>]<sup>3-</sup>)-*b*-PEO micelles and TA**

(QP2VP+[Fe(CN)<sub>6</sub>]<sup>3-</sup>)-*b*-PEO micelles which were prepared at 25 °C in the presence of 3.25x10<sup>-4</sup> M K<sub>3</sub>Fe(CN)<sub>6</sub> or (QP2VP+[Fe(CN)<sub>6</sub>]<sup>3-</sup>)-*b*-PEO micelles which were prepared at 37.5 °C in the presence of 2.45x10<sup>-4</sup> M K<sub>3</sub>Fe(CN)<sub>6</sub> were used as building blocks for the multilayer assembly. Both BCMs were LbL deposited at the surface using TA. The driving force for multilayer assembly was hydrogen bonding interactions among the ether oxygens of PEO coronal chains and protonated hydroxyl group of TA as shown in scheme 2. Note that, TA has a pK<sub>a</sub> of approximately 8.5 [95] and hydroxyl groups of TA are partially ionized at pH 7.5.

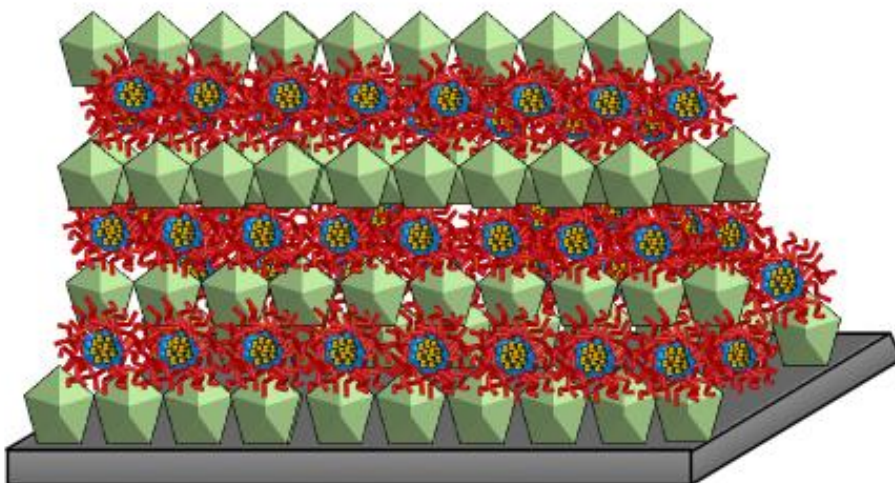
Panel A



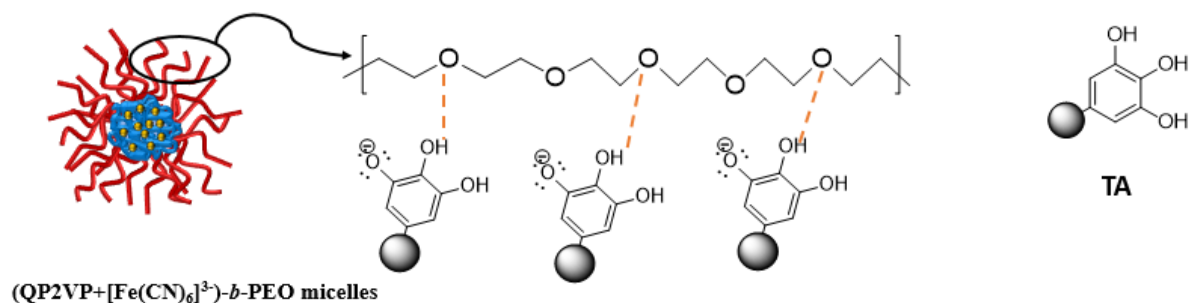
Tannic Acid



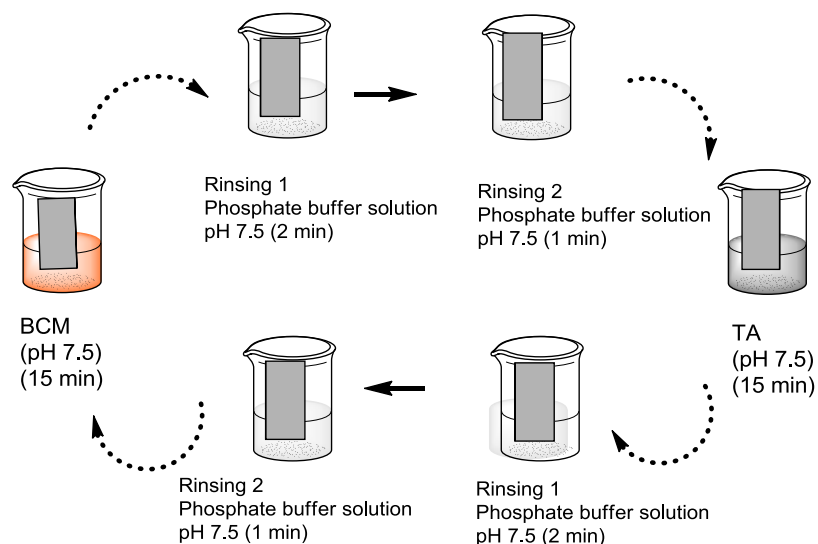
(QP2VP+[Fe(CN)<sub>6</sub>]<sup>3-</sup>)-*b*-PEO micelles



### H-bonding interactions among PEO-corona and TA



#### Panel B



**Scheme 2.** Schematic representation of the hydrogen bonding interactions among TA and  $(QP2VP+[Fe(CN)_6]^{3-})-b-PEO$  micelles (Panel A). Schematic representation of LbL process and multilayers of  $(QP2VP+[Fe(CN)_6]^{3-})-b-PEO$  micelles and TA.

Figure 19 shows the LbL growth of multilayer films. As seen in Figure 19A, multilayers deposited at 25°C demonstrated a zig-zag growth mode after the sixth layer where the substrate effect was diminished. This can be explained by sweeping away TA molecules from the surface by  $(QP2VP+[Fe(CN)_6]^{3-})-b-PEO$  micelles due to high

hydrophilicity of PEO chains and the tendency of (QP2VP+[Fe(CN)<sub>6</sub>]<sup>3-</sup>)-*b*-PEO micelles and TA complexes to go into the solution. In contrast, multilayers of (QP2VP+[Fe(CN)<sub>6</sub>]<sup>3-</sup>)-*b*-PEO micelles and TA which were constructed at 37.5 °C demonstrated a linear growth profile (Figure 19B). The increment per bilayer at 37.5 °C was higher than that at 25 °C. The difference can be explained by the enhanced hydrophobicity of PEO chains as the temperature was increased from 25 °C to 37.5 °C. Note that PEO has a LCST of 100 °C [93] in aqueous solution and it has been reported that the hydration of PEO chains decreased as the temperature increased even at temperatures well below the LCST. It has also previously been reported that hydrophobicity significantly contributes to the growth of hydrogen-bonded LbL films [96]. It is important to mention that a layer of (QP2VP+[Fe(CN)<sub>6</sub>]<sup>3-</sup>)-*b*-PEO micelles had a thickness of ~2.5 nm and ~ 3.5 nm at 25 °C and 37.5 °C respectively. Both thickness values were much lower than the hydrodynamic sizes of the BCMs which were ~ 30 nm and ~23 nm at 25°C and 37.5 °C, respectively. This important difference was a result of several factors. First, hydrodynamic size measurements were performed in aqueous environment using DLS technique. However, thickness measurements concerned the dry mass of adsorbed layer. Second, the spherical structure of BCMs could lead to low surface coverage which is critical in ellipsometric thickness measurements. Of note, ellipsometric thickness is averaged over square millimeter (mm<sup>2</sup>) surface area. Third, multiple binding points between the PEO coronal chains and the TA could cause flattening and spreading of BCMs at the surface which resulted in lower thickness values compared to hydrodynamic sizes of (QP2VP+[Fe(CN)<sub>6</sub>]<sup>3-</sup>)-*b*-PEO micelles[97].

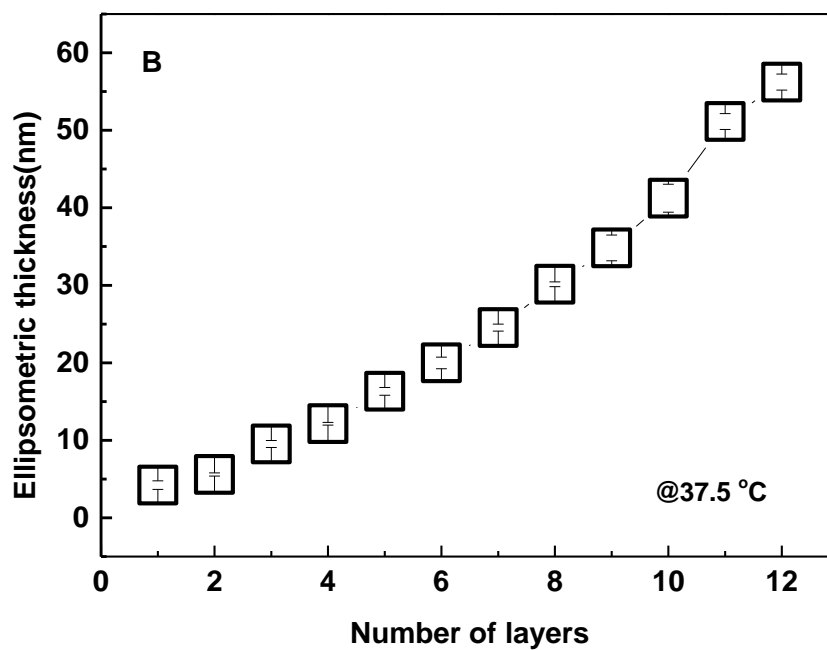
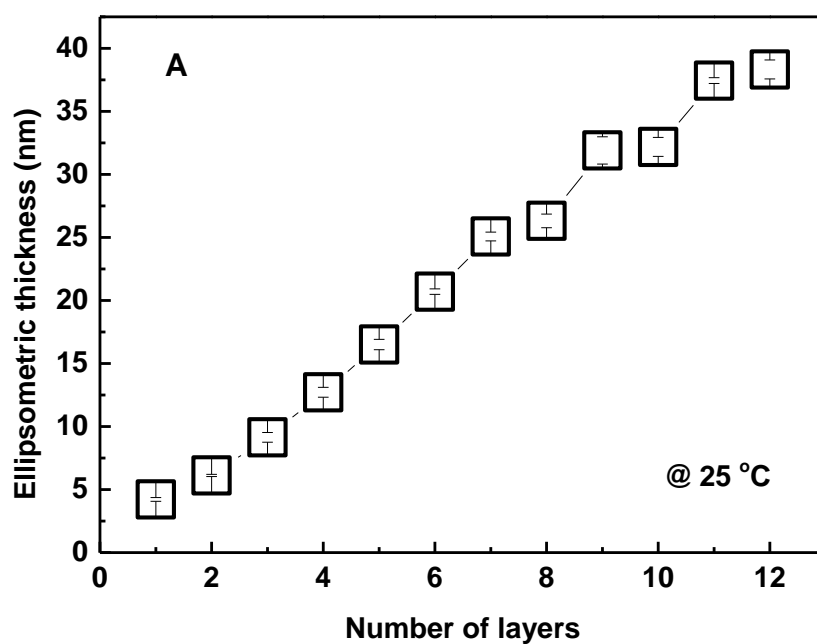


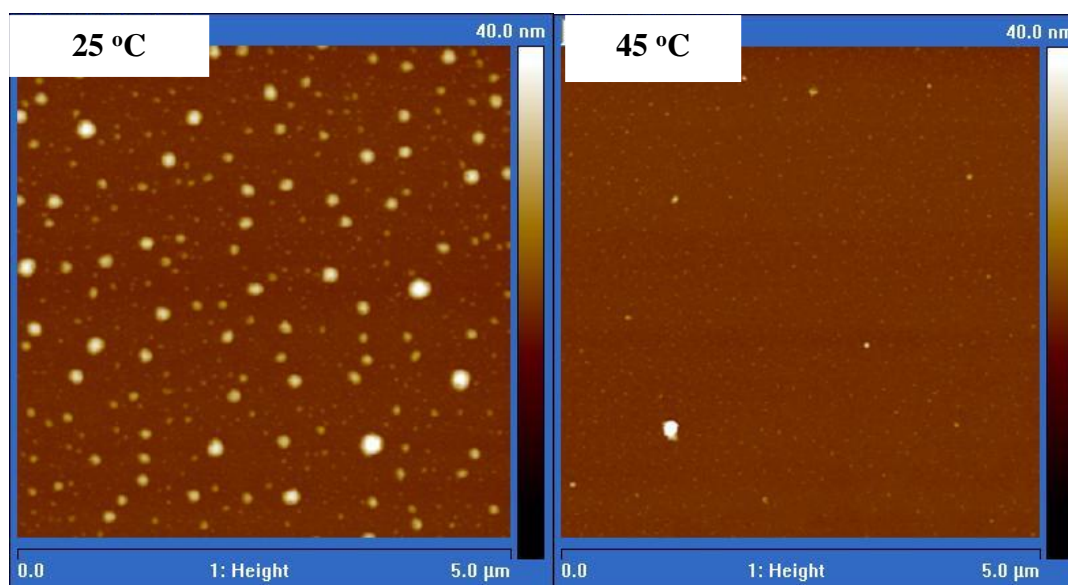
**Figure 19.** Ellipsometric thickness of multi-layer films of (QP2VP+[Fe(CN)<sub>6</sub>]<sup>3-</sup>)-*b*-PEO micelles deposited at pH 7.5 and 25 °C (Panel A) or 37.5 °C (Panel B).

### 3.5.2. Temperature-response of multilayers

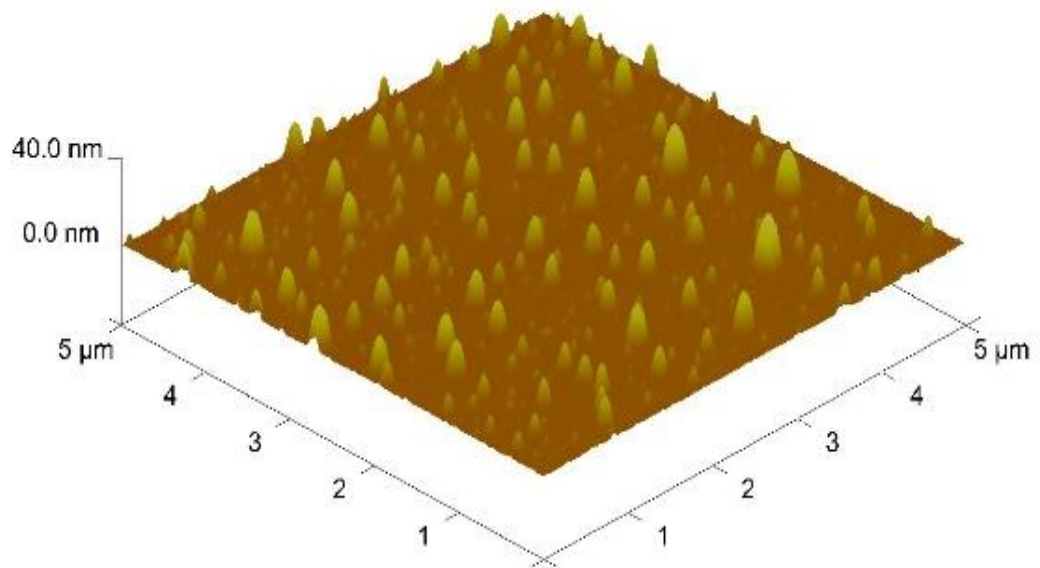
#### 3.5.2.1. Temperature-response of a monolayer of (QP2VP+[Fe(CN)<sub>6</sub>]<sup>3-</sup>)-*b*-PEO micelles

Prior to multilayer assembly, a monolayer of (QP2VP+[Fe(CN)<sub>6</sub>]<sup>3-</sup>)-*b*-PEO micelles (prepared at 25 °C in the presence of 3.25x10<sup>-4</sup> M K<sub>3</sub>Fe(CN)<sub>6</sub>) was deposited onto the surface at 25 °C and exposed to 45 °C in PBS to assure the disintegration of BCMs even if they were deposited at the surface. Figure 20A shows the AFM images of a monolayer of (QP2VP+[Fe(CN)<sub>6</sub>]<sup>3-</sup>)-*b*-PEO micelles before and after exposure to 45 °C. The disappearance of spherical aggregates after exposing the film to PBS solution at 45 °C for 60 minutes showed that surface-attached (QP2VP+[Fe(CN)<sub>6</sub>]<sup>3-</sup>)-*b*-PEO micelles disintegrated at 45 °C. Thickness of a monolayer film decreased from ~4.3 nm to ~2.5 nm after exposing the film to 45 °C for 1 hour. This indicates that disintegration of (QP2VP+[Fe(CN)<sub>6</sub>]<sup>3-</sup>)-*b*-PEO micelles did not result in complete removal of the coating from the surface. QP2VP-*b*-PEO went into a rearrangement and deposited as unimers at the surface resulting in lower surface roughness. Figure 20B contrasts the ellipsometric thicknesses and rms roughness values before and after exposure to 45 °C.

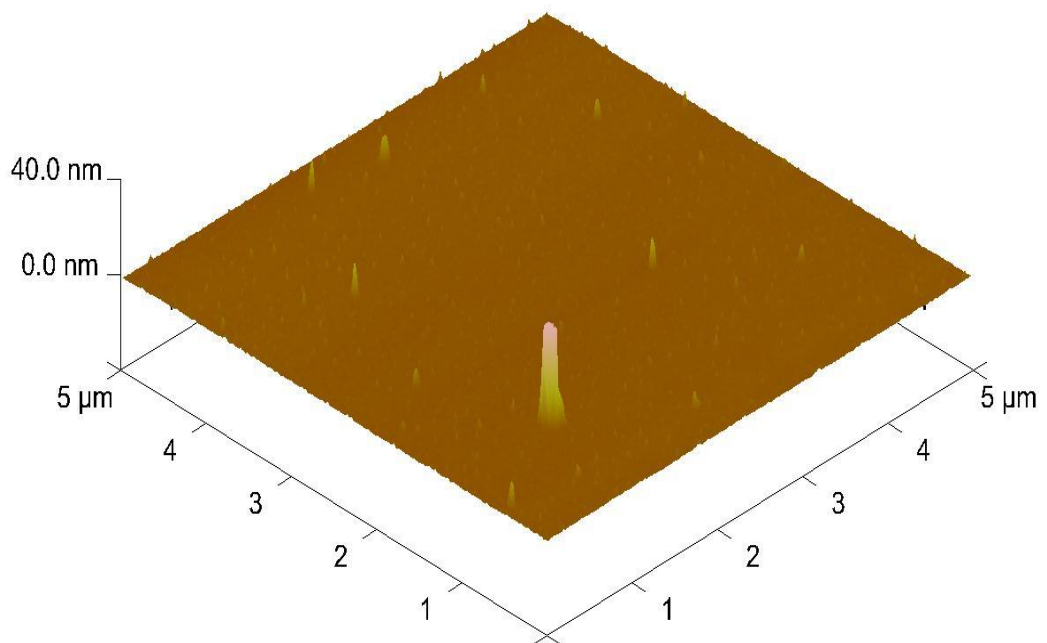
**Panel A**



25 °C



45 °C



**Panel B**

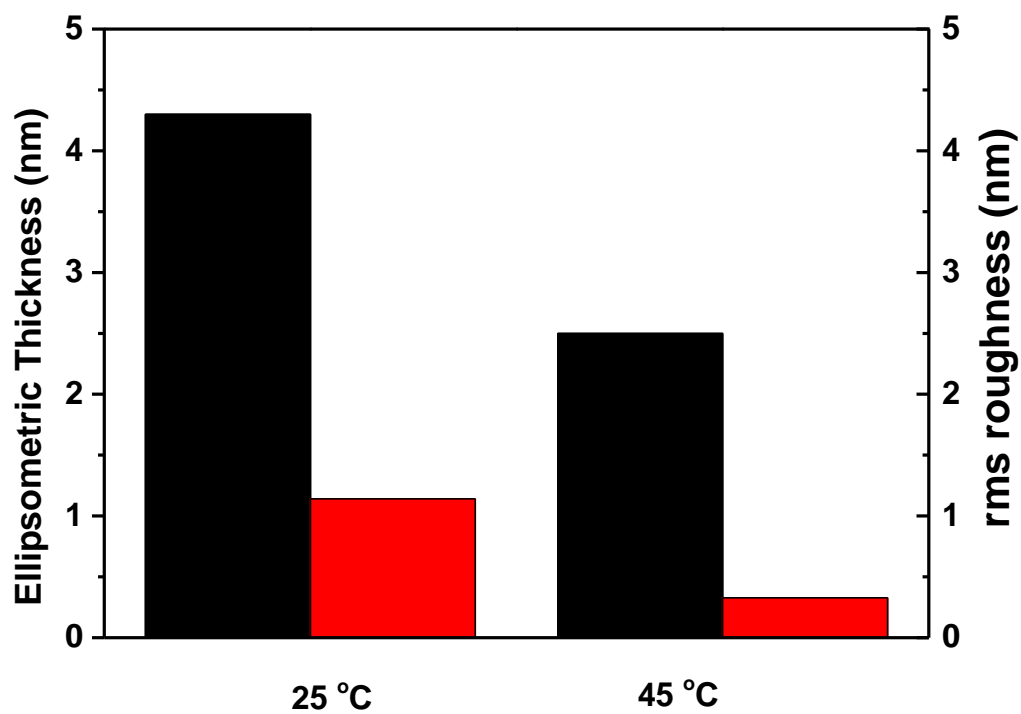
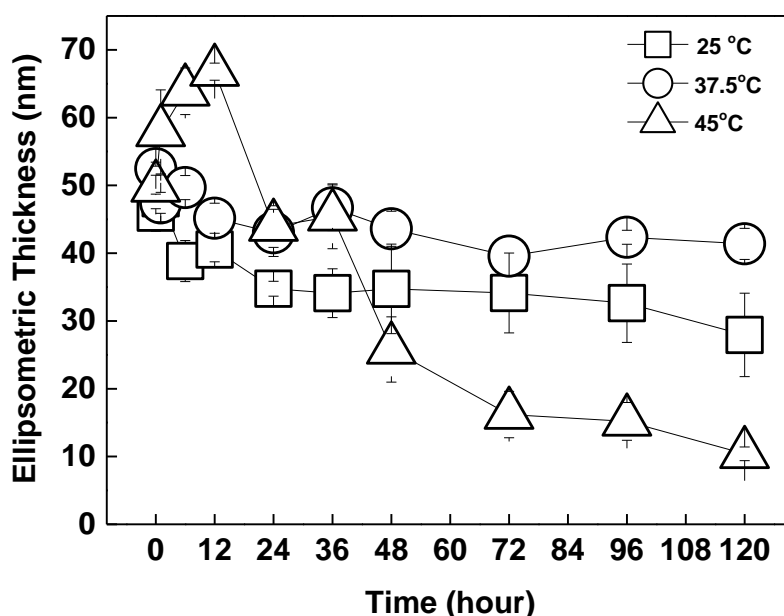


**Figure 20.** AFM topography images of a monolayer of (QP2VP+[Fe(CN)<sub>6</sub>]<sup>3-</sup>)-*b*-PEO micelles before and after exposure to 45 °C (Panel A) in PBS solution at pH 7.5 as 2D and 3D; ellipsometric thicknesses (black bars) and rms roughness (red bars) of a monolayer film before after exposure to 45 °C in PBS solution(Panel B).

### 3.5.2.2. Temperature-response of multilayers of (QP2VP+[Fe(CN)<sub>6</sub>]<sup>3-</sup>)-*b*-PEO micelles and TA

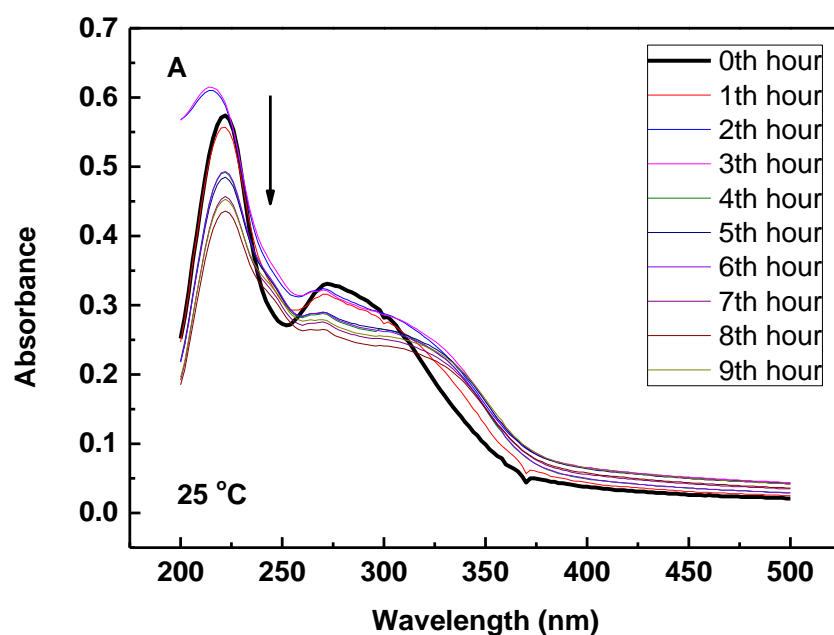
#### 3.5.2.2.1. Temperature-response of multilayers constructed at 25 °C

For multilayers, which were constructed at 25 °C, temperature-response was followed at 37.5 °C and 45 °C. Remember that (QP2VP+[Fe(CN)<sub>6</sub>]<sup>3-</sup>)-*b*-PEO micelles which were prepared in the presence of 3.25x10<sup>-4</sup> M K<sub>3</sub>Fe(CN)<sub>6</sub> at 25 °C disintegrated at 45 °C. Therefore, temperature-response of the multilayers was followed at the physiological pH at 37.5 °C and 45 °C in PBS buffer to mimic the biological environment. As a control experiment, stability of the multilayers in PBS buffer was followed at 25 °C as well. As seen in Figure 21, the thickness of the films gradually increased at 45 °C and a 40% increment was recorded after twelve hours. Film thickness was then followed on a daily basis and only 20 % of the film remained at the surface on the fifth day. In contrast, no significant change in film thickness was recorded in the first hour at 37.5 °C and 25 °C. Film thicknesses decreased by approximately 18 % after a day and no significant change in thickness was recorded later on for both of the films.



**Figure 21.** Evolution of thickness of 20-layer films of (QP2VP+[Fe(CN)<sub>6</sub>]<sup>3-</sup>)-*b*-PEO micelles and TA at 25°C and 45°C.

The loss in film thickness at 25°C and 37.5°C can be correlated with the enhanced ionization of TA at high ionic strength (in PBS solution). It has earlier been reported that the presence of salt ions shifted the disintegration pH of the hydrogen-bonded multilayers to lower pH values [98]. The increment in thickness at 45°C could possibly be correlated with loosening of the film structure due to partial loss of hydrogen bonding interactions among the layers with increasing temperature and penetration of salt ions as well as water molecules into the multilayers. Indeed, it was also possible that multilayers partially disintegrated in the first twelve hours and the increase in thickness was due to adsorption/absorption of the salt ions. To further explore, we examined the stability of multilayers using UV-Vis Spectroscopy technique. Figure 22 demonstrates the UV-Vis spectra of the films at 25°C (Panel A), 37.5°C (Panel B) and 45°C (Panel C).



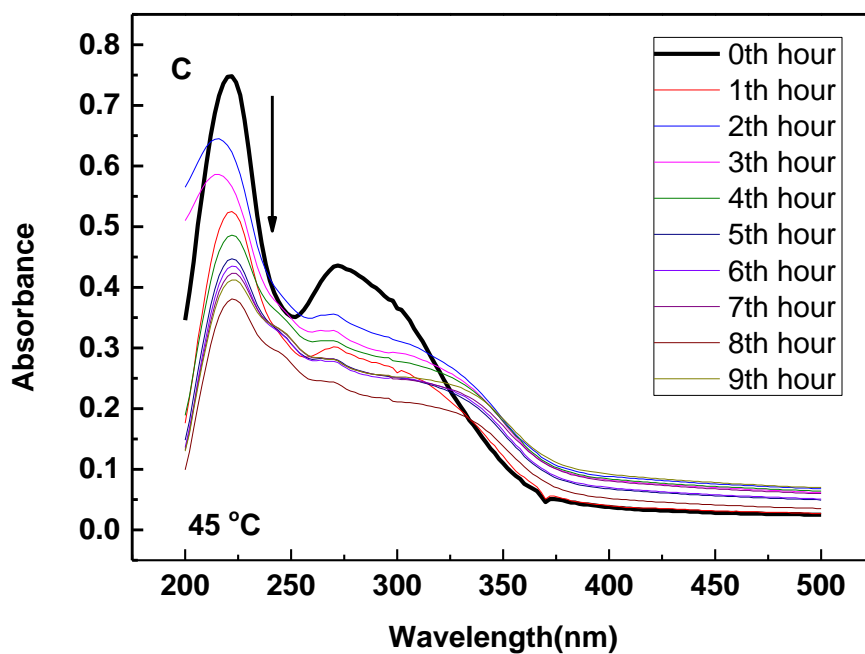
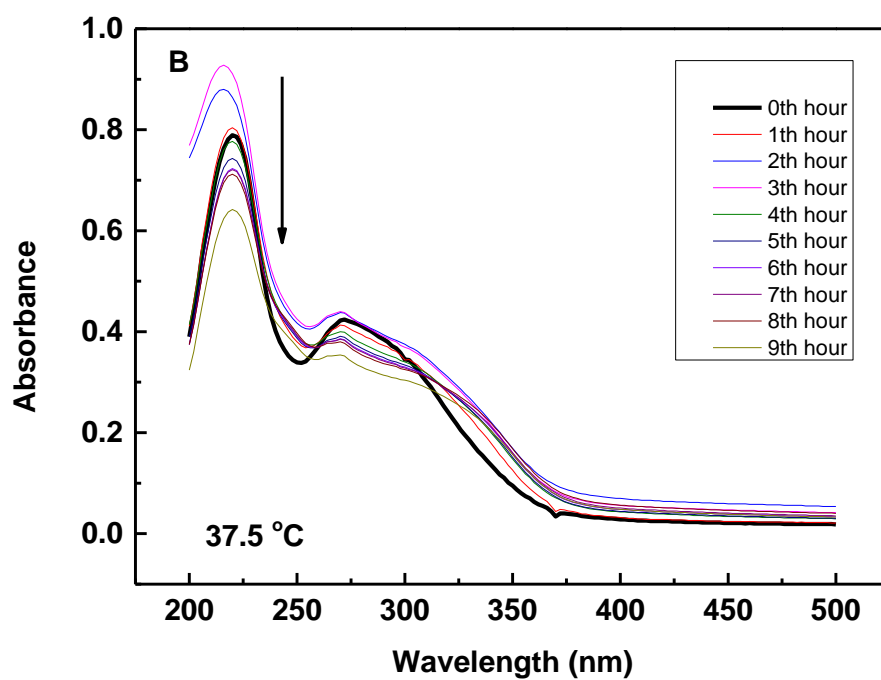


**Figure 22.** UV-Vis spectra of the (QP2VP+[Fe(CN)<sub>6</sub>]<sup>3-</sup>)-b-PEO micelles/TA films at 25 °C (Panel A), 37.5 °C (Panel B) and 45 °C (Panel C).

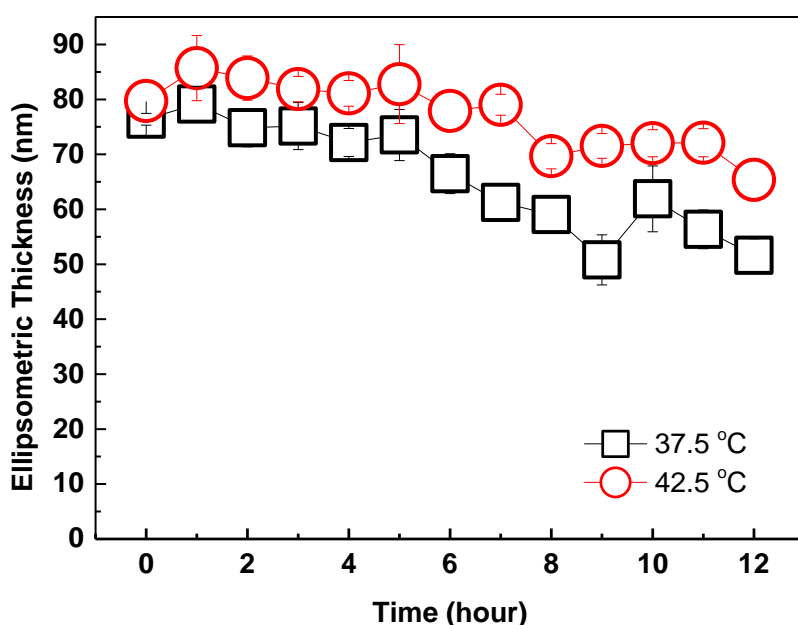
QP2VP-*b*-PEO has 2 peaks with centered at 205 nm and 260 nm. TA has 2 peaks with centered at 212 nm and 280 nm.  $K_3Fe(CN)_6$  has 2 peaks with centered at 260 nm and 302 nm. UV-Vis spectra of QP2VP-*b*-PEO, TA and  $K_3Fe(CN)_6$  are presented in Appendix. Unfortunately, the release of each component could not be evaluated individually due to overlapping of the peaks. However, the decrease in the intensity of the overall spectrum indicates loss of material from the surface. Results obtained at 25 °C and 37.5 °C using UV-Visible Spectroscopy technique were in good agreement with the results obtained from ellipsometric thickness measurements. The decrease in the intensity of the peaks was not significant up to 5 hours. The decrease in the intensity of the peaks was more obvious between 5-9 hours. However, at 45 °C, in contrast to results obtained from ellipsometric film thickness measurements, the intensity of the peaks decreased in the first hour. The decrease between 1 hour and 5 hours was smaller than that observed in the first hour. Still, the intensity of the peaks decreased gradually, indicating the disintegration of the polymer layers from the surface.

The disintegration of the multilayers can be correlated with: i) the disintegration of the micellar cores with increasing temperature which might have resulted in a charge imbalance within the multilayers and ii) weakening of the hydrogen bonding interactions among the layers with increasing temperature.

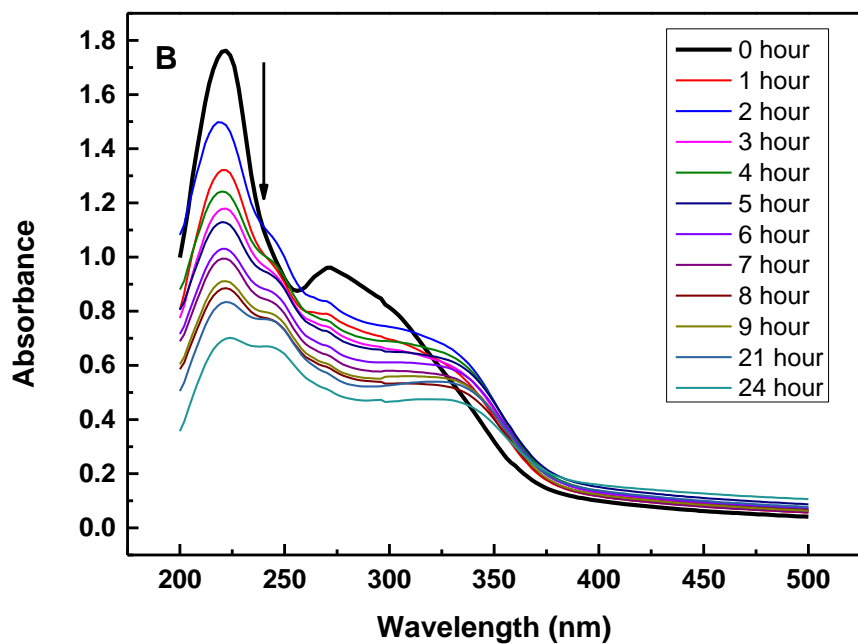
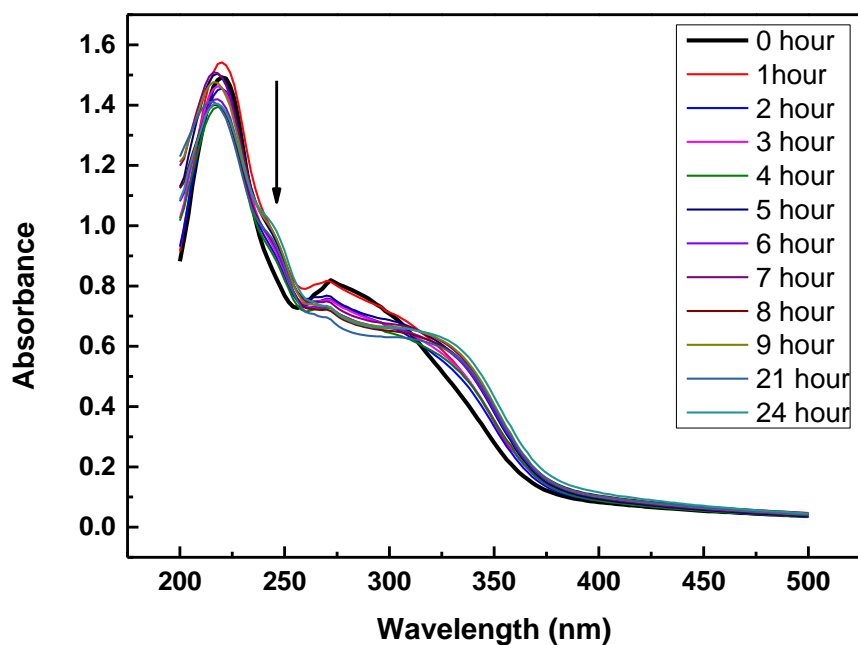
To further confirm the contribution of the loss of hydrogen-bonding interactions among the multilayer to the disintegration of the films, a control experiment has been performed. In this control experiment, instead of QP2VP-*b*-PEO micelles with cores exhibiting UCST-type behaviour, P2VP-*b*-PEO micelles was used as building blocks during multilayer assembly. Note that, P2VP-*b*-PEO micelles with pH-sensitive P2VP cores are not sensitive to temperature. A comparison of the UV-Visible spectra of multilayers of P2VP-*b*-PEO micelles/TA and (QP2VP+[Fe(CN)<sub>6</sub>]<sup>3-</sup>)-*b*-PEO micelles/TA at 45 °C showed that P2VP-*b*-PEO micelles/TA films also disintegrated at 45 °C (Appendix 4). Thus, it was concluded that disintegration of the layers occurred due to dissolution of the (QP2VP+[Fe(CN)<sub>6</sub>]<sup>3-</sup>) micellar cores as well as loss in hydrogen bonding interactions among the layers as the temperature increased.

### 3.5.2.2.2. Temperature-response of multilayers constructed at 37.5°C

Multilayers which were constructed at 37.5 °C were exposed to PBS solution at 37.5 °C and 42.5 °C. Film thickness and UV-Visible spectrum of the multilayers was recorded every one hour. Figure 23 indicates evolution of thickness of 20-layer films of (QP2VP+[Fe(CN)<sub>6</sub>]<sup>3-</sup>)-*b*-PEO micelles and TA at 37.5 °C and 42.5 °C. Similar to results obtained with films which were constructed at 25 °C, the results obtained from ellipsometry and UV-Visible Spectroscopy techniques were in good agreement for the experiment performed at 37.5 °C. No decrease in thickness was recorded in the first 5 hours. Similarly, the decrease in the intensity of the overall absorption spectrum was insignificant. At 42.5 °C, an increase in film thickness was recorded in the first hour. In contrast, significant decrease in the absorption spectrum was recorded for the same time period. As discussed in section 3.5.2.2.1, the increase in thickness can be correlated with the loose film structure due to weakening/loss of interactions among the layers which resulted in adsorption/absorption of salt ions within the multilayers at 42.5 °C. According to results obtained by UV-Visible Spectroscopy, half of the film was disintegrated after 7 hours.



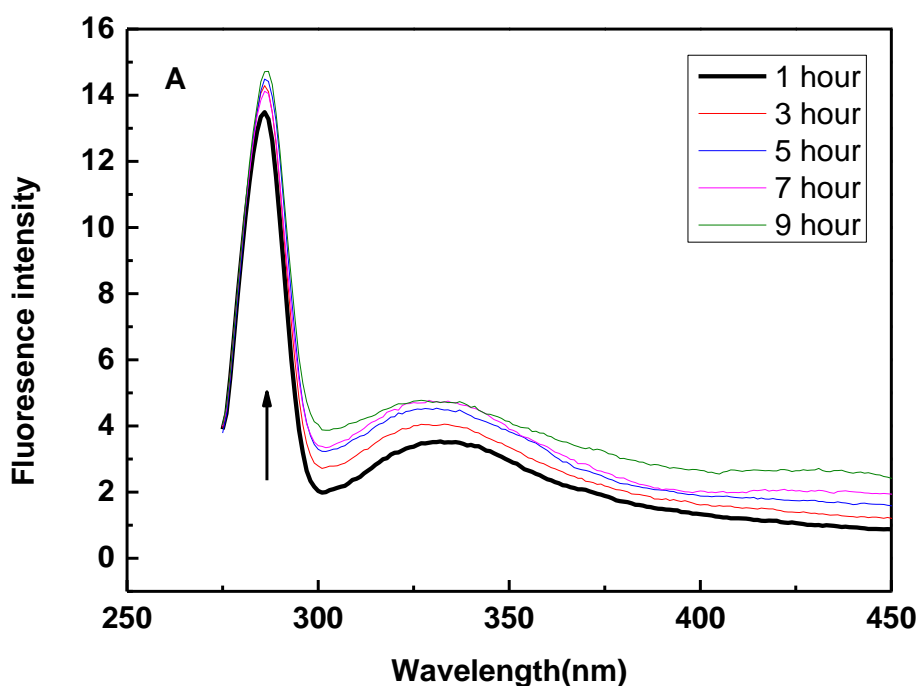
**Figure 23.** Evolution of thickness of 20-layer films of (QP2VP+[Fe(CN)<sub>6</sub>]<sup>3-</sup>)-*b*-PEO micelles and TA at 37.5 °C and 42.5 °C.



**Figure 24.** UV-Vis spectra of the (QP2VP+[Fe(CN)<sub>6</sub>]<sup>3-</sup>)-*b*-PEO micelles/TA films at 37.5°C (Panel A) and 42.5°C (Panel B).

### 3.5.2.2.3 Fluorescence Spectroscopy Studies

Fluorescence spectroscopy technique was used to analyze the multilayers which were immersed into PBS solutions. Emission spectra of QP2VP-*b*-PEO, TA and  $K_3Fe(CN)_6$  were recorded prior to the experiment. When excited at 260 nm, QP2VP-*b*-PEO exhibits one peak centered at 390 nm TA has one peak with centered at  $\sim 350$  nm.  $K_3Fe(CN)_6$  has one peak with centered at  $\sim 310$  nm (Appendix ). Unfortunately, the peaks observed in the emission spectra of the release solutions could not be assigned to individual film components. However, the fluorescence intensity of the peaks increased with time which also confirmed the disintegration of the layers from the surface. Figure 25 presents the emission spectra of the release solutions of the multilayers which were constructed at 25 °C and exposed to 45 °C (Panel A) and multilayers which were constructed at 37.5 °C and exposed to 42.5 °C (Panel B).



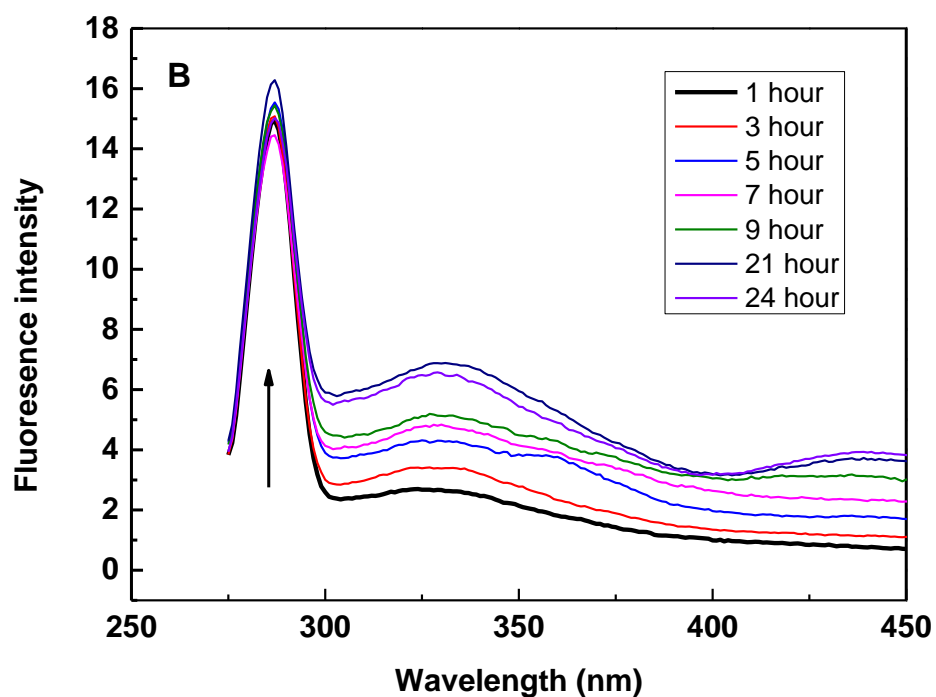


**Figure 25.** Fluorescence spectra of the release solutions of the (QP2VP+[Fe(CN)<sub>6</sub>]<sup>3-</sup>)-*b*-PEO micelles/TA films which were constructed 25°C and exposed to 45°C (Panel A) and (QP2VP+[Fe(CN)<sub>6</sub>]<sup>3-</sup>)-*b*-PEO micelles/TA films which were constructed at 37.5°C and exposed to 42.5°C (Panel B).

## CHAPTER 4

### CONCLUSIONS AND OUTLOOK

BCMs with cores exhibiting UCST-type phase behaviour at physiological pH were prepared using P2VP-*b*-PEO. First, the pyridine units on the P2VP blocks of P2VP-*b*-PEO were partially quaternized to obtain permanent positive charge on P2VP. The resulting polymer, QP2VP-*b*-PEO, was self-assembled into micellar aggregates in the presence of  $K_3Fe(CN)_6$  at pH 7.5 via electrostatic interactions among the QP2VP block and  $[Fe(CN)_6]^{3-}$  anions. The BCMs, QP2VP+ $[Fe(CN)_6]^{3-}$ -*b*-PEO micelles, had the PEO-corona and (QP2VP+ $[Fe(CN)_6]^{3-}$ )-core structure. The micellar cores demonstrated UCST-type phase behavior between a temperature range of 40-45 °C due to loss in electrostatic interactions among QP2VP and  $[Fe(CN)_6]^{3-}$  anions with increasing temperature. The micellization and the critical temperature values were highly dependent on the  $[Fe(CN)_6]^{3-}$  concentration. QP2VP+ $[Fe(CN)_6]^{3-}$ -*b*-PEO micelles did not form below a critical concentration of  $K_3Fe(CN)_6$ . Increasing  $K_3Fe(CN)_6$  concentration also resulted in loss of UCST-type behavior between 40-45 °C. The critical temperature values were also affected by the micellization temperature. For example, the amount of  $K_3Fe(CN)_6$  to form QP2VP+ $[Fe(CN)_6]^{3-}$ -*b*-PEO micelles was lower at 37.5 °C than that required for the micellization at 25 °C. Moreover, QP2VP+ $[Fe(CN)_6]^{3-}$ -*b*-PEO micelles formed at 37.5 °C were responsive to temperature changes in a more narrow range.

In the second part of this study, QP2VP+ $[Fe(CN)_6]^{3-}$ -*b*-PEO micelles were layer-by-layer deposited at the surface using TA at pH 7.5 at either 25 °C or 37.5 °C. The primary driving force for multilayer assembly was the hydrogen bonding interactions among hydrogen donating TA and hydrogen accepting PEO coronal chains. Multilayers prepared at 25 °C were quite stable in the first couple of hours at 37.5 °C, however demonstrated a gradual disintegration when the temperature was raised to 45 °C. Similarly, multilayers which were prepared at 37.5 °C gradually disintegrated

when the films were exposed to 42.5 °C. The disassembly of the multilayers can be correlated with the dissolution of the micellar cores above the critical temperature resulting in a charge imbalance within the multilayers. In addition, the disruption of the hydrogen bonds among the layers with increasing temperature could have also played a role in the multilayer disassembly.

This study differs from others concerning UCST-type behavior by their stability at physiological pH values. Moreover, BCMs were responsive to physiologically related temperature values. Although there are many studies on LbL films of polymers with LCST-type phase behavior, there are no studies concerning LbL films constructed using polymers with UCST-type phase behavior as the building blocks. In this context, this study is the first demonstrating temperature-induced erasable films from the surface.

In a future study, magnetic nanoparticles will be incorporated into the multilayer films. The disintegration of the films via AC magnetic field application will be examined. The magnetic nanoparticles are expected to increase the temperature within the multilayers upon AC magnetic field application. In this way, the disintegration of the multilayers will be induced via AC magnetic field rather than direct temperature increase.

## REFERENCES

- [1] C. Weber, R. Hoogenboom, U.S. Schubert, Progress in Polymer Science Temperature responsive bio-compatible polymers based on poly ( ethylene oxide ) and poly ( 2-oxazoline )s, *Prog. Polym. Sci.* 37 (2012) 686–714. doi:10.1016/j.progpolymsci.2011.10.002.
- [2] D. Schmaljohann, Thermo- and pH-responsive polymers in drug delivery, *Adv. Drug Deliv. Rev.* 58 (2006) 1655–1670. doi:10.1016/j.addr.2006.09.020.
- [3] M. a. Ward, T.K. Georgiou, Thermoresponsive polymers for biomedical applications, *Polymers (Basel)*. 3 (2011) 1215–1242. doi:10.3390/polym3031215.
- [4] P. Bawa, V. Pillay, Y.E. Choonara, L.C. Toit, Stimuli-responsive polymers and their applications in drug delivery, doi:10.1088/1748-6041/4/2/022001.
- [5] N. Yamada, T. Okano, H. Sakai, F. Karikusa, Y. Sawasaki, Y. Sakurai, Thermo-responsive polymeric surfaces; control of attachment and detachment of cultured cells, *Die Makromol. Chemie, Rapid Commun.* 11 (1990) 571–576. doi:10.1002/marc.1990.030111109.
- [6] P. Muthiah, S.M. Hoppe, T.J. Boyle, W. Sigmund, Thermally Tunable Surface Wettability of Electrospun Fiber Mats: Polystyrene/Poly(N-isopropylacrylamide) Blended versus Crosslinked Poly[(N-isopropylacrylamide)-co-(methacrylic acid)], *Macromol. Rapid Commun.* 32 (2011) 1716–1721. doi:10.1002/marc.201100373.
- [7] N. Mori, H. Horikawa, H. Furukawa, T. Watanabe, Temperature-Induced Changes in the Surface Wettability of SBR + PNIPA Films, *Macromol. Mater. Eng.* 292 (2007) 917–922. doi:10.1002/mame.200700102.
- [8] Y.H. Bae, T. Okano, R. Hsu, S.W. Kim, Thermo-sensitive polymers as on-off switches for drug release, *Macromol. Rapid Commun.* 8 (1987) 481–485. doi:10.1002/marc.1987.030081002.
- [9] Y. Oni, W.O. Soboyejo, Swelling and diffusion of PNIPA-based gels for

- localized chemotherapy and hyperthermia, *Mater. Sci. Eng. C.* 32 (2012) 24–30. doi:10.1016/j.msec.2011.09.006.
- [10] V. Bulmuş, S. Patir, S. a Tuncel, E. Pişkin, Stimuli-responsive properties of conjugates of N-isopropylacrylamide-co-acrylic acid oligomers with alanine, glycine and serine mono-, di- and tri-peptides., *J. Control. Release.* 76 (2001) 265–74. <http://www.ncbi.nlm.nih.gov/pubmed/11578741>.
- [11] W.L. Hinrichs, N.M. Schuurmans-Nieuwenbroek, P. van de Wetering, W.E. Hennink, Thermosensitive polymers as carriers for DNA delivery., *J. Control. Release.* 60 (1999) 249–59. doi:S0168-3659(99)00075-9 [pii].
- [12] A.T. and E.P. Sevil Dincer, A Potential Gene Delivery Vector : N - Isopropylacrylamide-ethyleneimine Block Copolymers, *Macromol. Chem. Phys.* 203 (2002) 1460–1465. doi:10.1002/1521-3935(200207)203:10.
- [13] H. Ikeda, F. Application, P. Data, Ullted States Patent [19], (1999).
- [14] H. Kanazawa, K. Yamamoto, Y. Matsushima, Temperature-Responsive Chromatography Using Poly ( N-isopropylacrylamide ) -Modified Silica, (1996) 341–346.
- [15] E.S. Gil, S.M. Hudson, Stimuli-reponsive polymers and their bioconjugates, *Prog. Polym. Sci.* 29 (2004) 1173–1222. doi:10.1016/j.progpolymsci.2004.08.003.
- [16] D. Fournier, R. Hoogenboom, H.M.L. Thijs, R.M. Paulus, U.S. Schubert, Tunable pH- and temperature-sensitive copolymer libraries by reversible addition-fragmentation chain transfer copolymerizations of methacrylates, *Macromolecules.* 40 (2007) 915–920. doi:10.1021/ma062199r.
- [17] C. de Las Heras Alarcon, S. Pennadam, C. Alexander, Stimuli responsive polymers for biomedical applications., *Chem. Soc. Rev.* 34 (2005) 276–285. doi:10.1039/b406727d.
- [18] M. Hrubý, S.K. Filippov, P. Štěpánek, Smart polymers in drug delivery systems on crossroads: Which way deserves following , *Eur. Polym. J.* 65 (2015) 82–97. doi:10.1016/j.eurpolymj.2015.01.016.
- [19] C. De, H. Alarco, S. Pennadam, C. Alexander, C. Alexander, Stimuli

responsive polymers for biomedical applications, (2005) 276–285.  
doi:10.1039/b406727d.

- [20] L.D. Taylor, L.D. Cerankowski, Preparation of Films Exhibiting a Balanced Solutions-A Study of Lower Consolute Behavior, 13 (1975) 2551–2570.
- [21] H.G. Schild, Poly ( n-isopropylacrylamide ): Experiment , Theory and Application been Appearing in the Literature with Increasing Frequency . As Fig . 1 " illustrates , growth has become rather explosive . CH<sub>3</sub> CH<sub>3</sub>, 17 (1992) 163–249.
- [22] B. Liu, J. Wang, G. Ru, C. Liu, J. Feng, Phase Transition and Preferential Alcohol Adsorption of Poly( N , N - diethylacrylamide) Gel in Water/Alcohol Mixtures, (2015). doi:10.1021/ma502393z.
- [23] S.A. Angelopoulos, C. Tsitsilianis, Thermo-Reversible Hydrogels Based on Poly ( N , N -diethylacrylamide ) - *block* -poly ( acrylic acid ) - *block* -poly ( N , N -diethylacrylamide ) Double Hydrophilic Triblock Copolymer, (2006) 2188–2194. doi:10.1002/macp.200600489.
- [24] X. Pang, S. Cui, Single-Chain Mechanics of Poly( N , N - diethylacrylamide) and Poly( N - isopropylacrylamide): Comparative Study Reveals the Effect of Hydrogen Bond Donors, (2013).
- [25] A.D. Little, Macromolecule Hydration and the Effect of Solutes on the Cloud Point of Aqueous Solutions of Polyvinyl Methyl Ether : A Possible Model for Protein Denaturation and Temperature Control in Homeothermic Animals I -- CH<sub>2</sub>--CH-- j , OCH<sub>3</sub> n, 35 (1971).
- [26] O. Confortini, F.E. Du Prez, Functionalized Thermo-Responsive Poly ( vinyl ether ) by Living Cationic Random Copolymerization of Methyl Vinyl Ether and 2-Chloroethyl Vinyl Ether, (1871) 1871–1882.  
doi:10.1002/macp.200700205.
- [27] J. Park, Y. Akiyama, Y. Yamasaki, K. Kataoka, Preparation and Characterization of Polyion Complex Micelles with a Novel Thermosensitive Poly ( 2-isopropyl-2-oxazoline ) Shell via the Complexation of Oppositely Charged Block Ionomers , (2007) 138–146.

- [28] R. Hoogenboom, Poly ( 2-oxazoline ) s : A Polymer Class with Numerous Potential Applications *Angewandte*, (2009) 7978–7994.  
doi:10.1002/anie.200901607.
- [29] G. Vancoillie, D. Frank, R. Hoogenboom, Progress in Polymer Science Thermoresponsive poly ( oligo ethylene glycol acrylates ), *Prog. Polym. Sci.* 39 (2014) 1074–1095. doi:10.1016/j.progpolymsci.2014.02.005.
- [30] E.E. Makhaeva, H. Tenhu, A.R. Khokhlov, Conformational Changes of Poly(vinylcaprolactam) Macromolecules and Their Complexes with Ionic Surfactants in Aqueous Solution, *Macromolecules*. 31 (1998) 6112–6118.  
doi:10.1021/ma980158s.
- [31] J. Seuring, S. Agarwal, Polymers with upper critical solution temperature in aqueous solution, *Macromol. Rapid Commun.* 33 (2012) 1898–1920.  
doi:10.1002/marc.201200433.
- [32] W. Wan, F. Cheng, F. Jäkle, A Borinic Acid Polymer with Fluoride Ion- and Thermo-responsive Properties that are Tunable over a Wide Temperature Range, (2014) 8934–8938. doi:10.1002/anie.201403703.
- [33] S.S. Yusa, As featured in : *Soft Matter*, *Soft Matter*. 11 (2015) 5204–5213.  
doi:10.1039/C5SM00499C.
- [34] D.N. Schulz, D.G. Peiffer, P.K. A, J. Larabee, J.J. Kaladas, Phase behaviour and solution properties of sulphobetaine polymers, 27 (1986) 1734–1742.
- [35] Y. Deng, Y. Xu, X. Wang, Q. Yuan, Y. Ling, H. Tang, Water-Soluble Thermoresponsive  $\alpha$  -Helical Polypeptide with an Upper Critical Solution Temperature : Synthesis , Characterization , and Thermoresponsive Phase Transition Behaviors, (2015) 453–458.
- [36] J. Seuring, S. Agarwal, Polymers with Upper Critical Solution Temperature in Aqueous Solution: Unexpected Properties from Known Building Blocks, (2013).
- [37] H. Zhang, X. Tong, Y. Zhao, Diverse Thermoresponsive Behaviors of Uncharged UCST Block Copolymer Micelles in Physiological Medium, (2014).

- [38] S. Kudaibergenov, J. Andre, *Polymeric Betaines : Synthesis , Characterization and Application*, (2006) 157–224.
- [39] J.E. Osterheld, *Intrinsic viscosities of polyelectrolytes. poly-(acrylic acid)'* , 1915 (2000).
- [40] R. Buscall, T. Corner, C. Colloid, S. Group, T. Heath, *ro ,. cl*, 18 (1982) 967–974.
- [41] P.A. Wood, Y. Zhu, Y. Pei, P.J. Roth, *Hydrophobically Modified Sulfobetaine Copolymers with Tunable Aqueous UCST through Postpolymerization Modification of Poly(penta fluorophenyl acrylate)*, (2014).
- [42] P. Mary, D.D. Bendejacq, M. Labeau, P. Dupuis, *Reconciling Low- and High-Salt Solution Behavior of Sulfobetaine Polyzwitterions*, (2007) 7767–7777.
- [43] K.E.B. Doncom, H. Willcock, A. Lu, B.E. Mckenzie, N. Kirby, R.K.O. Reilly, *Soft Matter Complementary light scattering and synchrotron micelle-to-unimer transition of polysulfobetaines*, (2015) 3666–3676.  
doi:10.1039/C5SM00602C.
- [44] N. Poly, F.A. Plamper, A. Schmalz, M. Ballauff, A.H.E. Mu, *Tuning the Thermoresponsiveness of Weak Polyelectrolytes by pH and Light : Lower and Upper Critical-Solution Temperature of*, (2007) 14538–14539.
- [45] Q. Zhang, F. Tosi, Ü. Sibel, S. Maji, R. Hoogenboom, *Tuning the LCST and UCST Thermoresponsive Behavior of Poly ( N , N -dimethylaminoethyl methacrylate ) by Electrostatic Interactions with Trivalent Metal Hexacyano Anions and Copolymerization*, (2015) 633–639.
- [46] J. Seuring, S. Agarwal, *First Example of a Universal and Cost-E ff ective Approach : Polymers with Tunable Upper Critical Solution Temperature in Water and Electrolyte Solution*, (2012).
- [47] N. Shimada, H. Ino, K. Maie, M. Nakayama, A. Kano, A. Maruyama, *Ureido-Derivatized Polymers Based on Both Poly(allylurea) and Poly(l-citrulline) Exhibit UCST-Type Phase Transition Behavior under Physiologically Relevant Conditions*.(2011)
- [48] S. Glatzel, *Well-Defined Uncharged Polymers with a Sharp UCST in Water*

- and in *Physiological Milieu*, (2011) 413–415. doi:10.1021/ma102677k.
- [49] M. Zhang, A.H.E. Mu, X. Andre, Thermo- and pH-Responsive Micelles of Poly ( acrylic acid ) - *block* -Poly ( N , N -diethylacrylamide ), (2005) 558–563. doi:10.1002/marc.200400510.
- [50] C.M. Schilli, M. Zhang, E. Rizzardo, S.H. Thang, ) Y. K. Chong, K. Edwards, G. Karlsson, A.H.E. Müller, A New Double-Responsive Block Copolymer Synthesized via RAFT Polymerization: Poly( N -isopropylacrylamide)- *block* -poly(acrylic acid), *Macromolecules*. 37 (2004) 7861–7866. doi:10.1021/ma035838w.
- [51] H. Wei, X.Z. Zhang, Y. Zhou, S.X. Cheng, R.X. Zhuo, Self-assembled thermoresponsive micelles of poly (N-isopropylacrylamide-b- methyl methacrylate), *Biomaterials*. 27 (2006) 2028–2034. doi:10.1016/j.biomaterials.2005.09.028.
- [52] X. Jia, D. Chen, M. Jiang, Preparation of PEO-b-P2VPH<sup>+</sup>-S2O8<sup>(2-)</sup> micelles in water and their reversible UCST and redox-responsive behavior., *Chem. Commun. (Camb)*. (2006) 1736–1738. doi:10.1039/b600859c.
- [53] K. Wu, L. Shi, W. Zhang, Y. An, X. Zhu, Z. Li, Formation of hybrid micelles between poly ( ethylene glycol ) - *block* -poly ( 4- vinylpyridinium ) cations and sulfate anions in an aqueous milieu , (2005) 455–459. doi:10.1039/b512610j.
- [54] J. Yin, J. Hu, G. Zhang, S. Liu, Schizophrenic Core – Shell Microgels: Thermoregulated Core and Shell Swelling/Collapse by Combining UCST and LCST Phase Transitions, (2014).
- [55] T. Industrial, Multilayers of Colloidal Particles , R. K. Iler, 594 (1966) 569–594.
- [56] Fuzzy Nanoassemblies : Toward Layered Polymeric Multicomposites, 277 (1997).
- [57] Y. Jang, S. Park, K. Char, Functionalization of polymer multilayer thin films for novel biomedical applications, 28 (2011) 1149–1160. doi:10.1007/s11814-010-0434-x.

- [58] G. Decher, J.B. Schlenoff, *Multilayer Thin Films - sequential assembly of nanocomposite materials*, Wiley-VCH, Weinheim, 2012.
- [59] S.S. Shiratori, M.F. Rubner, pH-dependent thickness behavior of sequentially adsorbed layers of weak polyelectrolytes, *Macromolecules*. 33 (2000) 4213–4219. doi:10.1021/ma991645q.
- [60] J.H. Cheung, W.B. Stockton, M.F. Rubner, *Molecular-Level Processing of Conjugated Polymers*. 3. Layer-by-Layer Manipulation of Polyaniline via Electrostatic Interactions, *9297 (1997) 2712–2716*.
- [61] B. Kim, S.W. Park, P.T. Hammond, *Hydrogen-Bonding Layer-by-Layer-Assembled Biodegradable Polymeric Micelles as Drug Delivery Vehicles from Surfaces*, 2 (n.d.) 386–392.
- [62] N. Kotov, *Layer-by-Layer self-assembly*, 12 (1999) 789–796.
- [63] M. Sato, M. Sano, van der Waals *Layer-by-Layer Construction of a Carbon Nanotube 2D Network*, (2005) 11490–11494.
- [64] J. Chen, L. Huang, L. Ying, G. Luo, X. Zhao, *Self-Assembly Ultrathin Films Based on Diazoresins*, (1999) 7208–7212.
- [65] G.K. Such, J.F. Quinn, A. Quinn, E. Tjipto, F. Caruso, *Assembly of Ultrathin Polymer Multilayer Films by Click Chemistry*, (2006) 9318–9319.
- [66] Y. Shimazaki, M. Mitsuishi, S. Ito, M. Yamamoto, *Preparation and Characterization of the Layer-by-Layer Deposited Ultrathin Film Based on the Charge-Transfer Interaction in Organic Solvents*, 7463 (1998) 2768–2773.
- [67] A. Rahim, H. Ejima, K.L. Cho, K. Kempe, M. Mu, J.P. Best, F. Caruso, *Coordination-Driven Multistep Assembly of Metal – Polyphenol Films and Capsules*, (2014).
- [68] H. Hong, T.E. Mallouk, *1,2-Ethanediybis(phosphonate)*, (1991) 2362–2369.
- [69] T.I. Diastereoselectivity, *J. Am. Chem.*, (1988) 618–620.
- [70] J.D. Hong, K. Lowack, J. Schmitt, G. Decher, *J. Gutenberg-universit, Layer-by-layer deposited multilayer assemblies of polyelectrolytes and proteins : from ultrathin films to protein arrays*, 102 (1993) 98–102.

- [71] S. Rauf, D. Zhou, C. Abell, D. Kang, Building three-dimensional nanostructures with active enzymes by surface templated layer-by-layer assembly {, (2006) 1721–1723. doi:10.1039/b517557g.
- [72] G.K. Such, A.P.R. Johnston, F. Caruso, Engineered hydrogen-bonded polymer multilayers: from assembly to biomedical applications., *Chem. Soc. Rev.* 40 (2011) 19–29. doi:10.1039/c0cs00001a.
- [73] D.M. DeLongchamp, P.T. Hammond, Highly Ion Conductive Poly ( ethylene oxide ) -Based Solid Polymer Electrolytes from Hydrogen Bonding Layer-by-Layer Assembly, 1 (2004) 5403–5411.
- [74] E. Kharlampieva, I. Erel-unal, S.A. Sukhishvili, Amphoteric Surface Hydrogels Derived from Hydrogen-Bonded Multilayers : Reversible Loading of Dyes and Macromolecules, (2007) 175–181.
- [75] S.A. Sukhishvili, S. Granick, Layered, erasable polymer multilayers formed by hydrogen-bonded sequential self-assembly, *Macromolecules.* 35 (2002) 301–310. doi:10.1021/ma011346c.
- [76] J.F. Quinn, F. Caruso, Facile Tailoring of Film Morphology and Release Properties Using Layer-by-Layer Assembly of Thermoresponsive Materials, (2004) 5388–5390.
- [77] K.B. Doorty, T. a. Golubeva, A. V. Gorelov, Y. a. Rochev, L.T. Allen, K. a. Dawson, W.M. Gallagher, A.K. Keenan, Poly(N-isopropylacrylamide) copolymer films as potential vehicles for delivery of an antimetastatic agent to vascular smooth muscle cells, *Cardiovasc. Pathol.* 12 (2003) 105–110. doi:10.1016/S1054-8807(02)00165-5.
- [78] S. Nayak, S.B. Debord, L.A. Lyon, Investigations into the Deswelling Dynamics and Thermodynamics of Thermoresponsive Microgel Composite Films, (2003) 7374–7379.
- [79] A.Sukhishvili, Temperature-Induced Swelling and Small Molecule Release with Hydrogen- Micelles, 3 (2009) 3595–3605. doi: 10.1021/nn900655z
- [80] M.J. Serpe, C.D. Jones, L.A. Lyon, Layer-by-Layer Deposition of Thermoresponsive Microgel Thin Films, (2003) 8759–8764.

- [81] C.M. Nolan, M.J. Serpe, L.A. Lyon, Thermally Modulated Insulin Release from Microgel Thin Films, (2004) 1940–1946.
- [82] M.J. Serpe, K.A. Yarmey, C.M. Nolan, L.A. Lyon, Doxorubicin Uptake and Release from Microgel Thin Films, 0400 (2005) 408–413.
- [83] J.A. Jaber, J.B. Schlenoff, Polyelectrolyte Multilayers with Reversible Thermal Responsivity, (2005) 1300–1306.
- [84] J. Reuber, H. Reinhardt, D. Johannsmann, Formation of Surface-Attached Responsive Gel Layers via Electrochemically Induced Free-Radical Polymerization, (2006) 3362–3367.
- [85] Z. Zhu, N. Gao, H. Wang, S.A. Sukhishvili, Temperature-triggered on-demand drug release enabled by hydrogen-bonded multilayers of block copolymer micelles, *J. Control. Release.* 171 (2013) 73–80. doi:10.1016/j.jconrel.2013.06.031.
- [86] L. Xu, Z. Zhu, S.A. Sukhishvili, Polyelectrolyte Multilayers of Diblock Copolymer Micelles with Temperature-Responsive Cores, 27 (2011) 409–415. doi:10.1021/la1038014.
- [87] W.S. Tan, R.E. Cohen, M.F. Rubner, S.A. Sukhishvili, Temperature-Induced, Reversible Swelling Transitions in Multilayers of a Cationic Triblock Copolymer and a Polyacid, (2010) 1950–1957. doi:10.1021/ma902459a.
- [88] I. Erel, H.E. Karahan, C. Tuncer, V. Bütün, a. L. Demirel, Hydrogen-bonded multilayers of micelles of a dually responsive dicationic block copolymer, *Soft Matter.* 8 (2012) 827. doi:10.1039/c1sm06248d.
- [89] I.Erel, pH-responsive layer-by-layer films of zwitterionic block copolymer micelles As featured in : *Polymer Chemistry*, (2014).doi:10.1039/c4py00040d.
- [90] K. Lipponen, S. Tähkä, M. Kostainen, M.L. Riekkola, Stable neutral double hydrophilic block copolymer capillary coating for capillary electrophoretic separations, *Electrophoresis.* 35 (2014) 1106–1113. doi:10.1002/elps.201300425.
- [91] S.K. Varshney, S. Antoun, R. Je, Water-Soluble Complexes Formed by Sodium Poly ( 4-styrenesulfonate ) and a Poly ( 2-vinylpyridinium ) - *block -*

- poly ( ethyleneoxide ) Copolymer, (2000) 9298–9305.
- [92] M. Orlov, I. Tokarev, A. Scholl, A. Doran, S. Minko, pH-responsive thin film membranes from poly(2-vinylpyridine): Water vapor-induced formation of a microporous structure, *Macromolecules*. 40 (2007) 2086–2091.  
doi:10.1021/ma062821f.
- [93] S. Hocine, M.-H. Li, Thermoresponsive self-assembled polymer colloids in water, *Soft Matter*. 9 (2013) 5839. doi:10.1039/c3sm50428j.
- [94] C. Guo, J. Wang, H.Z. Liu, J.Y. Chen, Hydration and conformation of temperature-dependent micellization of PEO-PPO-PEO block copolymers in aqueous solutions by FT-Raman, *Langmuir*. 15 (1999) 2703–2708.  
doi:10.1021/la981036w.
- [95] I. Erel , S.A. Sukhishvili, Hydrogen-Bonded Multilayers of a Neutral Polymer and a Polyphenol, (2008) 3962–3970.
- [96] E. Kharlampieva, V. Kozlovskaya, J. Tyutina, S.A. Sukhishvili, Hydrogen-bonded multilayers of thermoresponsive polymers, *Macromolecules*. 38 (2005) 10523–10531. doi:10.1021/ma0516891.
- [97] I. Erel, Z. Zhu, A. Zhuk, S.A. Sukhishvili, Journal of Colloid and Interface Science Hydrogen-bonded layer-by-layer films of block copolymer micelles with pH-responsive cores, *J. Colloid Interface Sci.* 355 (2011) 61–69.  
doi:10.1016/j.jcis.2010.11.083.
- [98] E. Kharlampieva, S.A. Sukhishvili, Hydrogen-Bonded Layer-by-Layer Polymer Films, *J. Macromol. Sci. Part C Polym. Rev.* 46 (2006) 377–395.  
doi:10.1080/15583720600945386.

## APPENDIX

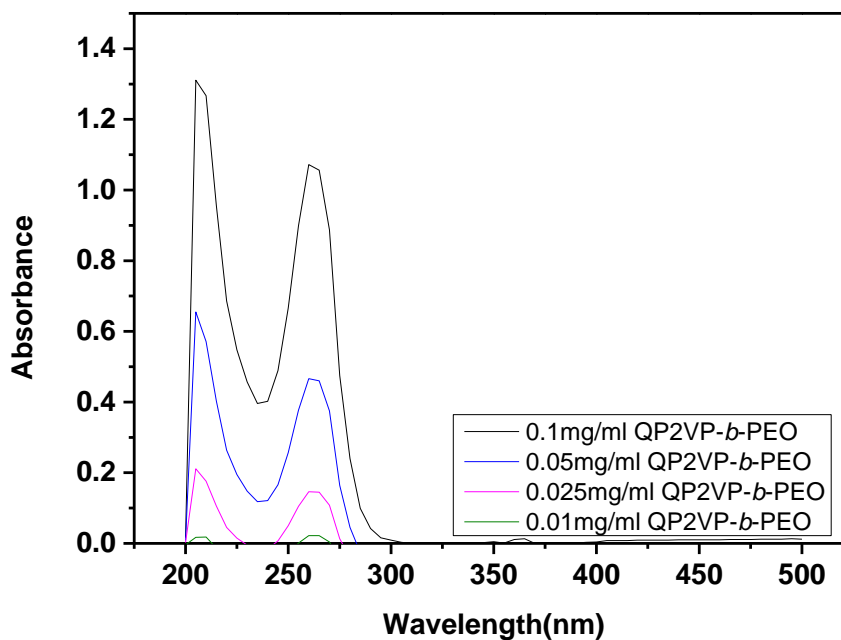


Figure A. 1 UV-Vis spectra of QP2VP-*b*-PEO.

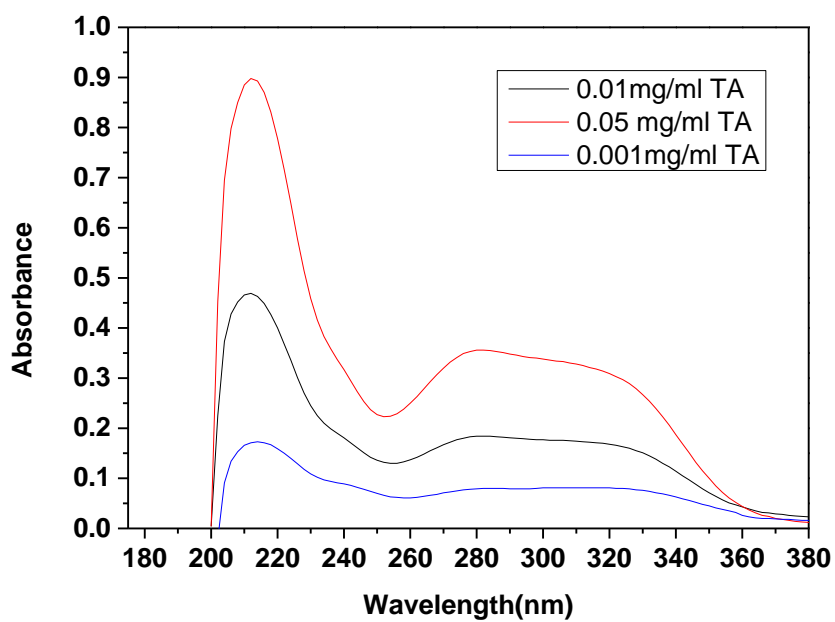


Figure A. 2. UV-Vis spectra of TA.

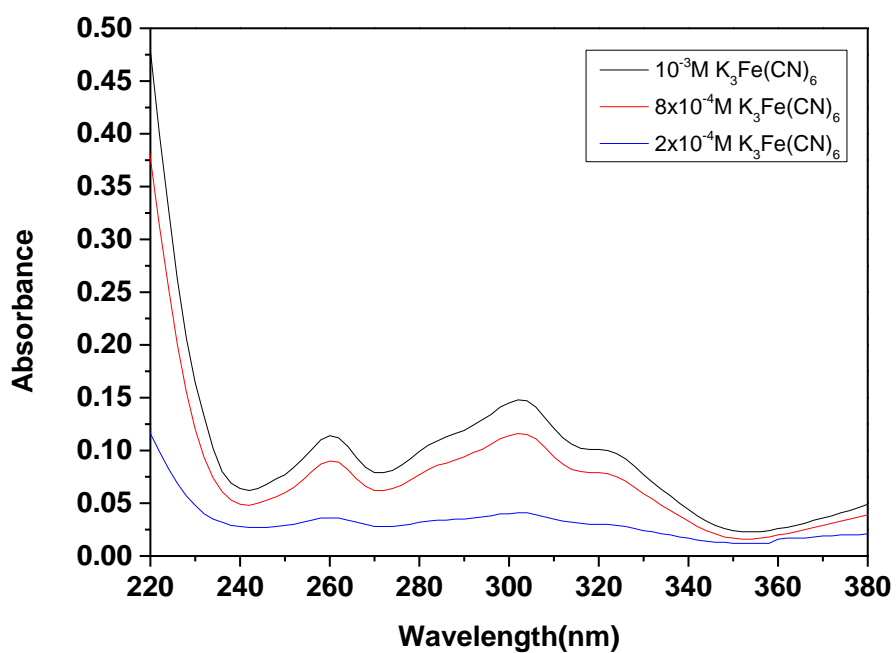


Figure A. 3. UV-Vis spectra of  $K_3Fe(CN)_6$ .

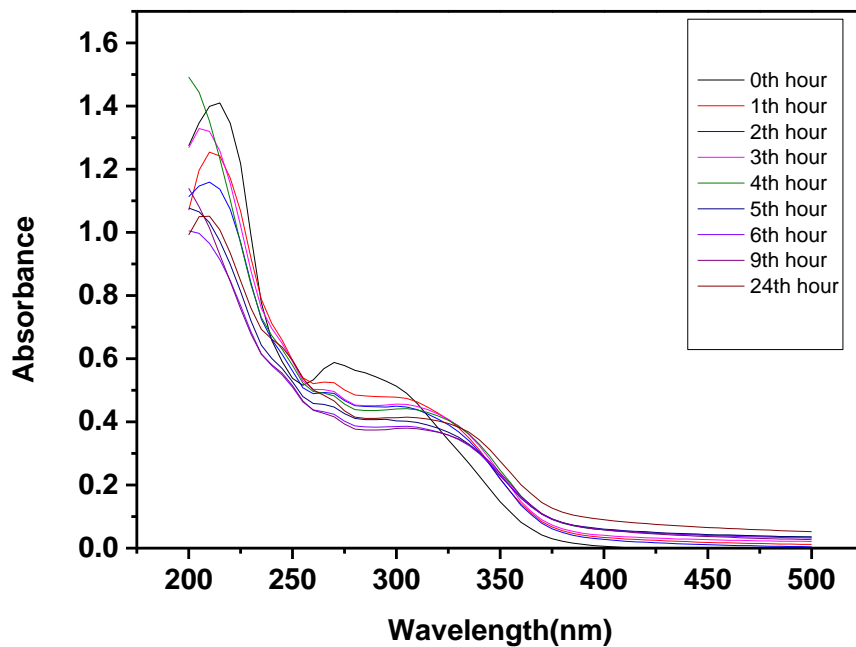


Figure A. 4. UV-Visible spectra of multilayers of P2VP-*b*-PEO micelles/TA at 45 °C.

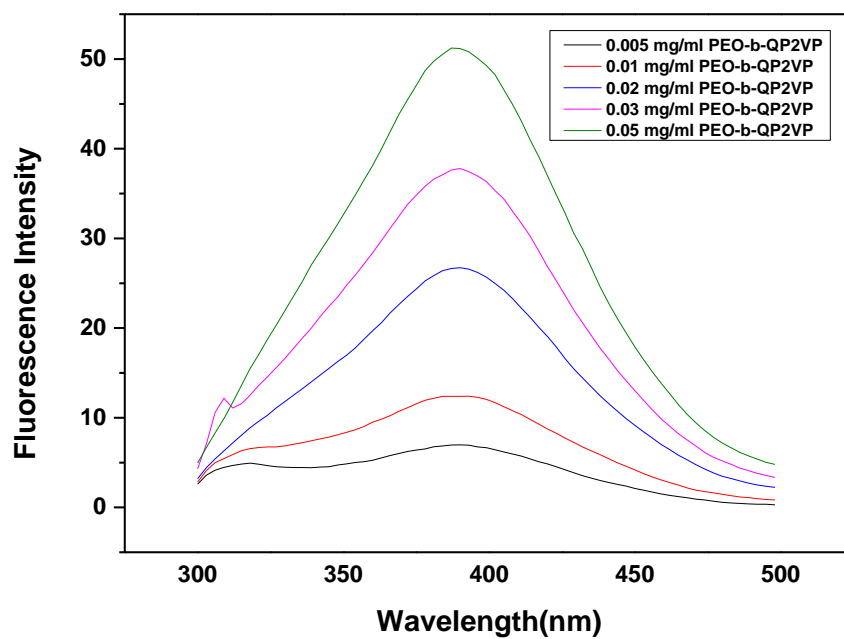


Figure A. 5. Fluorescence spectra of QP2VP-*b*-PEO.

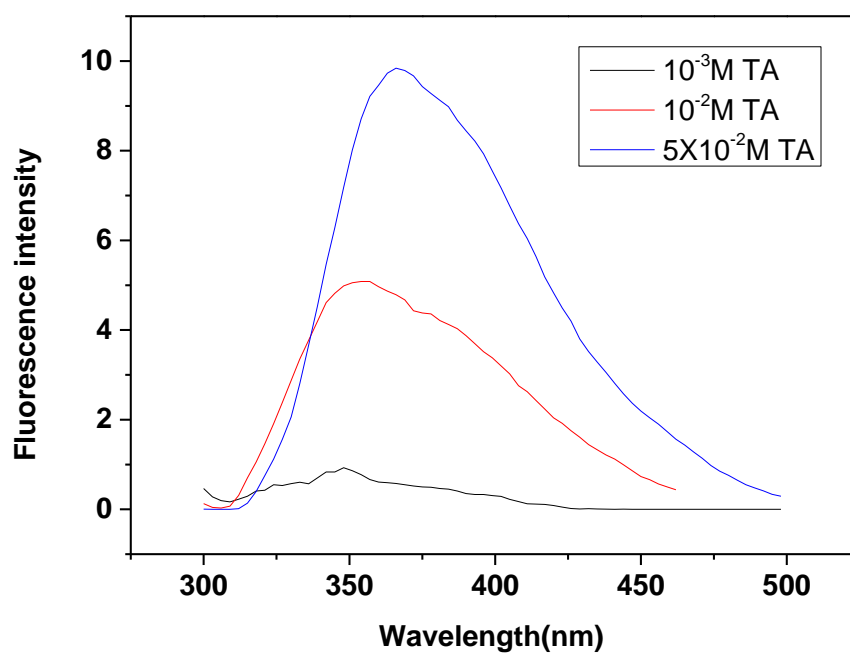
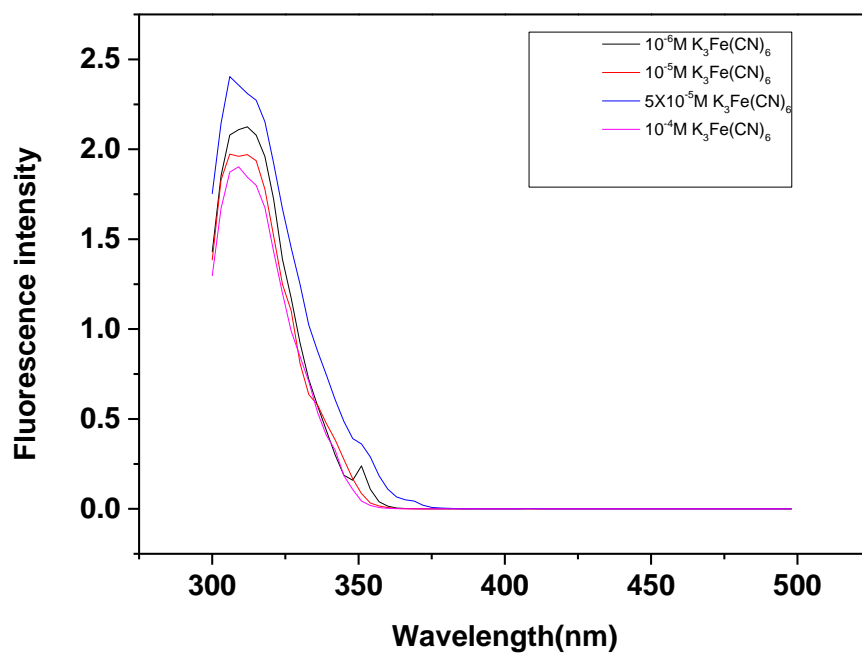


Figure A. 6. Fluorescence spectra of TA , ext  $\lambda=260$ nm.



**Figure A. 7.** Fluorescence spectra of  $K_3Fe(CN)_6$ , ext  $\lambda=260nm$ .